VOL. 256 MARCH 1958 No. 3

American Journal of Science

Established in 1818 by Benjamin Silliman

EDITORS
JOHN RODGERS—JOSEPH T. GREGORY

ASSOCIATE EDITORS

GEORGE GAYLORD SIMPSON, NEW YORK, N. Y.
A. F. BUDDINGTON, PRINCETON, N. J.
CARL O. DUNBAR
MATT WALTON
HENRY MARGENAU
RICHARD F. FLINT
HORACE WINCHELL
HAROLD G. CASSIDY
EDWARD S. DEEVEY, JR.
G. EVELYN HUTCHINSON, NEW HAVEN, CONN.
LEASON H. ADAMS
WILMOT H. BRADLEY, WASHINGTON, D. C.
HOWEL WILLIAMS, BERKELEY, CALIF.
C. R. LONGWELL, PALO ALTO, CALIF.
ADOLPH KNOPF, STANFORD, CALIF.
FREDERICK J. ALCOCK, OTTAWA, CANADA
CECIL E. TILLEY, CAMBRIDGE, ENGLAND

STERLING TOWER
YALE UNIVERSITY
NEW HAVEN, CONNECTICUT

Published 10 times a year. Ten dollars a year. One dollar twenty-five cents a copy.
Foreign, ten dollars sixty cents Canada, ten dollars thirty-five cents.

AMERICAN JOURNAL OF SCIENCE

Established in 1818 by Benjamin Silliman

THE FIRST SCIENTIFIC JOURNAL IN THE UNITED STATES

DEVOTED TO THE GEOLOGICAL SCIENCES AND TO RELATED FIELDS

Editors: JOHN ROGERS—JOSEPH T. GREGORY

Managing Editor: BETH A. BADGLEY

Entered as second-class matter at the Post Office at New Haven, Conn., under the Act of March 3, 1879. Published monthly, except July and September, at Sterling Tower, Yale University, New Haven, Conn.

Subscription rate $10 per year ($1.25 a number). Student rate $5 per year (application blanks available on request). Postage prepaid to the United States; 35 cents per year to Canada; 60 cents per year elsewhere.

The JOURNAL completed its *first* series of 50 volumes in 1845, its *second* series of 50 volumes in 1870, its *third* series of 50 volumes in 1895, its *fourth* series of 50 volumes in 1920, its *fifth* series of 36 volumes in 1938. Since 1938 the numbering by series has been discontinued, and volumes are annual and bear the whole numbers as of 1818, that for 1939 being volume 237.

Back numbers and volumes, also cumulative indices of all series, may with few exceptions be obtained from the office of the AMERICAN JOURNAL OF SCIENCE, Sterling Tower, New Haven, Conn. Positive microfilm copies of each complete volume may be purchased by subscribers to the paper edition from *University Microfilms*, 313 N. First St., Ann Arbor, Michigan. Regular subscribers may purchase each past year in microcard form, from *The Microcard Foundation*, Wesleyan University, Middletown, Connecticut.

INSTRUCTIONS TO CONTRIBUTORS

Manuscripts of articles submitted should follow the recommendations in the pamphlet "Suggestions to Authors" (Lane, 1935) and should be preceded by brief abstracts. They should be checked with special care before being submitted, to avoid changes in proof other than printer's errors.

References to literature should be listed alphabetically by authors at the end of the article; all references should be complete. For articles in journals or other serial publications, the reference should give in order: Author's name, year of publication, full title; name of periodical or series, volume number, inclusive pages. For books or other unnumbered publications, it should give: Author's name, year of publication, full title; place of publication, publisher. This form follows the recommendations in the pamphlet "Abbreviations used in publications of the U. S. Geological Survey", which is also the standard used for abbreviating names of periodicals, etc. Citations within an article should be to author and year, with specific pages wherever appropriate.

Plates (photographs), *figures* (line drawings), and *footnotes* should each be numbered consecutively through each article, using arabic numerals. If two photographs form one plate, they are figures 1 and 2 of that plate.

Illustrations should be neat and legible and should include explanations of symbols used. Copy that cannot be reproduced cannot be accepted. Plates and figures should be capable of reduction to not more than 4 by 7 inches, all lettering being at least 1/16th inch high after reduction. When necessary, one large map or table can be accepted, if it will not exceed 7 inches in width after reduction. Line drawings should be in black India ink on white drawing board, tracing cloth, or coordinate paper printed in blue. Photographs should be positive glossy prints. Photostatic and typewritten material cannot be accepted as copy for illustrations.

Reprints. Thirty separate copies of each article will be furnished to the author free of cost and without previous notice from him; these will be without a cover. Additional copies will be furnished at cost, which will of course be greater if the article is accompanied by plates involving unusual expense. Copies will be furnished with a printed cover giving the title, author, volume, page, and year, when specially ordered.

REFERENCE

Lane, R. H., 1935, Suggestions to authors of papers submitted for publication by the United States Geological Survey: U. S. Geol. Survey, Washington, D. C. (For sale by Superintendent of Documents, Washington, D. C. 40c.)

[American Journal of Science, Vol. 256, March 1958, P. 145-158]

American Journal of Science

MARCH 1958

STRUCTURAL PETROLOGY OF CAMBRO-ORDOVICIAN LIMESTONES OF THE NORTH-WEST HIGHLANDS OF SCOTLAND

C. B. CRAMPTON

ABSTRACT. Petrofabric analyses of dolomite and calcite marbles in the Durness Limestone from Loch Broom to Loch Glencoul in the North-West Highlands of Scotland are described. The preferred orientation of compression axes (and initial [0001]-axes) constructed for twinned {0221}-lamellae of dolomite measured in these limestones shows a transition from partial girdles characterised by two mutually perpendicular and prominent maxima to complete girdles disposed vertically either south-east and north-west or south-west and north-east. A tentative kinematic interpretation of these fabrics is attempted.

INTRODUCTION

Both calcite and dolomite have been investigated under conditions of experimental deformation (Griggs, Turner, Borg and Sosoka, 1953; Handin and Fairbairn, 1953; Turner, Griggs, Heard and Weiss, 1954). Some aspects of certain fabrics of naturally deformed calcite and dolomite marbles have been interpreted on the basis of the experimental data (Turner, 1953; Gilmour and Carman, 1954; Crampton, 1956). Petrofabric analyses of chiefly dolomite and some calcite marbles in the Durness Limestone succession of the North-West Highlands of Scotland from Loch Broom to Loch Glencoul are here described.

Situation and general features of analyzed specimens.—Loch Broom limestone: collected from the north-east cliffs of Loch Broom at Gadcaisceig, one mile south-east of Ullapool, not far below the Moine Thrust. The bedding plane dips 13° south-east.

Lochan Fasaidh limestone: collected just below the Moine Thrust a quarter of a mile north of Lochan Fasaidh. The foliation dips 47° south-south-west. Dip and bearings of sections cut for fabric analysis are 44°/337°, 61°/085° and 47°/205°.

Loch Urigill limestone: collected from the shore of Loch Urigill at the base of the north-east slopes of Druim na Doire Duibhe, mid-way between the thrust planes and sole. The foliation is strongly ruckled, but at the point of collection dips 44° west. Dip and bearing of sections cut for fabric analysis are 85°/176°, 52°/088° and 35°/280°.

Elphin limestone: collected from the south-west slopes of Cnoc Breac just east of Elphin and the sole of the thrusts. The rudimentary foliation dips 30° west-north-west. Dip and bearing of sections cut for fabric analysis are 30°/293°, 70°/132° and 73°/032°.

Ledbeg limestone: collected from the banks of the Ledbeg River near Ledbeg, close to the sole of the thrusts. The rock is cut by a set of parallel calcite veins along which splitting tends to occur thus giving rise to a well

defined joint system. The foliation dips 14° east, and carries a fine lineation dipping 11° north-east. This lineation lies normal to the calcite veins. Dip and bearing of sections cut for fabric analysis are 82°/325°, 81°/220° and 14°/032°.

Cnoc Chaornaidh limestone: collected from the lower slopes of Cnoc Chaornaidh, alongside the road to Benmore Lodge and near the Benmore Thrust. The strongly ruckled foliation at the point of collection dips 20° west. Dip and bearing of sections cut for fabric analysis are 90°/311°, 82°/135° and 08°/315°.

Loch Glencoul limestone: collected immediately below the Glencoul Thrust plane near the shores of Loch Glencoul. The bedding dips 20° south-east.

In thin section the Loch Broom limestone shows angular dolomite and quartz grains of sedimentary character. A little nearer the Moine Thrust plane there is some evidence of recrystallization, and the dolomite grains are larger and flattened normal to the optic axis. Against the lower surface of the Glencoul Thrust plane the Loch Glencoul limestone shows a mosaic of dolomite crystals intersected by zones of fracture, which sometimes contain lenticles of quartz.

Some specimens were collected from recrystallized masses within the metamorphic aureole of the Cnoc na Sroine syenite. Within the Lochan Fasaidh and Elphin limestones, clusters of dolomite crystals are enclosed by granulated dolomite. In the Ledbeg limestone individual dolomite porphyroblasts with irregular outline are isolated by the dolomite granules (plate 1), while within the Cnoc Chaornaidh limestone large flattened dolomite porphyroblasts are enveloped by granoblastic calcite and brucite (plate 2).

LOCHAN FASAIDH LIMESTONE

In thin section clusters of dolomite porphyroblasts are enclosed by granular dolomite. A little marginal granulation suggests slight external rotation of some porphyroblasts since crystallization. Most grains possess {0221}-lamellae and {1011}-cleavages, these planes being identified by their angular and zonal relationships. Slight internal distortion of some porphyroblasts is indicated by undulose extinction and flexed lamellae and cleavages.

Petrofabric analysis.—Because in no case were nearly all twinned lamellae in the fabric accessible for measurement in one section only, three mutually perpendicular sections were cut from all specimens described within this study and used for investigation of preferred orientation. 200 grains were measured in each section. Unless the figures have been presented in the horizontal plane showing peripheral geographical co-ordinates, the plane of projection of each diagram coincides with the plane of that section yielding the highest proportion of twinned grains. Plotted points representing measurements made in the other two sections have been rotated to the plane of the former.

Within this particular specimen only two sections revealed a significant proportion of twinned grains. Figure 1 shows the distribution of 400 twinned and untwinned grains measured in these two sections. The restricted range of orientation of the initial [0001]-axis of those grains with optically identifiable

{0221}-twins contrasts sharply with apparently random distribution of [0001] of twinned and untwinned grains considered collectively. Hence the range of lattice orientation does not limit the range of possible orientation of {0221}-twins within the fabric.

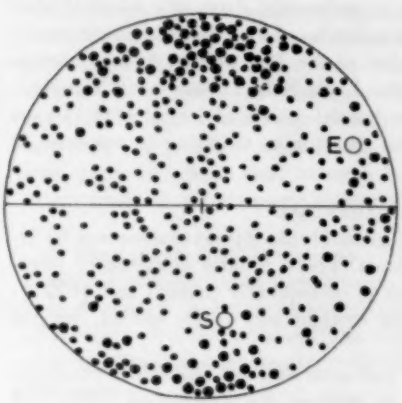

Fig. 1

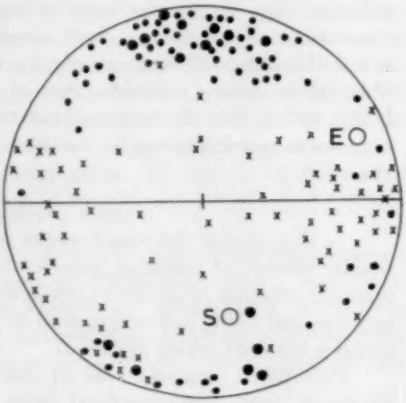

Fig. 2

Fig. 1. Loch Fasaidh limestone. Dolomite: 75 initial [0001]-axes of twinned grains (large circles), and 325 [001]-axes of untwinned grains (small circles), measured in two mutually perpendicular sections. Foliation left to right; E, S indicate compass points. All figures constructed in lower hemisphere of equal-area projection.

Fig. 2. Loch Fasaidh limestone. Dolomite: compression axes (63 from the section parallel to the plane of projection of the diagram (small circles), and 18 rotated from the other section (large circles), and tension axes (crosses) constructed for 81 twinned {0221}-lamellae measured in two mutually perpendicular sections. Foliation left to right; E, S indicate compass points.

Most grains showing twinning possess only one set of twin lamellae. The preferred orientation of {0221}-poles for twinned lamellae define two statistical *s*-planes diverging 45° either side of the foliation. During experimental deformation of dolomite (Turner, Griggs, Heard and Weiss, 1954) twin gliding along {0221}-lamellae was restricted to those grains in which [0001] was originally inclined to the axis of compression at a small angle, the normal to the intersection of {0221} with {0001} being the glide direction and the sense of shear such that upper layers of the lattice are displaced away from the initial [0001]-axis. A compression and a tension axis most favorably oriented to effect twin gliding on {0221} were constructed graphically for all twinned lamellae measured in both of the mutually perpendicular sections. Figure 2 shows the resultant distribution.

The preferred orientation of compression axes follows closely that of initial [0001]-axes of twinned grains because of twinning geometry. Compression axes constructed from the lower proportion of measured grains with {0221}-twins in the section normal to the plane of projection of the diagram confirm the maximal concentration of such axes normal to the foliation. The collective preferred orientation of tension axes is, however, slightly weaker.

Interpretation of fabric data.—Because of the slightly higher preferred

orientation of compression axes, more of the observed twinning could have been produced by a simple compressive stress operating normal to the foliation than by a simple tensile stress. The preferred orientation of initial [0001]-axes of twinned grains within a maximal concentration normal to the foliation (fig. 1), on the basis of the experimental data, is consistent with these tentative conclusions. Such compression would be directed north-north-east and south-south-west, nearly parallel to the line of the thrust outcrop. This fabric closely resembles that of the Loch Shin Limestone (Crampton, 1956) except that the textures and the partial girdle of initial [0001]-axes suggests minor intergranular rotation in addition to twinning in response to stress.

LOCH URIGILL LIMESTONE

In thin section the rock consists of granoblastic dolomite dissected by irregular strings of dolomite porphyroblasts. There is little evidence of intergranular rotation. Undulatory extinction is infrequently present and {02$\bar{2}$1}-lamellae and {10$\bar{1}$1}-cleavages tend to be straight and widely spaced. Sutural contacts between grains are usual.

Petrofabric analysis.—As in the previous and all following examples discussed (with one exception) there is random distribution of [0001] of twinned and untwinned grains considered collectively. Hence there is no restriction to possible orientation of twinned lamellae other than orientation of the stress system to which twinning may be considered a response.

Figure 3 shows the distribution within two coincident maxima nearly

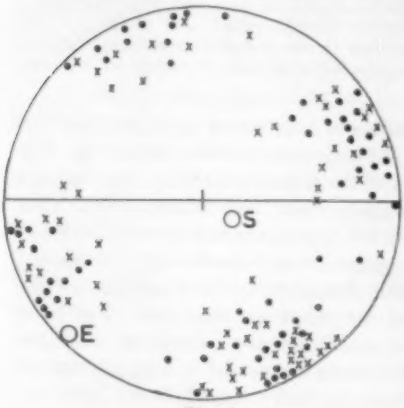

Fig. 3

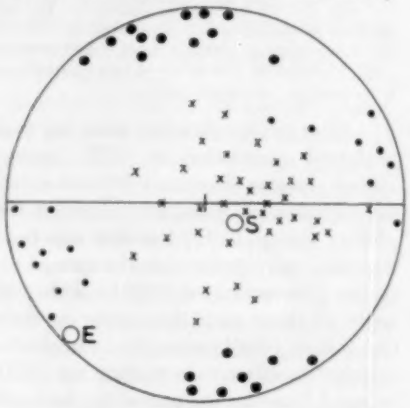

Fig. 4

Fig. 3. Loch Urigill limestone. Dolomite: compression axes (small circles), and tension axes (crosses), constructed for 68 twinned {02$\bar{2}$1}-lamellae measured in the section parallel to the plane of projection of the diagram. Foliation left to right; E, S indicate compass points.

Fig. 4. Loch Urigill limestone. Dolomite: 20 compression axes (large circles) rotated from one section, and 17 compression axes (small circles) rotated from the other section normal to the plane of projection of the diagram, and 37 tension axes (crosses), constructed for twinned {02$\bar{2}$1}-lamellae measured in these two sections. Foliation left to right; S, E indicate compass points.

parallel and normal to the foliation of compression and tension axes constructed for {0221}-lamellae of twinned grains measured in the section revealing the highest proportion of grains with {0221}-twins. Figure 4 shows the distribution of these same axes gained from the other two of the three mutually perpendicular sections cut from each specimen. A comparison of the two figures confirms the reality of the two maxima of compression axes at right angles to one another, which are coincident with the preferred orientation of initial [0001]-axes of these same grains. A similar comparison regarding tension axes reveals that these are distributed within two girdles at right angles to one another, each being normal to one of the maxima of compression axes. It follows that twinned lamellae poles will tend to be distributed along small circles arranged around each of the two maxima of initial [0001]-axes.

Interpretation of fabric data.—Because of the stronger and homogeneous preferred orientation of compression axes most observed twinning could have been produced by compressive stresses, these being of insufficient intensity to cause inter-granular rotation. The two maximal concentrations of compression axes are directed, one nearly vertically, and the other nearly horizontally east and west.

Regional data.—Analyses of the Elphin, Loch Glencoul and Loch Broom limestones reveal fabrics essentially similar to that described above. Figure 5 shows the distribution of compression and tension axes constructed for {0221}-twins measured in three mutually perpendicular sections cut from the Elphin limestone. The two marked concentrations of compression axes are quite distinct, one nearly vertical and the other nearly horizontal south-east

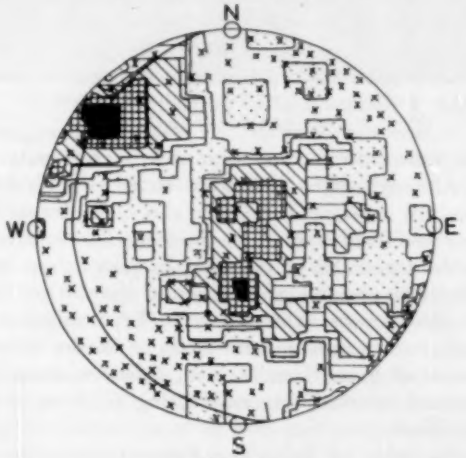

Fig. 5

Fig. 5. Elphin limestone. Dolomite: compression axes (contoured), and tension axes (crosses), constructed for 154 twinned {0221}-lamellae measured in three mutually perpendicular sections. Plane of diagram is the geographic horizon; NSEW indicate compass points; foliation shown as full arc. Contours; ½-1-2-3-5% per 1% area.

and north-west, both within a south-east and north-west girdle. The lower preferred orientation of tension axes is also apparent, these being distributed within two girdles, one nearly horizontal and the other nearly vertical, with a maximal concentration at their intersection.

The maximal concentration of compression axes nearly normal to the foliation is common to all these limestone fabrics, but the other concentration and also the orientation of the girdle of such axes vary approximately parallel or normal to the general trend of the thrust outcrop. Analysis of the Loch Broom limestone near the Moine Thrust plane reveals the two maximal concentrations of compression axes within a partial girdle disposed north-north-east and south-south-west, contrary to that of the Elphin limestone near the sole. The fabric of the Loch Broom limestone shows an exceptional weak preferred orientation of [0001] of twinned and untwinned grains considered collectively normal to the foliation, and coincident with one of the maxima within the much higher preferred orientation of initial [0001]-axes of twinned grains. Experimental deformation of dolomite (Turner, Griggs, Heard and Weiss, 1954) did not produce fabric changes of sufficient magnitude to allow definite conclusions, but a slight migration of [0001] towards the axis of compression was reported.

LEDBEG LIMESTONE

Dolomite is present in two forms. The granoblastic dolomite is segregated into alternating layers of varying grain size thus giving rise to the foliation. These layers usually maintain a constant orientation except in the region of porphyroblasts where they are strongly flexed. The dolomite porphyroblasts display strongly developed undulatory extinction, and are frequently fractured and granulated around their margins. They contain irregularly shaped $\{02\bar{2}1\}$-lamellae and $\{10\bar{1}1\}$-cleavages which are often flexed, the region of flexing being characterised by a greater development of twinned lamellae. There is sometimes a marked loss of parallelism of $\{02\bar{2}1\}$-lamellae within each set. These textures are illustrated by plate 1, and suggest that the porphyroblasts have undergone severe inter- and intra-granular rotation since their formation. Although slight elongation of the porphyroblasts helps produce the lineation, this is mainly defined by elongated brucite lenticles.

The calcite veins lying normal to the lineation tend to possess sharp boundaries with the remainder of the rock. In places these veins are flexed, this being accompanied by some granulation of the calcite. Undulose extinction is present in some grains. While many $\{01\bar{1}2\}$-lamellae are fine, straight and widely spaced, some grains possess zones of flexure in which there is a profuse development of broad lamellae with diffuse margins. These textures suggest limited crystal rotation, this never being as severe as that within the dolomite porphyroblasts.

Analysis of the fabric of dolomite.—Figure 6 shows the distribution of 600 [0001]-axes of twinned and untwinned grains measured in three mutually perpendicular sections, the plane of projection of the diagram lying normal to the lineation and parallel to the calcite veins. If only the initial [0001]-axis of all measured grains with $\{02\bar{2}1\}$-twins is selected there is an obvious pre-

PLATE 1

Ledbeg limestone; isolated and fractured porphyroblast showing flexed and disturbed twinned {0221}-lamellae and {1011}-cleavages. Polaroids crossed; ×40.

ferred orientation within a girdle normal to the lineation. The full range of lattice orientation does not restrict the range of possible orientation of {0221}-twins within the fabric.

Despite the irregular outline and sometimes diffuse boundary between lamellae, in the majority of porphyroblasts the initial lattice could be distinguished from the twinned lattice. Figure 7 shows the distribution of compression and tension axes constructed from twinned lamellae of grains measured in the section normal to the lineation. Both axes apparently lie within a girdle normal to the lineation. The girdle of compression axes must follow from the distribution of initial [0001]-axes of twinned grains shown in figure 6, but the preferred orientation of tension axes needs further investigation.

Compression and tension axes determined for twinned lamellae of grains measured within the remaining two sections, one parallel to the foliation and the other normal to the foliation and veins, have been rotated to the plane of projection of figure 7. If the distribution of tension axes within figures 7 and 8 are considered collectively it can be seen that such axes possess random

orientation. Any apparently preferred orientation results from consideration of measurements made within one section only. Compression axes shown in figures 7 and 8 fall within coincident girdles. It follows geometrically that twinned lamellae poles are distributed within a weak girdle normal to the lineation.

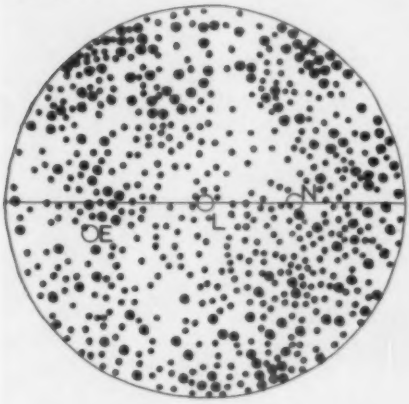

Fig. 6

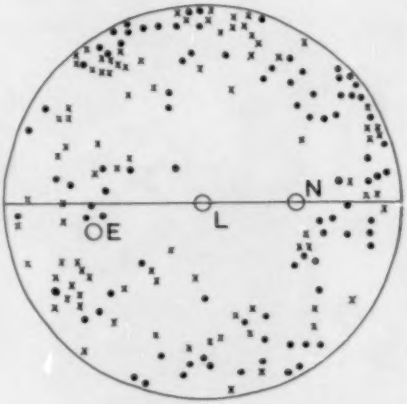

Fig. 7

Fig. 6. Ledbeg limestone. Dolomite: 150 initial [0001]-axes of twinned grains (large circles), and 450 [0001]-axes of untwinned grains (small circles), measured in three mutually perpendicular sections. Foliation left to right; lineation (L); E, N indicate compass points.

Fig. 7. Ledbeg limestone. Dolomite: compression axes (small circles), and tension axes (crosses), constructed for 93 twinned $\{02\bar{2}1\}$-lamellae, measured in the section parallel to the plane of projection of the diagram. Foliation left to right; lineation (L); E, N indicate compass points.

Interpretation of fabric data.—Within figure 12 all measured axes from the three mutually perpendicular sections have been rotated to their geographical orientation. The contoured distribution of compression axes within a vertical girdle disposed south-east and north-west, parallel to the calcite veins and normal to the foliation and lineation, contrasts with random orientation of tension axes. Within the Elphin limestone textures suggesting crystal rotation are weakly developed as is the girdle of compression axes shown in figure 5. In the Ledbeg limestone the textures of dolomite suggest that intense crystal rotation has occurred subsequent to crystallisation and much of the twinning. Although the two maximal concentrations of compression axes in figure 12 retain a similar orientation compared with figure 5, the well developed girdle is now the prominent feature of the preferred orientation.

Interpretation of fabric of calcite.—Only two sections revealed a significant proportion of twinned grains within the total 200 grains measured in each section. Figure 9 shows the distribution of compression and tension axes constructed from $\{01\bar{1}2\}$-lamellae of these twinned grains. Within the girdle of compression axes normal to the lineation there is a weighted maximum near the foliation. The girdle of tension axes is less well developed.

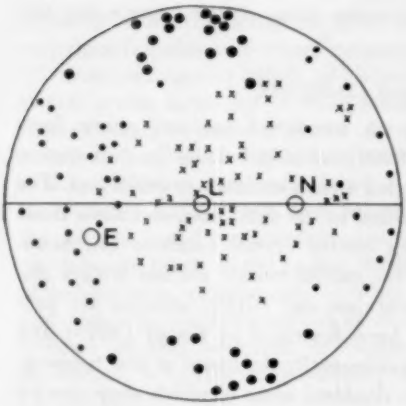

Fig. 8

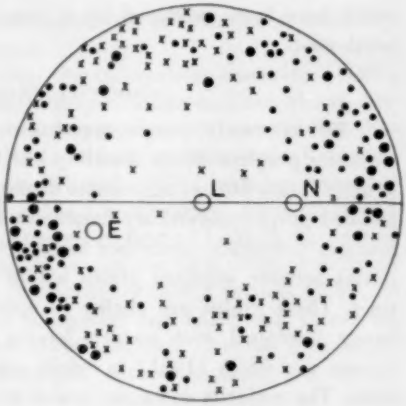

Fig. 9

Fig. 8. Ledbeg limestone. Dolomite: 40 compression axes (small circles) rotated from one section, and 29 compression axes (large circles) rotated from the other section normal to the plane of projection of the diagram, and 69 tension axes (crosses), constructed for twinned $\{0\bar{2}21\}$-lamellae measured in these two sections. Foliation left to right; lineation (L); E, N indicate compass points.

Fig. 9. Ledbeg limestone. Calcite: compression axes (small circles), and tension axes (crosses), constructed for 120 twinned $\{01\bar{1}2\}$-lamellae measured in two of the three mutually perpendicular sections. 30 acute glide line bisectors (large circles) constructed for twinned lamellae of doublets superposed. Foliation left to right; lineation (L); E, N indicate compass points.

Of 90 twinned grains, 30 are doublets. This proportion of doublets need not imply that tension was a significant stress during deformation since limited crystal rotation suggested by the textures would probably bring more than one $\{01\bar{1}2\}$-lamella in a grain into a position conducive to twinning. The orientation of acute bisectors of glide lines constructed from the $\{01\bar{1}2\}$-lamellae of these doublets is superposed upon figure 9. When the development of twinning has been caused by a compressive stress, this should be approximately parallel to the acute bisector of the two sets of lamellae in those grains that show double twinning (Turner, 1953). Most of the acute glide line bisectors shown in figure 9 are located within the broad maximum of compression axes.

Comparison of dolomite and calcite fabrics.—Symmetrologically the fabrics of dolomite and calcite are similar. The parallel veins containing calcite cut the dolomite porphyroblasts, and because they bear a suitable relationship with the lineation and preferred orientation of compression axes, are interpreted as *ac* joints which formed after the plastic deformation of dolomite had ceased. Two deformation phases must therefore be postulated. Since dolomite is considerably stronger than calcite and the textures suggesting crystal rotation show weaker development within calcite, the earlier deformation phase characterised by plastic deformation of dolomite was far more severe than the late minor deformation phase during which calcite experienced plastic deformation, after the formation of *ac* joints. Twinning within calcite

could have been produced by a compressive stress directed south-east and north-west.

CNOC CHAORNAIDH LIMESTONE

An extremely rough appearance on weathered surfaces arises from dolomite porphyroblasts standing out from enclosing calcite. In thin section brucite forms fibrous aggregates displaying strong undulatory extinction. The isolated porphyroblasts are flattened normal to the optic axis, and show those textures previously described suggesting limited crystal rotation. The boundaries between adjacent grains within the calcite mosaic are not always distinct. These grains are chalky in appearance and {01$\bar{1}$2}-lamellae are profusely developed, such textures having been described by Knopf (1949) and Turner and Ch'ih (1951) in calcite experimentally deformed at low temperatures. The majority of calcite grains are doublets, some of which show one set

PLATE 2

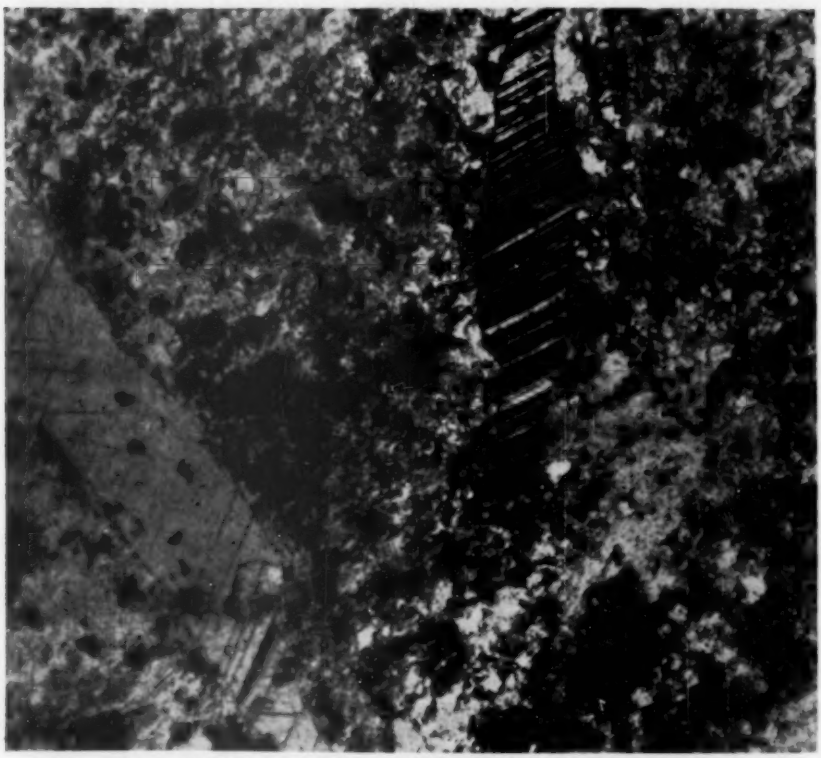

Cnoc Chaornaidh limestone; isolated and flattened porphyroblasts showing twinned {0221}-lamellae, enveloped by calcite and brucite. Polaroids crossed; ×40.

profusely developed while the other set consists of widely spaced, relatively very thick lamellae with crenulate margins.

Interpretation of fabric of dolomite.—As in previous examples, [0001] of 600 grains measured in three mutually perpendicular sections shows random orientation, while selection of twinned grains reveals a coincident preferred orientation of the initial [0001]-axis and compression axis. Compression and tension axes constructed from twinned $\{02\bar{2}1\}$-lamellae measured in all three sections have been rotated to their geographical orientation and the distribution of compression axes contoured in figure 11. As in the case of the dolomite fabric of the Ledbeg limestone, in contrast to random orientation of tension axes, compression axes are distributed within a vertical girdle, in this case with the contrary orientation south-west and north-east. Closer inspection of this preferred orientation reveals crossed girdles with slight divergence, a feature only partially developed within the Ledbeg limestone (figure 12).

At the intersection of the two girdles, the vertical maximal concentration of compression axes normal to the foliation, characteristic of most dolomite fabrics, is still retained. The horizontally disposed maximal concentration within the girdle is, however, replaced by two sub-maxima, one in each of the crossed girdles.

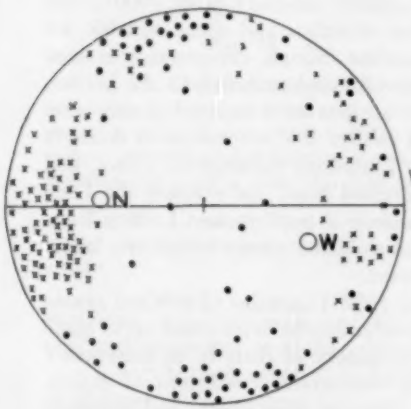

Fig. 10

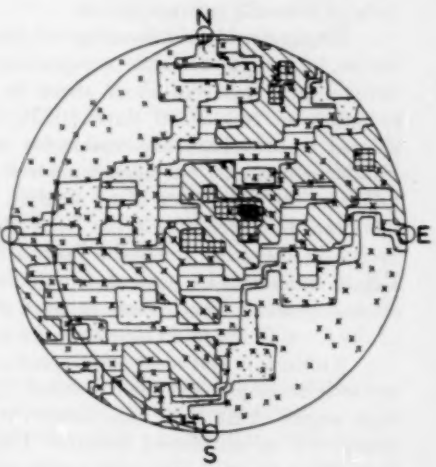

Fig. 11

Fig. 10. Cnoc Chaornaidh limestone. Calcite: 66 acute glide line bisectors (small circles), and 132 tension axes (crosses), constructed for twinned $\{01\bar{1}2\}$-lamellae of 66 doublets within a total 100 measured twinned grains located within the section parallel to the plane of projection of the diagram. Foliation left to right; N, W indicate compass points.

Fig. 11. Cnoc Chaornaidh limestone. Dolomite: compression axes (contoured), and tension axes (crosses), constructed for 223 twinned $\{02\bar{2}1\}$-lamellae measured within three mutually perpendicular sections. Plane of diagram is the geographic horizon; NSEW indicate compass points; foliation shown as full arc. Contours; ½-1-2-4-5% per 1% area.

Textures suggesting crystal rotation are more strongly developed within dolomite of the Ledbeg limestone. Presumably rotation of the dolomite porphyroblasts would be more easily accomplished in the softer calcite of the Cnoc Chaordaidh limestone than within the granular dolomite of the Ledbeg limestone.

Interpretation of the fabric of calcite.—Two sections revealed very few twinned grains. Within the section parallel to the plane of projection of the diagram all grains have twinned. Thus calcite had recrystallized with a preferred orientation of [0001]-axes severely restricting the range of possible orientation of $\{01\bar{1}2\}$-twins within the fabric. The distribution of acute glide line bisectors and tension axes constructed from twinned $\{01\bar{1}2\}$-lamellae of 66 doublets of a total 100 measured grains is shown in figure 10. The high proportion of doublets implies that a tensile stress could have given rise to most of the observed twinning, further confirmation of this being given by the lower preferred orientation of acute glide line bisectors.

Because dolomite porphyroblasts have experienced some crystal rotation whereas calcite which is more easily deformed has not, the dolomite fabric reflects an earlier and more severe deformation phase. The weighted maximum of tension axes of calcite twinned grains coincides with the unoccupied area separating the acute angle between the crossed girdles of compression axes of dolomite twinned grains.

Singlet-doublet relationships of dolomite.—The geometry of the dolomite lattice is such that simple compression applied sub-parallel to [0001] can develop high resolved shear stress in the direction and sense suitable for twinning on two or all three $\{02\bar{2}1\}$-lamellae. Simple compression is considered to have been responsible for most observed twinning in the Lochan Fasaidh limestone, but only 8 percent of all measured twinned grains were doublets, the remainder being singlets. A similar low proportion of doublets has been described within the Loch Shin Limestone (Crampton, 1956), and occurs in the other limestone fabrics discussed here; for example the Loch Urigill limestone 10 percent, Elphin limestone 7 percent, and Ledbeg limestone 8 percent. The highest proportion of doublets occurs within the fabric of the Cnoc Chaornaidh limestone, 24 percent.

Within this and most other specimens $\{02\bar{2}1\}$-lamellae of twinned grains are well developed and their twinned character can be determined up to quite high angles of tilt thus minimizing the possibility of their being mistakenly interpreted as untwinned lamellae. Under comparable conditions of experimental deformation dolomite was much stronger than calcite and twinning far less easily induced (Turner, Griggs, Heard and Weiss, 1954). The absence of extensive doublet formation in dolomite might thus be a reflection of this greater resistance to plastic deformation by twin gliding, and the wider separation of $\{02\bar{2}1\}$-lamellae within the dolomite lattice.

SUMMARY AND CONCLUSIONS

The calcite fabrics of the Ledbeg and Cnoc Chaornaidh limestones are symmetrically similar to the dolomite fabrics within those specimens but belong to a late minor deformation phase. It is of interest that the textures of the

Cnoc Chaordaidh limestone suggest cool conditions during deformation by comparison with experimental work, and those of the Ledbeg limestone late introduction or segregation into veins and subsequent twinning.

If compression axes of all dolomite fabrics analyzed within this regional study are rotated to their geographical orientation and combined in figure 13, it is apparent that such axes tend to lie in two vertical girdles, one directed

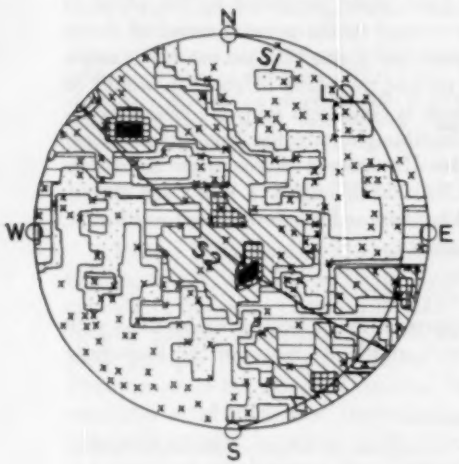

Fig. 12

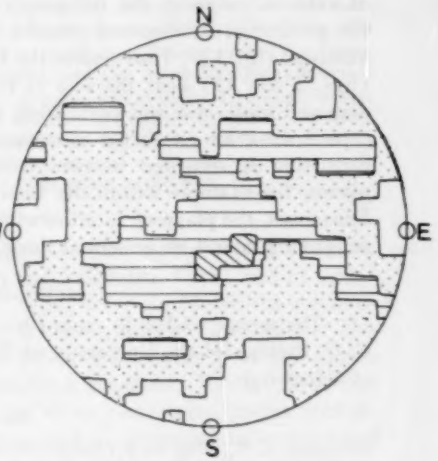

Fig. 13

Fig. 12. Ledbeg limestone. Dolomite: compression axes (contoured), and tension axes (crosses), constructed for 162 twinned {0221}-lamellae measured in three mutually perpendicular sections. Plane of diagram is the geographic horizon; NSEW indicate compass points; foliation shown as full arc. Contours; ½-1-2-4-5% per 1% area. Foliation (*S1*), calcite veins (*S2*), and lineation (*L*) superposed.

Fig. 13. Composite diagram. Dolomite: 1037 compression axes. Plane of diagram is the geographic horizon; NSEW indicate compass points. Contours; 1-2-3% per 1% area.

south-east and north-west and the other south-west and north-east, with a maximal concentration at the point of intersection of the two girdles.

A maximal concentration of compression axes (and initial [0001]-axes) of twinned grains oblique but more usually nearly normal to the foliation is present in all the dolomite fabrics. In all cases but one the foliation plane is gently inclined to the horizontal and hence this concentration is disposed nearly vertically. The exception, the fabric of the Lochan Fasaidh limestone, shows a single maximum normal to the foliation (fig. 2). The remaining fabrics show a transition from partial girdles characterised by two mutually perpendicular and pronounced maxima to complete girdles in which the two maxima, although present, are less dominant (figs. 3, 5 and 12). Figures 11 and 12 show the tendency towards the development of crossed girdles, with the maximal concentration at the girdle intersection and the unoccupied area

indicating the acute bisectrix of the two girdles near the horizontal plane. Figure 11, representing the end of this transition series, shows the reduction of one of the two usually typical maxima.

Attempting a tentative kinematic interpretation of fabric symmetry, if the axis of symmetry of the girdles of compression axes or initial [0001]-axes (the lineation in the fabric of the Ledbeg limestone) is equivalent to the axis of external rotation, the deformation (*ac*) plane suggested by the plane of the girdle can be disposed parallel or normal to the general trend of thrust outcrops (fig. 13). Thus within the Elphin and Legbed limestones for example (figs. 5 and 12) near the sole of the thrusts the plane of rotation would be disposed south-east and north-west, which is consistent with the generally accepted direction of thrust movements, although only the final stage of deformation is recorded in twin lamellae. In certain places near the thrust planes, for example within the Cnoc Chaordaidh (fig. 11) and Loch Broom limestones, the plane of rotation would be disposed south-west and north-east, suggesting lateral movement at these points.

ACKNOWLEDGMENTS

The writer wishes to record his appreciation of helpful discussions with F. C. Phillips of the University of Bristol, and L. E. Weiss of the University of Edinburgh.

REFERENCES

Crampton, C. B., 1956, Loch Shin limestone—comparison of dolomite and calcite fabrics: Edinburgh Geol. Soc. Trans., v. 16, p. 334-337.

Gilmour, P., and Carman, M. F., 1954, Petrofabric analysis of the Loch Tay limestone: Geol. Mag., v. 91, p. 49-60.

Grigg, D. T., Turner, F. J., Borg, I., and Sosoka, J., 1953, Deformation of Yule marble, Part 5—Effects at 300°C: Geol. Soc. America Bull., v. 64, p. 1329-1342.

Handin, J., and Fairbairn, H. W., 1953, Experimental deformation of Hasmark dolomite: Geol. Soc. America Bull., v. 64, p. 1429-1430.

Knopf, E. B., 1949, Fabric changes in Yule marble after deformation in compression, Part 1: Am. Jour. Sci., v. 247, p. 433-461.

Turner, F. J., 1953, Nature and dynamic interpretation of deformation lamellae in calcite of three marbles: Am. Jour. Sci., v. 251, p. 276-298.

Turner, F. J., and Ch'ih, C. S., 1951, Deformation of Yule marble, Part 3—Effects at room temperature: Geol. Soc. America Bull., v. 62, p. 887-906.

Turner, F. J., Griggs, D. T., Heard, H., and Weiss, L. E., 1954, Plastic deformation of dolomite at 380°C: Am. Jour. Sci., v. 252, p. 477-488.

University of Bristol
England*

* Now at 30, Mount Preston
Leeds, 2
England

[American Journal of Science, Vol. 256, March 1958, P. 159-170]

DYNAMIC INTERPRETATION OF THE FABRIC OF A DOLOMITE FROM THE MOINE THRUST-ZONE IN NORTH-WEST SCOTLAND

JOHN M. CHRISTIE

ABSTRACT. Petrofabric studies on naturally and experimentally deformed dolomite indicate that the main mechanisms of plastic deformation of dolomite, under most conditions, are twin-gliding on {0221} and translation-gliding on {0001}. The fabric of a dolomite with mylonitic textures is analysed and interpreted in dynamic terms. The grains in the rock contain numerous {0221} twin lamellae and also internally rotated lamellae of the type observed in experimentally deformed dolomite and designated L_e. Compression and tension axes inferred from twinned {0221} lamellae are statistically parallel to those inferred from L_e lamellae. The strain calculated from the amount of rotation of L_e lamellae varies from 5 to 18 percent for individual grains; it is concluded that these figures are probably less than the total post-crystalline strain in the rock.

INTRODUCTION

Recent fabric studies of experimentally deformed dolomite rock (Turner, Griggs, Heard, and Weiss, 1954; Handin and Fairbairn, 1955) and of single crystals of dolomite (Higgs and Handin, 1954) have elucidated the mechanisms of plastic deformation of dolomite at temperatures below 400°C. The present paper describes the fabric of a dolomite tectonite from the Moine Thrust-zone in the Assynt district of Sutherland, Scotland.[1] The fabric of this specimen is of particular interest as some of its constituent grains contain internally rotated lamellae of the type recorded in experimentally deformed dolomite but not hitherto described in naturally deformed rocks. A dynamic interpretation of the {0221} twin lamellae and rotated lamellae is made in the light of the experimentally established data, and the mechanism of deformation of the rock is tentatively discussed.

INTRAGRANULAR DEFORMATION OF DOLOMITE

Inferred from Natural Fabrics.—The first detailed study of dolomite orientation in deformed rocks was made by Fairbairn and Hawkes (1941). Analyses of the orientation of the lattice and twin lamellae in a number of specimens from Montana, Vermont and Ontario were recorded and a possible mechanism of deformation was inferred from the data. The authors found that {0221} twin lamellae were extensively developed in all the specimens, and the orientation of the lamellae in the fabric of the rocks led them to conclude that the sense of gliding in twinning on {0221} was opposite to that for twinning on {01$\bar{1}$2} in associated calcite. They considered that translation-gliding on {0001}, which had been produced experimentally by Johnsen (1902), might also be of some importance as an orienting mechanism, though this would be difficult to prove in view of the difficulty of identifying the process by optical means.

In a comprehensive study of Alpine dolomite-tectonites, Ladurner (1953)

[1] The specimen (M14) was collected from a body of crystalline dolomite underlying the Moine Thrust at Benmore Lodge near Loch Ailsh. It is one of five similar specimens analyzed as part of a detailed structural study of the area. The fabrics of the remaining four specimens are described elsewhere (Christie, 1956) and related to the visible megascopic structures in the rocks of the thrust-zone.

recorded the orientation of [0001]-axes in more than 40 specimens from various parts of the Alps. On the basis of the preferred orientation of [0001]-axes he classified the rocks into *S*-tectonites and three types of *B*-tectonite, according to the number of *s*-planes and symmetry planes which he recognized in the fabrics. The similarity between synoptic diagrams showing maxima of [0001]-axes in dolomite-tectonites and analogous diagrams for calcite-tectonites led Ladurner (1953, p. 290, 296) to assume that the same mechanism was responsible for producing the preferred orientation in dolomites as was postulated by Felkel (1929) for calcite: namely, gliding on $\{01\bar{1}2\}$, combined with rotation of the $\{01\bar{1}2\}$ planes about the *B*-axis of the fabric. This conclusion is invalidated by the experimental work of Turner, Griggs and Heard (1954), who have shown that translation-gliding in calcite occurs, not on $\{01\bar{1}2\}$, as thought by Felkel, but on $\{10\bar{1}1\}$, and at room temperatures on $\{02\bar{2}1\}$. Moreover, experimental work on dolomite up to the present time (see below) gives no indication that gliding on $\{01\bar{1}2\}$ occurs in dolomite, nor is such a mechanism compatible with the geometry of the dolomite lattice.

Determined by Experimental Deformation of Dolomite.—Early attempts to produce twinning experimentally in dolomite were unsuccessful but Johnsen (1902) recorded translation-gliding in deformed crystals with {0001} as the glide plane and one of the *a* crystal axes as the glide line. More recently two glide mechanisms were demonstrated for dolomite (Dover Plains dolomite rock) compressed 9.4 percent at 380°C and 3,000 atmospheres confining pressure (Turner, Griggs, Heard and Weiss, 1954):

1. "twin-gliding on $\{02\bar{2}1\}$, the sense of shear being such that the upper layers of the crystal lattice are displaced downwards from the upper end of the *c*-axis," that is, with a *negative* sense of shear (Turner, Griggs and Heard, 1954, p. 897);
2. "translation-gliding on {0001}, with the *a*-axes as probable glide directions."

Deformation of single crystals of dolomite at room temperature and at 300°C (Higgs and Handin, 1954) confirms the above conclusions: the crystals deformed at 300°C by translation-gliding on {0001} and by twin-gliding on $\{02\bar{2}1\}$ with a negative sense of shear; the latter mechanism was not identified in crystals deformed at room temperature. Twin-gliding on $\{02\bar{2}1\}$ was also found by Handin and Fairbairn (1955) in their experiments on Hasmark dolomite rock. Bradley, Burst and Graf (1953) have shown, moreover, that these two glide mechanisms would account for the progressive changes observed in the lattice of dolomite after prolonged grinding.

DYNAMIC INTERPRETATION OF LAMELLAE IN NATURALLY DEFORMED DOLOMITE ROCK

Inferences of two independent kinds, concerning the dynamics of deformation, may be drawn from $\{02\bar{2}1\}$ lamellae in naturally deformed dolomite rocks:

The first is analogous to the dynamic interpretation of twin lamellae in calcite marbles, described by Turner (1953). Figure 1a shows the orientation of $\{02\bar{2}1\}$ twin lamellae in relation to the [0001]-axis in dolomite twinned on

{02$\bar{2}$1}. The angle between [0001] and the pole of the lamellae, {02$\bar{2}$1}, is 62½°. The applied stresses which would be most effective in causing twin-gliding on {02$\bar{2}$1} with a negative sense are also shown in figure 1a: a compression applied in a direction designated C, or a tension in a direction T. For either, the coefficient of resolved shear stress on {02$\bar{2}$1} would have the maximum possible value, 0.5.

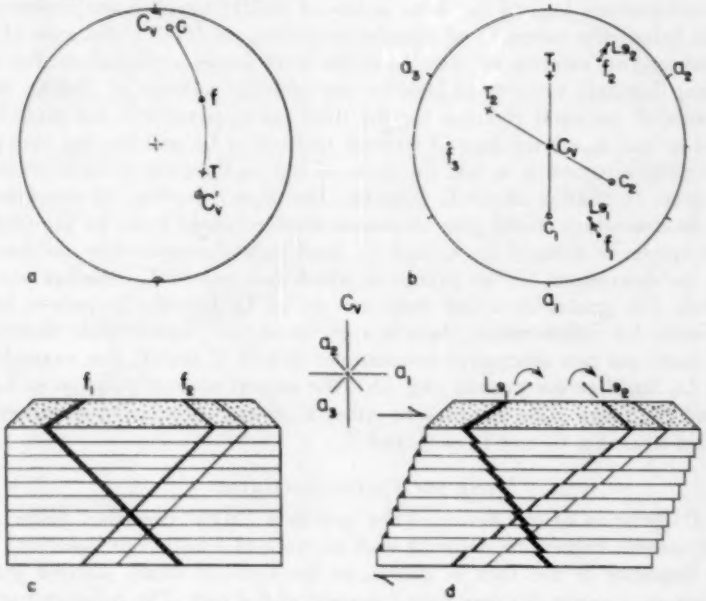

Fig. 1. a. Projection showing the orientation of [0001] in the host lattice (C_v) and in the twinned lattice (C_v') in dolomite. C and T are respectively the axes of compression and tension which give maximum resolved shear stress on {02$\bar{2}$1} = f, for gliding with a negative sense.

b. Projection showing the orientation of {02$\bar{2}$1} and L9 lamellae in the dolomite lattice. For fuller explanation, see text.

c, d. Diagrams illustrating the internal rotation of {02$\bar{2}$1} lamellae, f_1 and f_2, to L_{9_1} and L_{9_2} by translation-gliding on (0001) parallel to a_1. C_v, a_1, a_2, a_3 are the crystal axes.

The second kind of inference is drawn from internally rotated {02$\bar{2}$1} lamellae of the type designated L_9 by Turner, Griggs, Heard and Weiss (1954). Following Turner, et al., it is assumed that these have been rotated by translation on {0001} parallel to one of the *a* crystallographic axes. In the experimentally deformed Dover Plains rock only one set of L_9 lamellae were found in any grain; but in the specimen here described two sets of L_9 lamellae are present in several grains, allowing unique identification of the active glide direction. The orientation of these two sets of lamellae in the dolomite lattice is shown in figure 1b. Figures 1c and d illustrate diagrammatically the phenomenon of translation-gliding on {0001} in dolomite. The lattice orienta-

tion (C_v, a_1, a_2, a_3) is unchanged by gliding. Pre-existing {02$\bar{2}$1} lamellae, f_1 and f_2, are internally rotated about axes which are the intersections of the lamellae {02$\bar{2}$1} with the glide plane {0001}, that is, the *a* crystal axes. The sense of internal rotation about the axes of internal rotation is the same as the sense of shear on the glide plane. Following gliding parallel to a_1 the lamellae f_1 and f_2 are rotated about a_3 and a_2 respectively and so assume the new orientations L_{e_1} and L_{e_2}. If three sets of {02$\bar{2}$1} lamellae are present in a grain before the inception of translation-gliding on {0001}, the axes of potential internal rotation are parallel to the three *a*-axes of the lattice. But it is evident that only two sets of lamellae can undergo rotation by gliding, since the axis of potential rotation for the third set is parallel to the glide line. Since a_2 and a_3 are the axes of internal rotation of L_{e_1} and L_{e_2}, the only possible glide direction is a_1 and the sense of slip on the glide plane is given by the sense of rotation of the L_e lamellae. Optimum directions of compression and tension which would give maximum resolved shear stress on the {0001} glide system so deduced are C_1 and T_1. Such axes of compression and tension may be determined for all grains in which two sets of L_e lamellae are recorded. For grains in which only one set of L_e lamellae is present or is accessible for measurement, there is a choice of two possible glide directions and there are two alternative orientations of both C and T. For example, if only L_{e_1} lamellae are present (fig. 1b), the axis of internal rotation of L_{e_1} is a_2 and the active glide line may be either a_1 or a_3; the inferred directions of applied stress are C_1 and T_1 or C_2 and T_2.

THE LOCH AILSH DOLOMITE

Description of the Fabric.—The specimen (M14) described below is a pure, massive crystalline dolomite with no trace of foliation or lineation. The only impurity in the rock is quartz, in the form of small, isolated grains making up considerably less than 1 percent of the rock. The dolomite grains, which are more or less uniform in size (average mean grain diameter = 0.54 mms.), show a high degree of post-crystalline strain: all contain well-developed {02$\bar{2}$1} twin lamellae, and a few show undulose extinction. There is considerable granulation along grain boundaries, the minute interstitial granules comprising approximately 27 percent of the rock (measured by means of a point counter in 3 mutually perpendicular sections). There is a weak dimensional orientation of the main grains: the majority of the grain sections in all three sections are equidimensional, but a limited number in each section are slightly elongate parallel to a common direction in the fabric.

To overcome limitations due to orientation of any single section relative to the fabric, the analysis was carried out on three mutually perpendicular sections cut from the specimen. Lamellae which are inclined at low angles (less than 35°) to a section are not accessible for measurement with the universal stage, so that there is a corresponding central "blind spot" in every fabric diagram. Since the three {02$\bar{2}$1} planes in dolomite are inclined to each other at approximately 80°, one set of lamellae is inaccessible in most grains. It should be noted that L_e lamellae can be recorded satisfactorily only if the intersection [L_e: 02$\bar{2}$1] can be rotated into parallelism with the micro-

scope axis. Consequently, in any section, L_0 lamellae can be measured only in grains with a limited range of orientation. The range of orientation of grains in which two sets of L_0 lamellae can be measured is obviously further restricted. Thus, in order to obtain a reliable statistical estimate of the orientation of L_0 lamellae in a rock it is necessary to examine at least three sections with different orientation.

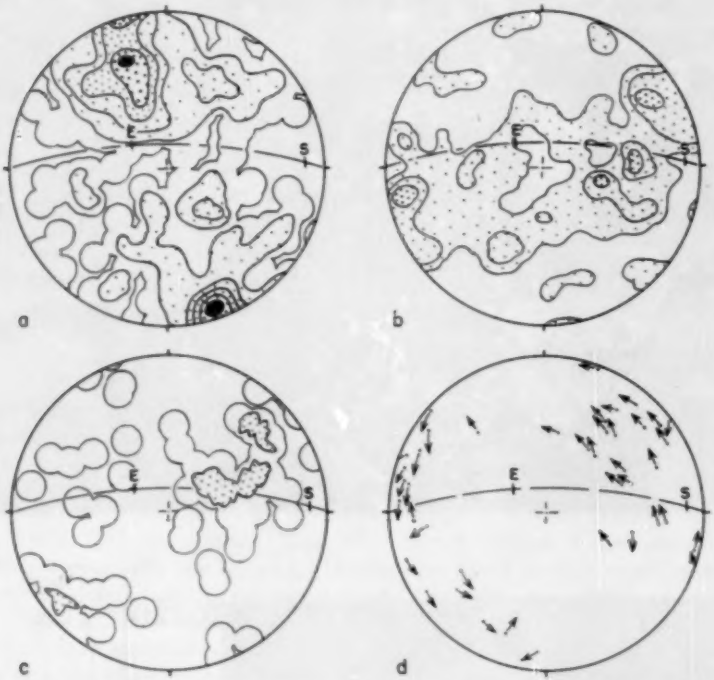

Fig. 2. Orientation data for the Loch Ailsh dolomite. All data are plotted on a lower hemisphere, equal area projection. Geographic orientation is given by the horizontal plane and east (E) and south (S) directions.

a. 310 [0001]-axes of dolomite. Contours: 1/3, 1, 2, 3, 4, 5% per 1% area.

b. 300 *a* crystallographic axes in 100 unselected grains. Contours: 1, 2, 3% per 1% area.

c. Poles of 60 twinned {0221} lamellae. Contours: 1½, 5% per 1% area.

d. Poles of {0221} lamellae (points) and associated L_0 lamellae (arrowheads) in 35 grains.

Figure 2a shows the preferred orientation of 300 [0001]-axes, 100 measured in each of three mutually perpendicular sections. A strong similarity in the three component partial diagrams (each containing 100 axes) indicates a high degree of homogeneity within the field of the specimen. There is a single area of concentration, containing two maxima of equal intensity approximately 30° apart, and there is some suggestion of a girdle, the axis of

which is nearly horizontal in figure 2a. The orientation of the *a* crystallographic axes (figure 2b) is restricted by the strong preferred orientation of the [0001]-axes: they are disposed in a broad zone normal to the maximum

PLATE 1

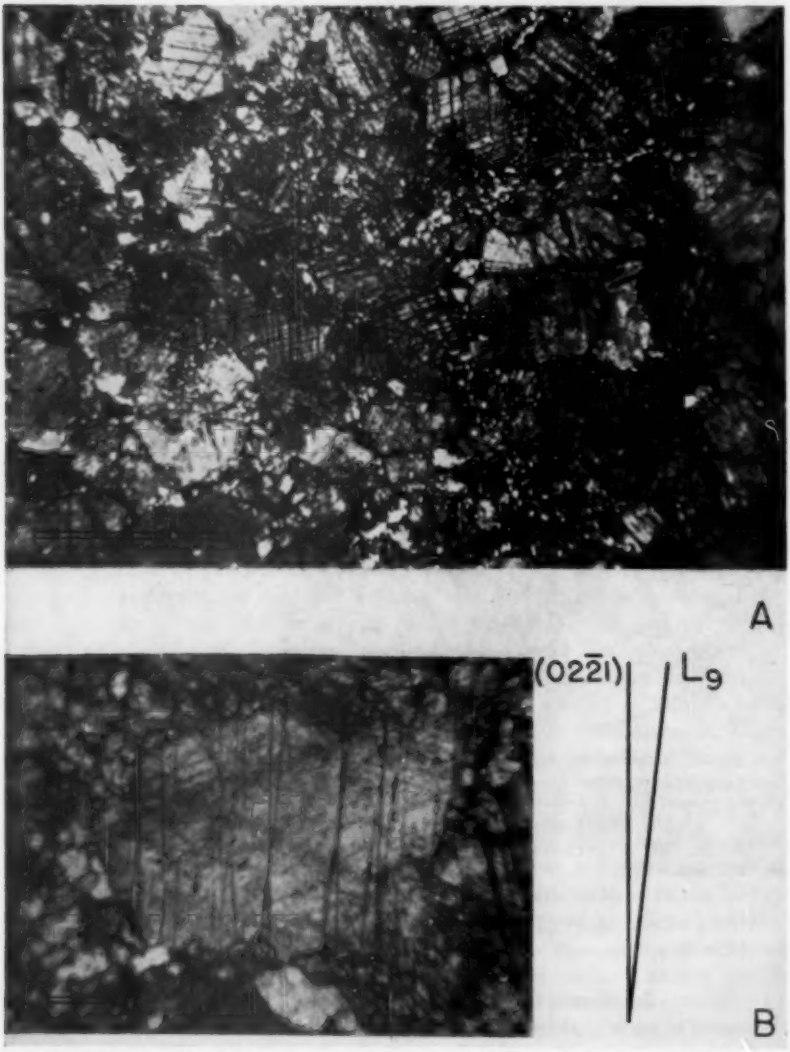

A. Photomicrograph showing the texture of the Loch Ailsh dolomite. Scale line represents 1mm.

B. Single grain showing L_9 lamellae intersected by later $\{02\bar{2}1\}$ lamellae. The intersection of the two sets of lamellae is vertical. Scale line represents .1mm.

of [0001]-axes, and there is a concentration near the periphery of the diagram (i.e. parallel to the girdle axis of the [0001] diagram).

As shown in plate 1A {02$\bar{2}$1} lamellae are strongly developed in all the grains. An analysis of the lamellae is given in tables 1 and 2. The majority of the grains contain three sets of {02$\bar{2}$1} lamellae; but it is remarkable that there is optically recognizable twinning in only 20 percent of the grains, and in these it is generally present on only one set of lamellae. The orientation of recognizably twinned lamellae (60 lamellae in 58 grains) is shown in figure 2c. The poles of the lamellae define a single maximum.

TABLE 1*

Percentage of Grains Showing Twinned and Non-twinned {02$\bar{2}$1} Lamellae

Number of sets of lamellae per grain	Percentage of grains
3 sets	71%
2 sets	25%
1 set	4%
No sets	0%

Rotated L_9 lamellae were recorded in 35 of the grains examined. These lamellae (plate 1B) differ from {02$\bar{2}$1} lamellae in being less sharply defined; they have a discontinuous, granular appearance and their orientation is consequently more difficult to measure accurately than that of twin lamellae and cleavages. The L_9 lamellae may frequently be recognized by this characteristic appearance; but as this is not invariably so, and to avoid errors of identification, they were recorded only where associated with later lamellae having rational {02$\bar{2}$1} orientation (plate 1B). Turner, Griggs, Heard and Weiss (1954) record only one set of L9 lamellae per grain in their experimentally deformed dolomite rock, but two sets of L_9 lamellae are present in four of the grains analyzed in the Loch Ailsh rock. Figure 2d shows the orientation of the L_9 and associated {02$\bar{2}$1} lamellae in the specimen; all but two of these sets of L_9 lamellae were measured in the section with the same orientation as the diagram. The angle between L_9 and {02$\bar{2}$1} varies between 5° and 12°,

TABLE 2*

Percentage of Grains Showing Twinned {02$\bar{2}$1} Lamellae

Number of sets of lamellae per grain	Percentage of grains
3 sets	0%
2 sets	1%
1 set	19%
No sets	80%

* The above analyses are based only on grains in which all three planes were accessible for measurement with the U-stage. Lamellae parallel to {02$\bar{2}$1} which are not recognizable as twin lamellae are described as "non-twinned" to distinguish them from lamellae in which the orientation is visibly different from that of the host grain ("twinned lamellae"), as in Borg & Turner, 1953.

with a mean value of 8½°, a figure which is comparable with that obtained in the dolomite deformed by Turner et al. The sense of rotation of {0221} to L_o is statistically constant.

Dynamic Interpretation of the Fabric.—The axes of compression and tension which would be most effective in causing the observed twinning are shown in figure 3a. It is clear that a strong compression parallel to the direction C, or a tension parallel to the direction T could account for all the observed twinning. Figure 3b shows the glide lines (a) and axes of compression (C) and tension (T) deduced for the four grains in which two sets of L_o lamellae were recorded. For the 31 grains with one set of visible L_o lamellae the 62 *possible* glide lines are shown contoured in figure 3c (unshaded

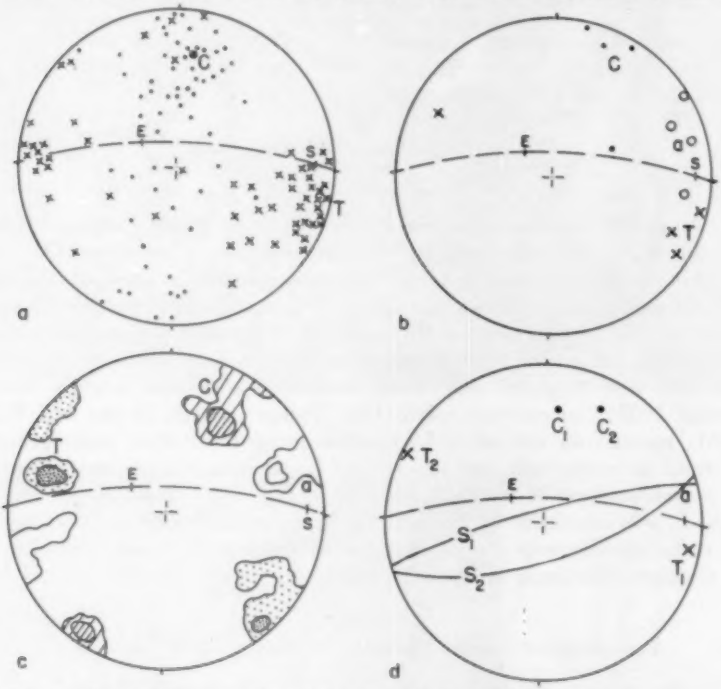

Fig. 3. Dynamic interpretation of data from the Loch Alish dolomite.

a. Axes of compression (points) and tension (crosses) which would give maximum resolved shear stress favorable for twinning on the observed twinned {0221} lamellae.

b. Active glide lines (circles) and axes of compression (points) and tension (crosses) which would give maximum resolved shear stress favorable for translation-gliding on {0001} in grains containing two sets of L_o lamellae.

c. Synoptic diagram showing maxima of *possible* glide-lines (a), tension axes (T) and compression axes (C) inferred for 31 grains containing one set of L_o lamellae.

d. Kinematic and dynamic interpretation of the data for the specimen. S_1 and S_2 are planes defined statistically by {0001}. C_1, T_1 and C_2, T_2 are stress axes inferred from twinned {0221} lamellae and L_o lamellae respectively.

contours). The *possible* axes of compression (shaded contours) and tension (stippled contours) deduced for the 31 grains are also shown in the figure (3c). Maxima for possible glide lines (a) and for axes of compression (C) and tension (T) in figure 3c have orientations close to the glide lines and axes of compression and tension inferred for grains with two sets of L_o lamellae (fig. 3b). The axes of compression and tension deduced from twinning (C_1 and T_1, fig. 3d) are also subparallel to those inferred from the L_o lamellae (C_2 and T_2, fig. 3d).

Absence of L_o lamellae in a grain does not denote absence of {0001} translation, since L_o lamellae appear only if {0221} lamellae were present in the grain prior to gliding on {0001}. The lattice orientation of grains with L_o lamellae (figs. 4a, b) is not obviously different from that of the other grains (figs. 2a, b); so that many or all of the grains in the rock may well have undergone some degree of translation-gliding on {0001}. Thus the planes defined statistically by the orientation of {0001} could represent statistical slip-planes in the fabric (S_1 and S_2, fig. 3d). Kinematic *a*-axes in these slip-planes would be given by the preferred orientation of the glide directions in individual grains (a).

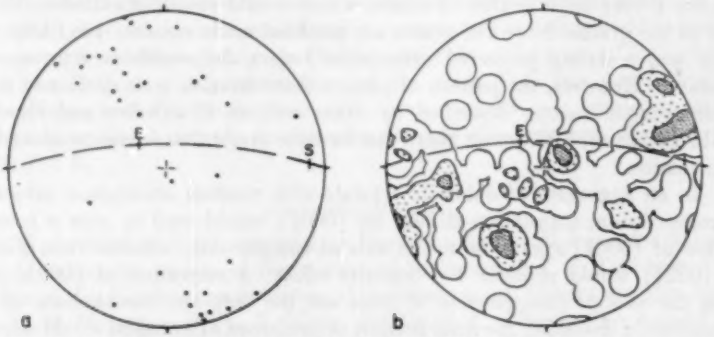

Fig. 4. Additional orientation data for the Loch Ailsh dolomite.
a. [0001]-axes in 35 grains containing L_o lamellae.
b. *a* crystallographic axes in the same 35 grains. Contours: 1, 3, 5% per 1% area.

The geometry of the dolomite lattice is such that a compression applied subparallel to [0001] will tend to produce twin-gliding simultaneously on two or three of the {0221} planes. But if a tensile force is applied normal to [0001] in such a way as to give high resolved shear stress on one {0221} plane, the resolved shear stress on the other two {0221} planes will be low and twin-gliding will take place on only one set of {0221} lamellae. Thus we might expect to find two or three sets of twin lamellae in each grain in rocks which have been deformed by compression, whereas tension should give a fabric in which most grains contain only one set of twin lamellae. The presence of two or three sets of {0221} lamellae in the majority of grains in the specimen under consideration indicates that these have been produced by compression. Although grains containing three sets of {0221} lamellae are very common,

only 20 percent of the grains contain optically recognizable twinned lamellae and the majority of these have only one such set. This feature, which is rather remarkable in view of the considerable post-crystalline deformation of the rock, may perhaps indicate a low temperature of deformation, for twinning has been produced experimentally only at temperatures above 300°C (Higgs and Handin, 1954).

Although the {02$\bar{2}$1} lamellae in some grains are closely spaced, there is no indication, even where optically recognizable twinning is present, that the grains are more than partially twinned. This fact, along with the paucity of optically twinned grains, suggests that twinning was of minor importance during the final stages of deformation. The evidence of the fabric, then, suggests that translation-gliding on {0001} was more important than twin-gliding on {02$\bar{2}$1} during the latest stage of the deformation of the rock.

Orienting Mechanism.—This study yields little evidence as to the mechanism by which the strong preferred orientation of [0001] was achieved. It is probable that the intracrystalline structures described and interpreted above reflect only the final stage in the deformation of the rock. To produce such a strong preferred orientation by gliding of the types discussed would require a very high degree of strain, which would result in extreme elongation of the grains. Since the grains are predominantly equant, it is likely that there was a strong preferred orientation before the visible structures were produced. However, the pattern of preferred orientation is so similar to those of dolomite tectonites described by other authors (Fairbairn and Hawkes, 1941; Ladurner, 1953) that there can be little doubt that it was produced by deformation.

In an aggregate of dolomite crystals with random orientation subjected to compression, translation-gliding on {0001} would tend to give a concentration of [0001]-axes close to the axis of compression, whereas twin-gliding on {02$\bar{2}$1} would produce the opposite effect—a migration of [0001]-axes from the axis of compression. If these are the only two mechanisms of deformation in dolomite, the final pattern of preferred orientation would depend solely on which of the two types of gliding was produced with the greatest ease. The observed concentration of [0001]-axes could have been brought about by basal translation with minor twinning on {02$\bar{2}$1} under compression directed parallel to the present [0001] concentration, but definite evidence as to the operative mechanism is lacking.

Calculation of Strain from Rotated Lamellae.—Theoretically it should be possible to estimate the post-crystalline strain in a rock from the degree of internal rotation of lamellae as a result of gliding according to a known system. In view of the extensive post-crystalline strain in the present specimen it should be well suited for such consideration (Turner, et al., 1956, p. 1292). The strain, ε, in individual grains is given by the equation:

$$\varepsilon = \frac{S_0\ (\cot\alpha - \cot\beta)}{\sin\gamma}$$

where α and β are the angles between the rotated lamellae and the glide-

plane before and after rotation (selected so that $\beta > \alpha$); γ is the angle between the glide line and the axis of internal rotation and S_0 is the coefficient of resolved shear stress. For the glide system under consideration γ is 60° and S_0 is given values of 0.4-0.5 (Turner, et al., 1954). For rotations of L_0 ranging from 5° to 12° the calculated strains are 5 to 18 percent.

There are certain limitations to the acceptance of these figures as a measure of the actual strain in the rock. Estimation of strain from the rotation of L_0 lamellae assumes that all the deformation was achieved by translation-gliding on {0001}, and there is evidence in most grains of limited twin-gliding. Moreover, many of the grains contain minute dark granules which may have resulted from the disruption of rotated lamellae. It is probable, in the writer's opinion, that L_0 lamellae become too diffuse for measurement and are eventually disrupted when the strain is much in excess of the values recorded above. Thus the strain recorded in the rotation of L_0 lamellae in individual grains is probably less, and perhaps considerably less, than the total post-crystalline strain in the rock.

CONCLUSION

The Loch Ailsh dolomite has a strongly-oriented tectonite fabric of unknown origin, with almost orthorhombic symmetry. The fabric yields a unified picture of translation-gliding on {0001} and twin-gliding on {02$\bar{2}$1}, dating from the final stage of deformation of the rock. This late post-crystalline deformation probably took place at a comparatively low temperature and was produced by a strong compression directed along an axis plunging 50° to N315° E.

ACKNOWLEDGMENTS

The author is deeply grateful to Professor Arthur Holmes, for valuable advice during the course of the work, and to Professor F. J. Turner and Dr. G. Oertel, for constructive criticism of the manuscript. Thanks are also due to Dr. D. B. McIntyre, Dr. L. E. Weiss and Dr. P. C. Gilmour, for helpful discussion and advice. The work was carried out at the University of Edinburgh, with generous financial assistance from the University Court, the Carnegie Trust for the Universities of Scotland and the Cross Trust.

REFERENCES

Borg, I., and Turner, F. J., 1953, Deformation of Yule Marble, Part 6: Geol. Soc. America Bull., v. 64, p. 1343-1351.

Bradley, W. F., Burst, J. F., and Graf, D. L., 1953, Crystal chemistry and differential thermal effects of dolomite: Am. Mineralogist, v. 38, p. 207-217.

Christie, J. M., 1956, A tectonic study of the post-Cambrian thrusts of the Assynt region: Thesis, University of Edinburgh.

Fairbairn, H. W., and Hawkes, H. E., Jr., 1941, Dolomite orientation in deformed rocks: Am. Jour. Sci., v. 239, p. 617-632.

Felkel, E., 1929, Gefugestudien an Kalktektoniten: Jahrb. d. Geol. Bundesanstalt, v. 79, p. 33-85.

Handin, J., and Fairbairn, H. W., 1955, Experimental deformation of Hasmark dolomite: Geol. Soc. America Bull., v. 66, p. 1257-1273.

Higgs, D. V., and Handin, J., 1954, Experimental deformation of dolomite single crystals (Abstract): Geol. Soc. America Bull., v. 65, p. 1263.

Johnsen, A., 1902, Biegungen und Translationen: Neues Jahrb. f. Min., Geol. Pal., v. 2, p. 133-153.

Ladurner, J., 1953, Allgemeine Kennzeichung und regionale Stellung alpiner Dolomittektonite: Jahrb. d. Geol. Bundesanstalt, v. 96, p. 253-300.

Turner, F. J., 1953, Nature and dynamic interpretation of deformation lamellae in calcite of three marbles: Am. Jour. Sci., v. 251, p. 276-298.

Turner, F. J., Griggs, D. T., and Heard, H., 1954, Experimental deformation of calcite crystals: Geol. Soc. America Bull., v. 65, p. 883-934.

Turner, F. J., Griggs, D. T., Heard, H., and Weiss, L. E., 1954, Plastic deformation of dolomite rock at 380°C: Am. Jour. Sci., v. 252, p. 477-488.

Turner, F. J., Griggs, D. T., Clark, R. H., and Dixon, H. R., 1956, Deformation of Yule Marble, Part 7: Geol. Soc. America Bull., v. 67, p. 1259-1294.

Department of Geology
Pomona College
Claremont, California

[American Journal of Science, Vol. 256, March 1958, P. 171-207]

PHASE EQUILIBRIA AT HIGH TEMPERATURES IN OXIDE SYSTEMS INVOLVING CHANGES IN OXIDATION STATES*

ARNULF MUAN*

ABSTRACT. Determination of phase equilibria in oxide systems involving changes in oxidation states requires careful control of atmospheric conditions. The desired O_2 partial pressure may be obtained experimentally by using vacuum techniques or by mixing O_2 with an inert gas in the range 1 to 10^{-9} atm. Under more reducing conditions the desired O_2 partial pressure is best obtained by mixing CO_2 and H_2 in various proportions. The resulting O_2 partial pressure is calculated from known equilibrium data.

In the description of phase equilibria in such systems, the O_2 partial pressure of the gas phase is an important parameter. Diagrams showing projections of the liquidus surface with liquidus isotherms and fractionation curves should be supplemented by curves showing equilibrium partial pressures of O_2 of the gas phase. New criteria for derivation of paths of equilibrium crystallization must be established. Compositions of condensed phases change during crystallization in a manner which is described by straight lines pointing towards the O apex of the model used to represent the system.

Iron oxide containing silicates are the best-known examples of systems where changes in oxidation states are involved. The systems Fe—O, FeO—Fe_2O_3—SiO_2 and MgO—FeO—Fe_2O_3—SiO_2 are used for the purpose of illustrating principles.

INTRODUCTION

A knowledge of equilibrium as well as kinetic relationships is necessary in order to understand and predict chemical reactions. In cases where reaction rates are very low, equilibrium data are of relatively little use for an evaluation of industrial processes, while they still may be of great importance for an understanding of geological processes, where the time factor is less critical. As reaction rates increase, equilibrium data become increasingly important. Although few, if any, industrial processes operate under perfect equilibrium conditions, equilibrium data have their great value in defining limits for the reactions taking place.

It is customary, for classification purposes, to distinguish between homogeneous and heterogeneous equilibria. Actually, a single homogeneous phase can not be isolated; it is not possible in practice to contain or support it without introducing one or more other phases. However, where the main reactions take place within the homogeneous part of the system, such as for instance in a gas phase, the equilibrium may be considered homogeneous. Heterogeneous equilibria, on the other hand, are those in which mass transfer across phase boundaries is an important part of the process. Such equilibria invariably involve condensed[1] phases, either liquid or solid or both. The conditions governing the coexistence of phases at equilibrium can be derived from classical thermodynamics, and are commonly expressed in the law referred to as Gibbs' Phase Rule.

$$P + F = C + 2$$

Here P designates the number of phases existing together at equilibrium, F is the number of degrees of freedom and C the number of components. The dependence of phase relationships on the variables of the system is best il-

* Contribution No. 57-4 from College of Mineral Industries, The Pennsylvania State University, University Park, Pennsylvania.

lustrated in the geometrical constructions known as phase diagrams. Among the variables influencing the phase assemblage may be temperature, pressure, chemical composition, electrical field, magnetic field etc. It has been found experimentally that the latter two may usually be ignored. Furthermore, in most cases reactions are carried out at a total pressure of 1 atm.[2], leaving temperature and chemical composition as the main variables. The dependence of phase relationships on these variables is what is usually illustrated in a phase equilibrium diagram.

A very substantial amount of phase equilibrium work on oxide systems has been described in the literature during the last decades.[3] In reviewing these studies one is impressed by the large amount of data available on systems made up from oxides of noble gas type ions, such as for instance SiO_2, Al_2O_3, MgO, CaO. The great interest in such oxides is, of course, well founded. These oxides are among the most abundant constituents of the earth's crust, and a knowledge of systems made up from these components is important in geological sciences as well as in technology. There are, however, a large number of other oxides, as well as other compounds, which are equally important, and becoming more so as new materials are developed. Many of these materials involve components made up from ions of transition elements where changes in oxidation states not only are possible but indeed very common. The study of phase equilibria in such systems is somewhat more complicated than the study of the systems just mentioned, because the gas phase plays an important role in the equilibria. The present paper discusses methods for studying and describing such systems.

METHODS FOR DETERMINING PHASE EQUILIBRIA IN OXIDE SYSTEMS

Ordinary Dry Silicate Systems.—In working out and describing phase equilibria in "ordinary dry" silicate systems[4] it is customary to ignore the vapor phase and treat the equilibria in terms of the condensed phase rule

$$P + F = C + 1$$

where P indicates the number of *condensed* phases present, while the other symbols have the same meaning as explained before. No serious error is introduced by doing this as long as the vapor pressure of each constitutent is low. Such systems are usually studied in an open quench furnace in air atmosphere. As an illustration, consider the system CaO—MgO—SiO_2 at liquidus temperatures. At equilibrium there is a certain partial pressure of each constituent in the gas phase coexisting with the condensed phases. These partial pressures vary with temperature and composition of the liquid, each assemblage of condensed phases requiring, at equilibrium, a very definite composition of the gas phase. During the time required for equilibrium to be

[1] The term condensed phases is used here and throughout the remainder of the paper to designate liquid and solid phases as distinguished from a gas phase.

[2] Pressure is, of course, an extremely important variable in geological sciences, as evidenced by the large amount of research work presently going on in the field of hydrothermal synthesis at high pressures and elevated temperatures.

[3] See for instance: Levin, E. M., McMurdie, H. R. and Hall, F. P., 1956, Phase diagrams for ceramists: Columbus, Ohio, Amer. Ceramic Soc.

attained among condensed phases the equilibrium composition of the gas phase over the charge may or may not be obtained, depending to a large extent on the degree or circulation of air through the furnace. Whether or not this true equilibrium composition of the gas phase over the sample is reached, is, however, not important in practice. This is because the vapor pressure of each constituent is so low[5] that the sample may build up, or try to build up, the equilibrium composition of the gas phase without changing appreciably the total composition of the condensed phases. Equilibria among the latter can therefore be studied without controlling the atmosphere, and the phase relationships can be discussed in terms of the condensed phase rule.

Systems Involving Changes in Oxidation States.—In cases where elements of changing oxidation states are involved in the equilibria, the situation is usually more complicated. Consider an arbitrary element Me forming two oxides MeO_x and MeO_y. Here the element Me occurs in two different states of oxidation, Me^{2x} and Me^{2y}, respectively. Suppose that these oxides are dissolved in a condensed phase in equilibrium with a gas phase. The following reaction is of critical importance:

$$(MeO_x)_{\text{in soln.}} = (MeO_y)_{\text{in soln.}} + \frac{(x-y)}{2} O_{2\,(g)}$$

It will be seen that a change in O_2 pressure causes a change in the relative proportions Me^{2x}/Me^{2y} in the condensed phase, and vice versa. Hence in treating systems involving such components the partial pressure of O_2 must be taken into consideration in addition to the vapor pressures of the components themselves. As long as all these pressures are very low (of the same order of magnitude as for CaO, MgO and SiO_2), such systems can be studied and described in a manner similar[6] to the treatment of CaO—MgO—SiO_2. The vapor pressures of the oxides *themselves* as a function of temperature are predetermined. For a large number of important oxides, such as for instance iron oxides, these pressures are very low up to liquidus temperatures. The equilibrium O_2 pressure, however, is a function of the ratio MeO_x/MeO_y in the condensed phases, increasing rapidly as this ratio increases. If the MeO_x/MeO_y ratio of the condensed phases in a mixture is such that the equilibrium O_2 pressure of the gase phase is low, phase equilibria for this mixture can be studied in a vacuum system or in a purified inert gas atmosphere. The basis for the use of this method is the slow exchange of O_2 between the gas phase and the condensed phases. As an illustration, assume that the MeO_x/MeO_y ratio in the liquid phase at the temperature considered is such that the corresponding partial pressure of O_2 is 10^{-9} atm. Assume furthermore that a completely "perfect" inert gas is used, with no O_2 present in the gas initially. The mixture when heated in a furnace through which this inert gas flows will try to build up the equilibrium O_2 pressure of 10^{-9} atm. The amount of

[4] The term "ordinary" is used in this paper to designate oxide systems involving only ions of noble gas type, as distinguished from systems containing transition elements. The term "dry" is used to indicate that no water is present, as distinguished from hydrothermal systems.

[5] The vapor pressures of CaO, MgO and SiO_2 at 1400°C in air are approximately (Brewer, 1953): CaO, 10^{-10} atm.; MgO, 10^{-9} atm.; SiO_2, 10^{-9} atm.

oxygen required to build up this low pressure in a moderate volume of gas (the inert gas flows through the furance at a moderate speed) is very small ($\frac{10^{-9}}{22.4} \cdot 32 = 1.4 \times 10^{-9}$ g oxygen per liter of gas). Hence the MeO_x/MeO_y ratio of the condensed phases is changed very little, and for practical purposes the composition of the condensed phases may be considered constant. If the inert gas is not "perfect", the situation is similar. Assume for the sake of argument that the inert gas (or the vacuum system) contains a small amount of oxygen corresponding to an O_2 pressure of 10^{-7} atm. In order to establish equilibrium between the gas phase and the condensed phases the latter phases must pick up O_2 from the gas phase. However, the difference $10^{-7} - 10^{-9}$ is very small, and again an enormous volume of gas would be required to change significantly the relative amounts MnO_x/MnO_y and hence the total composition of the condensed phases ($\sim 1.4 \times 10^{-7}$ g oxygen per liter of gas). For all practical purposes, therefore, the total composition of the condensed phases may be considered constant. This is the basis for the method used by Schuhmann, Powell and Michal (1953) in their study of a part of the system $FeO—Fe_2O_3—SiO_2$. They made up mixtures in the low Fe_2O_3 part of the system by weighing up the three components FeO, Fe_2O_3 and SiO_2 in required proportions. The mixtures were heated in platinum containers in an inert gas atmosphere, and the results interpreted on the basis of the assumption that the total composition of the condensed phases did not change during the period of time necessary to attain equilibrium among the condensed phases.[7]

An alternative method for studying such systems under reducing conditions is the one used by Bowen and Schairer (1932) in their investigation of phase equilibria in iron silicates. Their work, which was started 25 years ago, was the pioneering effort in the field and represented the first real breakthrough in experimental studies of iron oxide containing systems. The method consists in examining equilibria among condensed phases in mixtures contained in Fe crucibles in a purified inert gas atmosphere, such as for instance N_2. The partial pressure of O_2 of the gas phase under these conditions is that corresponding to the equilibria

$$Fe_2O_{3\,(\text{in melt})} = 2FeO_{(\text{in melt})} + \frac{1}{2}O_{2\,(g)}$$

and

$$Fe_2O_{3\,(\text{in melt})} + Fe_{(s)} = 3FeO_{(\text{in melt})}$$

at any particular temperature. In the binary system Fe – O only one degree of freedom exists in the presence of the phases above (liquid, metallic Fe, gas), and the O_2 pressure is a function of temperature alone. In a ternary system, such as for instance $FeO—Fe_2O_3—SiO_2$, one additional degree of freedom exists with the same phase assemblage, and the equilibrium O_2 pressure is a function of temperature as well as the amount of one of the com-

[6] Air atmosphere can not be used for the experimental study of such equilibria. This point will be discussed in more detail below.

[7] These authors were fully aware of the composition changes caused by iron going into the platinum of the container, according to the reaction $3FeO = Fe + Fe_3O_4$. However, in most instances this reaction was not extensive enough to change the results significantly.

ponents of the liquid phase. If wüstite (FeO)[8] is one of the phases present, this O_2 pressure is equal to the equilibrium pressure at which FeO and Fe coexist in equilibrium in the binary system Fe – O, at the temperature in question. (For data on this equilibrium, see papers by Darken and Gurry (1945, 1946). If wüstite is not present as a phase, at temperatures below its melting point (1371°C), this O_2 pressure is lower than the pressure corresponding to the FeO/Fe equilibrium.

At considerably higher levels of O_2 pressures, equilibrium may be reached between an O_2 containing gas phase and the condensed phases within a reasonable period of time. As an example, one liter of O_2 gas of 1 atm. pressure corresponds to 1.43 g oxygen. Hence a moderate rate of flow of gas through the furnace in this case will supply enough oxygen to change the MeO_x/MeO_y ratio of the condensed phases to the equilibrium value within a reasonable period of time. It is therefore possible in practice to study equilibria in oxide systems, involving a gas phase at 1 atm. O_2, and in air (corresponding to $p_{O_2} = 0.21$ atm.). If the O_2 pressure of the gas is decreased, either by using a vacuum or by mixing with an inert gas, the volume of gas necessary to bring about the change in composition of condensed phases required for equilibrium increases rapidly (proportional to $\left(\frac{1}{p_{O_2}}\right)$. An O_2 pressure of approximately 10^{-3} atm. is a practical lower limit for studying the equilibria when oxygen is present only as O_2 molecules in the gas phase.

It is possible, however, to obtain equilibrium between the gas phase and the condensed phases also below these levels of O_2 pressures by using indirect methods of creating the desired O_2 partial pressures. The most convenient way of doing this is to use an oxygen-containing gas which upon heating in the furnace decomposes to another gas species under liberation of O_2. Gases suitable for this purpose are H_2O and CO_2, which decompose upon heating according to the equations:

$$2H_2O = 2H_2 + O_2, \text{ and}$$
$$2CO_2 = 2CO + O_2, \text{ respectively.}$$

The equilibrium constant for each of these reactions as a function of temperature is well known. If CO_2 or H_2O is used alone, and the total pressure is kept constant, the O_2 pressure is a function of temperature alone. This means that O_2 pressure and temperature can not be varied independently if the pure gases are used, and this of course is a serious drawback. If, however, some H_2 is mixed with the H_2O or some CO with the CO_2,[9] the dissociations of H_2O or CO_2 are suppressed to a degree which can be controlled by varying the mixing ratios of the gases. The O_2 pressure now is a function of temperature as well as H_2O/H_2 or CO_2/CO mixing ratios. O_2 pressure and

[8] Wüstite is a defect structure with a considerable variation in the Fe/O ratio (Darken and Gurry, 1945, 1946). Although the stoichiometric composition FeO can not be realized in practice, the formula for wüstite is usually written as FeO for the sake of convenience.

[9] These gases are interchangeable; CO may be mixed with H_2O and H_2 with CO_2. The interdependence of the equilibrium ratios H_2O/H_2, CO_2/CO, CO_2/H_2 and H_2O/CO at a certain O_2 pressure is expressed by the equilibrium constant for the "water gas equation" $CO_2 + H_2 = CO + H_2O$.

temperature can therefore be varied independently. The advantage of using mixed gas atmospheres rather than vacuum or inert gas is the presence of oxygen not only as O_2 but in bound form (H_2O or CO_2) as well. At temperatures high enough to make the gas reactions rapid, a mechanism is available by which the O_2 exchange between the gas phase and the condensed phases can take place within a reasonable period of time in spite of the low *partial* pressure of O_2. As soon as O_2 is removed from the gas phase by reaction with the condensed phases, the equilibrium amount is restored by the decompositions $2H_2O = 2H_2O + O_2$ or $2CO_2 = 2CO + O_2$, whatever the case may be. It is emphasized that such methods for equilibrium studies can be used only at temperatures sufficiently high to make the gas reactions rapid.

REPRESENTATIONS OF PHASE RELATIONSHIPS

The System Fe – O.—Systems containing iron oxides as components have been studied more thoroughly than any other oxide systems in which changes in oxidation states are involved. These will be used as examples in the following.

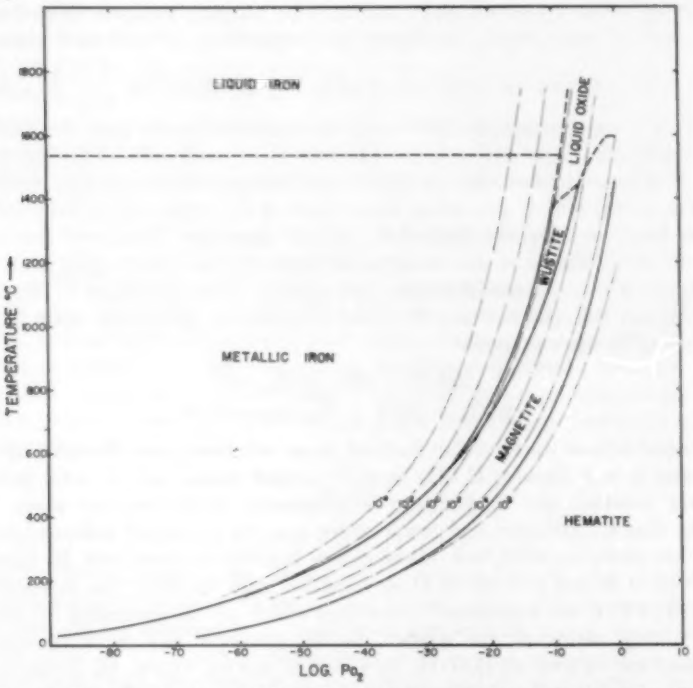

Fig. 1. Diagram showing stability relationships among the phases hematite (Fe_2O_3), magnetite ($FeO.Fe_2O_3$), wüstite (FeO), metallic iron (Fe), liquid oxide and liquid iron as a function of temperature (in °C) and O_2 pressure (in atm.). Heavy solid lines are boundary curves separating the various phase areas labelled in the diagram. Light dash-double dot lines are lines of equal p_{H_2O}/p_{H_2} ratios of the gas phase at 1 atm. total pressure.

A thorough understanding of phase equilibria in the system Fe – O is essential as a background for discussing more complicated multicomponent iron silicates. The most recent and complete reports on the system are the excellent papers in 1945 and 1946 by Darken and Gurry (1945, 1946). These authors summarize results of earlier work in addition to providing a large amount of new data. The following discussion is based on data contained in their papers as well as data available in a recent compilation of thermodynamic constants by Coughlin (1954).

The importance of controlling the O_2 pressure was emphasized in the last section. The diagram shown in figure 1 is intended to bring out this point more clearly and in a quantitative way for the Fe—O system. In this plot phase equilibrium relationships among metallic iron (Fe), wüstite (FeO), magnetite ($FeO.Fe_2O_3$), hematite (Fe_2O_3), liquid iron and liquid oxide are illustrated as a function of temperature (°C) and partial pressure of O_2. The diagram has been constructed from data explained in detail later in connection with figure 2. The following rules should be observed when using the diagram in figure 1. In an area where one condensed phase exists in equilibrium with a gas, the system possesses 2 degrees of freedom. Hence, in a field such as for instance that of wüstite both temperature as well as O_2 pressure may be changed without causing any phase changes. Along a bound-

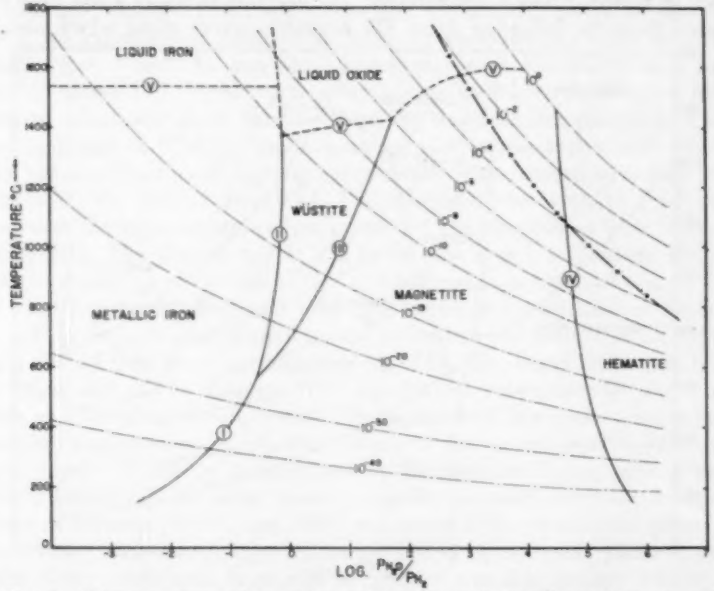

Fig. 2. Diagram presented in order to illustrate stability relationships among iron oxides and metallic iron as a function of temperature (in °C) and ratios of H_2O/H_2 of the gas phase in equilibrium with the condensed phases. Heavy solid lines are boundary curves separating the various phase areas labelled in the diagram. Light dash-dot lines are O_2 isobars. The heavy dash-cross line shows equilibrium ratios p_{H_2O}/p_{H_2} of pure water vapor as a function of temperature at a total pressure of 1 atm.

ary curve, however, where 2 condensed phases coexist in equilibrium with a gas phase, the system has only 1 degree of freedom. Hence, if temperature is chosen, the O_2 pressure is fixed and vice versa. It will be noticed that the O_2 pressures of the gas phase in equilibrium with the various condensed phases in the system vary over a very large range, as temperatures vary between room temperature and liquidus temperatures. This of course is directly related to the large heat effects associated with each of the reactions represented by the boundary curves. $\left(\frac{d \ln p_{O_2}}{dT} = \frac{\Delta H^\circ}{RT^2} \right.$, where ΔH° is the heat of reaction per mole of O_2 for each reaction, such as for instance: $6Fe_2O_3 = 4Fe_3O_4 + O_2$). Oxygen pressures at the lowest temperatures shown in figure 1 are so low as to have little or no physical meaning. Physically more meaningful are ratios p_{H_2O}/p_{H_2} or p_{CO_2}/p_{CO} of the gas phase in equilibrium with the various oxides. Lines representing equilibrium values of p_{H_2O}/p_{H_2} ratios are plotted as dash double dot lines in figure 1. It is seen that these lines fall close to and are nearly parallel to the boundary curves separating the various phase areas. More "spread out" and readable diagrams are obtained by plotting p_{H_2O}/p_{H_2} and p_{CO_2}/p_{CO} ratios of the gas phase in equilibrium with the various condensed phases as a function of temperature, as shown in figures 2 and 3, respectively. The diagram in figure 2 has been constructed from the following data: The boundary curve along which metallic

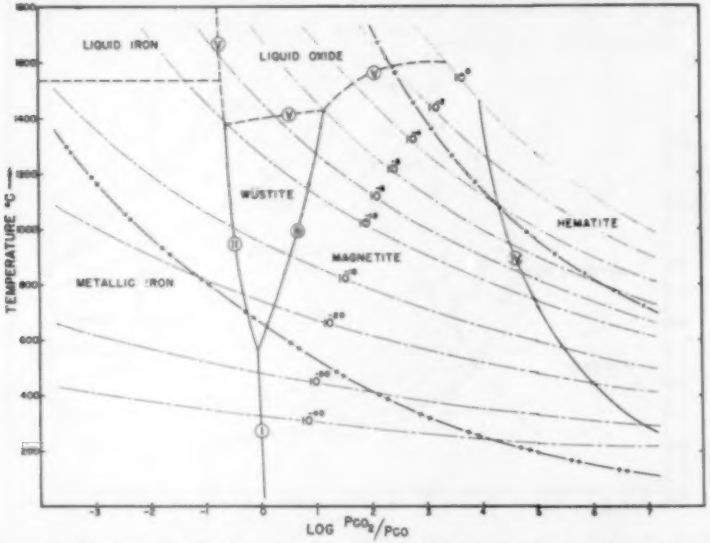

Fig. 3. Diagram illustrating stability relationships among iron oxides and metallic iron as a function of temperature and ratios of CO_2/CO of the gas phase in equilibrium with the condensed phases. Heavy solid lines and light dash-dot lines have the same meanings as in last diagram. The heavy dash-double cross line indicates ratios p_{CO_2}/p_{CO} in equilibrium with carbon (graphite) as a function of temperature at a total pressure of 1 atm.

iron and wüstite or liquid oxide coexist in equilibrium with gas (curve II), as well as part of the curve where magnetite, wüstite and gas exist together in equilibrium (curve III), have been plotted from data obtained by direct measurements of H_2O/H_2 ratios of the gas in equilibrium with these phases, as reported in the literature. The lower temperature part of curve II (600-1000°C) was constructed from the data of Emmetts and Shultz (1930), while the upper region (1200-1515°C) was plotted from the data of Chipman and Marshall (1940). The low temperature part of curve III (600-800°C) was drawn on the basis of the data of Emmetts and Shultz (1930). The upper part of this curve (1096-1388°C) was constructed on the basis of data reported by Darken and Gurry (1946). These authors used CO_2/CO and CO_2/H_2 gas mixtures rather than H_2O/H_2 to study the equilibrium described by this line. Their data have been converted to values of H_2O/H_2 ratios by use of the equilibrium data for the reactions

$$2CO_2 = 2CO + O_2$$
$$2H_2O = 2H_2 + O_2$$

as tabulated in a recent publication by Coughlin (1954). The liquidus curve V, as well as that part of the hematite-magnetite boundary curve IV falling between 1100 and 1450°C, likewise, have been constructed from the data of Darken and Gurry (1946) by conversion to H_2O/H_2 ratios as described above. No experimental data are available for the boundary curve magnetite-metallic iron (curve I) and the hematite-magnetite boundary curve below 1100°C (curve IV). These parts of the curves have been constructed on the basis of calculated values obtained from the standard free energy data tabulated by Coughlin (1954). For checking purpose, curves were also constructed from calculated values in regions where direct measurements have been made (curves II, III, part of curve IV). The calculated curves are in good agreement with the experimental curves except for the magnetite-wüstite boundary (curve III). The discrepancy in the latter case is not surprising. The data listed in the tables of Coughlin refer to wüstite of composition $Fe_{0.947}O$, while the wüstite in equilibrium with magnetite varies in composition in the range $Fe_{0.950}O$ to $Fe_{0.839}O$ (see phase diagram of Darken and Gurry (1945, 1946)). Light dashed lines show partial pressures of O_2. The heavy dash-cross line in the upper part of the diagram gives equilibrium values of p_{H_2O}/p_{H_2} of pure water as a function of temperature. The position of this curve relative to the boundary curves shows the stability ranges of the various iron oxides in pure water vapor. It will be noticed that at temperatures below approximately 1070°C hematite is the stable phase in equilibrium with water vapor. At temperatures between 1070°C and 1595° magnetite is the equilibrium phase in a water vapor atmosphere, and above 1595°C a liquid oxide phase is stable under these conditions. It should be pointed out that neither wüstite nor metallic iron are equilibrium phases in water vapor at any temperature at a total pressure of 1 atm. In order to study equilibria in regions of the diagram falling below this dissociation curve for pure H_2O it is necessary to mix H_2 (or some other reducing agent) with the H_2O in amounts that may be *calculated* from the diagram in figure 2. One important relationship should be

made clear at this point: The values of H_2O/H_2 ratios plotted in figure 2 are the *equilibrium* ratios at any particular temperature. In order to study experimentally equilibria among the iron oxide phases it is usually necessary to mix the two gases in fixed proportions at room temperature and heat this gas mixture to whatever temperature is desired for the study of the equilibria among the condensed phases. These two ratios (original mixing ratio at room temperature and equilibrium ratio at the elevated temperature) are not the same. They are related to each other in the following way: Let $p_{H_2O(i)}$ and $p_{H_2(i)}$ be the partial pressures of H_2O and H_2, respectively, in the starting gas mixture at room temperature. Upon heating, H_2O decomposes according to the equation

$$2H_2O = 2H_2 + O_2$$

At equilibrium we have the relationship

$$K = \frac{p_{O_2(eq.)} \; p_{H_2(eq.)}}{p_{H_2O(eq.)^2}}$$

where $p_{O_2(eq.)}$ etc. are the partial pressures of the gases at equilibrium at the high temperature, and K is the equilibrium constant at the same temperature. Let us call $p_{O_2(eq.)} = x$. Then we have the following relationships:

$$p_{O_2(eq.)} = x$$

$$p_{H_2(eq.)} = (1-x)\; p_{H_2(i)} + 2x$$

$$p_{H_2O(eq.)} = (1-x)\; p_{H_2O(i)} - 2x$$

Hence:

$$K = \frac{x\left((1-x)p_{H_2(i)} + 2x\right)^2}{\left((1-x)p_{H_2O(i)} - 2x\right)^2}$$

and

$$\frac{p_{H_2O(eq.)}}{p_{H_2(eq.)}} = \frac{(1-x)p_{H_2O(i)} - 2x}{(1-x)p_{H_2(i)} + 2x}$$

If $x << p_{H_2O(i)}$ and $x << p_{H_2(i)}$ we have

$$\frac{p_{H_2O(eq.)}}{p_{H_2(eq.)}} \cong \frac{p_{H_2O(i)}}{p_{H_2(i)}}$$

and likewise

$$K \cong \frac{x \cdot p_{H_2(i)^2}}{p_{H_2O(i)^2}},$$

or $x \cong Kr^2$, where r = mixing ratio $\dfrac{p_{H_2O(i)}}{p_{H_2(i)}}$

These approximations are valid in all regions of the diagram in figure 2 except in close proximity of the line for dissociation of pure water. For pure water the following relationships hold:

$$p_{O_2(eq.)} = x$$

$$p_{H_2(eq.)} = 2x$$

$$p_{H_2O(eq.)} = 1 - 3x$$

$$K = \frac{x \cdot (2x)^2}{(1 - 3x)^2}, \text{ or } K = \frac{4x^3}{(1 - 3x)^2}$$

At moderate or low temperatures, where K is small, $x << 1$, and the following approximation is valid:

$$K \cong 4x^3; \; x \cong \left(\frac{K}{4}\right)^{1/3}$$

Hence

$$\frac{p_{H_2O(eq.)}}{p_{H_2(eq.)}} \cong \left(\frac{p_{O_2}}{K}\right)^{1/2} \cong \left(\frac{\left(\frac{K}{4}\right)^{1/3}}{K}\right)^{1/2} \cong \frac{1}{1.25 \cdot K^{1/3}}$$

In order to study equilibria above the dissociation curve for pure water (fig. 2), on the other hand, it is necessary to mix O_2 with the H_2O. At moderate or low temperatures, where the dissociation of water is small, this amounts to practically the same as mixing O_2 with an inert gas; the partial pressure of O_2 in the mixture is practically the same as the proportion of O_2 mixed with the gas.

It will be observed that some of the boundary curves in figure 2 have a positive slope, some have a negative slope, and one (the Fe—wüstite and Fe—liquid oxide boundary) is practically vertical. The latter case illustrates a situation in which the ratio p_{H_2O}/p_{H_2} of the gas in equilibrium with the two condensed phases remains essentially constant over a large temperature interval (1000-1600°C). The reason for this is that the heat of reduction of iron oxide to Fe is balanced by an almost identical heat effect of opposite sign, the oxidation of H_2 to H_2O:

$$FeO + H_2 = Fe + H_2O$$

Therefore, ΔH° for this reaction is very small, and the equilibrium constant (ratio H_2O/H_2) is almost independent of temperature. Curves with positive slope (for example the Fe—Fe_3O_4 boundary curve) result when the heat of reduction of the oxide to the next lower oxide or to metallic iron is larger than the heat of oxidation of H_2 taking part in the reaction. Conversely, the negative slope of the hematite-magnetite boundary curve illustrates an example of an overall exothermic reaction.

The diagram in figure 3 shows equilibrium ratios p_{CO_2}/p_{CO} of the gas phase in stable equilibrium with condensed phases in the system Fe—O, as a function of temperature. The diagram has been constructed from the same data as explained in connection with figure 2. It will be observed that the two diagrams in figures 2 and 3 are almost identical. The reason for this is that the dissociation constants of H_2O and CO_2 are closely similar, the former being slightly higher at temperatures above 800°C, the latter being slightly

higher at lower temperatures. The various lines have the same meanings as in the last diagram (fig. 2) with p_{CO_2}/p_{CO} ratios replacing the p_{H_2O}/p_{H_2} ratios. An additional line of great importance in the present case is the dash-double cross line illustrating p_{CO_2}/p_{CO} ratios in equilibrium with graphite according to the equation

$$2CO_{(g)} = C_{(c)} + CO_{2\ (g)}$$

This line indicates limiting ratios of p_{CO_2}/p_{CO} at various temperatures. If, at a chosen temperature, CO_2/CO ratios of the gas phase are decreased from a value represented by a point in the upper part of the diagram, graphite starts depositing, with CO_2/CO ratio remaining constant, when the latter ratio reaches a value corresponding to the point on the dash-cross curve for this temperature. The reaction $2CO_{(g)} = C_{(c)} + CO_{2\ (g)}$ is strongly exothermic, as evidenced by the steep negative slope of the dash-cross curve in figure 3. In order to obtain a gas with low CO_2/CO ratios, it is therefore necessary to go to high temperatures. It will be noticed that the dash-double cross line intersects the Fe_3O_4—FeO and the FeO—Fe boundary curves at approximately 660 and 720°C, respectively. These are the lowest temperatures at which wüstite and metallic iron, respectively, can exist in equilibrium with C - O gases. This relationship of course is of fundamental importance for an understanding of the blast furnace process, and has some important implications in certain fields of geochemistry. During the last couple of years geochemists have taken a great deal of interest in equilibrium relationships of carbonates at high CO_2 pressures. (See for instance papers by Harker and Tuttle, 1956; Harker and Hutta, 1956). One of the carbonates of great interest in geochemistry is siderite ($FeCO_3$). The graph in figure 3, although constructed for a total pressure of 1 atm., may be used to judge the possibility of studying experimentally the reaction

$$FeCO_{3\ (c)} = FeO_{(c)} + CO_{2\ (g)}$$

It is evident from the diagram that a considerable proportion, the exact amount depending on temperature, of CO must be mixed with the CO_2 in order to prevent oxidation of FeO to Fe_3O_4. (See curve III in fig. 3). The disproportionation of CO to CO_2 and C, represented by the dash-double cross curve, however, puts a limit on the CO/CO_2 ratios that can be reached. The intersection between this curve and curve III at 660°C defines a limiting temperature below which FeO can not exist as an equilibrium phase in the presence of C and O at a total pressure of 1 atm. Higher pressures will cause a shift in the dash-double cross curve towards the right, while the boundary curve III may be expected to be comparatively little effected by an increase in pressure. The lowest temperature at which siderite may be decomposed to give wüstite as an equilibrium phase, therefore, is higher than 660°C at higher pressures. The *metastable* equilibrium $FeCO_3 = FeO + CO_2$ may be *calculated*, below these temperatures, from experimental equilibrium data on the reaction $3FeCO_3 = Fe_3O_4 + CO + 2CO_2$, if such become available, combined with thermodynamic data referred to above (Darken and Gurry, 1945, 1946; Coughlin, 1954).

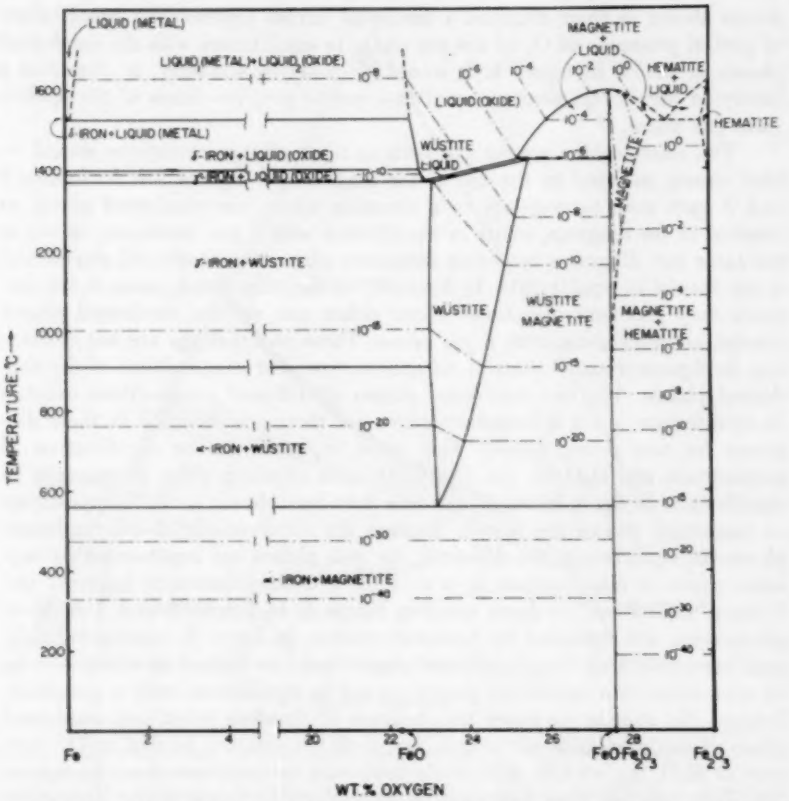

Fig. 4. Diagram to show phase equilibrium relationships in the system Fe—O, mainly after Darken and Gurry (1945, 1946). Heavy solid lines are boundary curves separating phase areas labelled in the diagram and light dash-dot lines are O_2 isobars (in atm.). Dashed curves in upper right part of the system are inferred boundary curves in a region where experimental data are lacking ($p_{O_2} > 1$ atm.).

The diagrams presented in figures 2 and 3 have one serious drawback: They do not show compositions of condensed phases. It is of course possible to draw a phase diagram for the system Fe—O showing compositions of condensed phases. This indeed has been done; the most complete diagram is that presented by Darken and Gurry (1945). They plot the diagram in the usual way with temperatures (in °C) along the vertical axis and composition (expressed in weight % O) along the horizontal axis. Their diagram also has one serious drawback, however: It does not show compositions of the gas phase in equilibrium with the condensed phases. The diagram presented in figure 4 of the present paper is intended to illustrate phase equilibria in the system Fe—O in a manner which eliminates the drawbacks mentioned above. The diagram is essentially a reproduction from Darken and Gurry (1946), the axes being temperature and composition. In addition to the boundary

curves shown in their diagram a family of curves representing equal values of partial pressures of O_2 of the gas phase in equilibrium with the condensed phases is shown in figure 4. It would be possible, similarly, to construct a family of curves representing equal p_{H_2O}/p_{H_2} or p_{CO_2}/p_{CO} ratios of the equilibrium gas phase.

The relationships among the various types of representations should be kept clearly in mind in the use of the diagrams in figures 2-4. In figures 2 and 3 each area corresponds to a situation where one condensed phase, as labelled in the diagram, exists in equilibrium with a gas. Boundary curves in the same two diagrams represent situations where two condensed phases and a gas coexist in equilibrium. In figure 4, on the other hand, areas in the diagram may represent situations where either one or two condensed phases coexist in equilibrium with a gas phase. These observations are not conflicting. In figures 2 and 3 there is no axis to represent compositions of the condensed phases. The two condensed phases of different compositions existing in equilibrium along a boundary curve are therefore recorded in these diagrams by one point, namely that point representing the combination of temperature and H_2O/H_2 (or CO_2/CO) ratio at which these phases exist in equilibrium. In fig. 4, however, the axes have been chosen so that compositions of condensed phases are shown. Because the compositions of the condensed phases in equilibrium are different, the two phases are represented by separate points in this diagram. It is as if the boundary curves in figures 2 and 3 were "pulled out" to form areas in figure 4. In figures 2 and 3 adjacent phase areas are separated by boundary curves, in figure 4, correspondingly, each one-phase area (one *condensed* phase) must be limited on either side by an area where two condensed phases coexist in equilibrium with a gas phase. Because the system possesses two degrees of freedom when one condensed phase exists in equilibrium with a gas, both temperature as well as O_2 pressure or H_2O/H_2 (or CO_2/CO) ratio may vary in one-phase areas in figures 2-4. Therefore the lines representing O_2 isobars in figure 4 run diagonally across such areas. In a two-phase area (two *condensed* phases), on the other hand, only one degree of freedom exists and p_{O_2} as well as H_2O/H_2 (or CO_2/CO) ratios in the gas phase are fixed if the temperature is chosen. The O_2 isobaric lines therefore must be horizontal lines parallel to the composition axis in a two-phase region.

Ternary and Quaternary Iron Silicates.—The methods used for describing phase equilibrium relationships in the binary system Fe—O can be extended into the more complicated ternary and quaternary systems. As an illustration of the former, consider the system $FeO—Fe_2O_3—SiO_2$, which is part of the ternary system Fe—Si—O. In the following we will focus our attention on the liquidus temperature region. In figure 5 is shown the usual plot of the projected liquidus surface with boundary curves and liquidus isotherms (Muan, 1955). When one crystalline and one liquid phase coexist with a gas phase, the system possesses two degrees of freedom. If temperature and liquid composition are chosen, O_2 pressures are fixed. It is therefore possible to draw a set of curves representing equal partial pressures of O_2

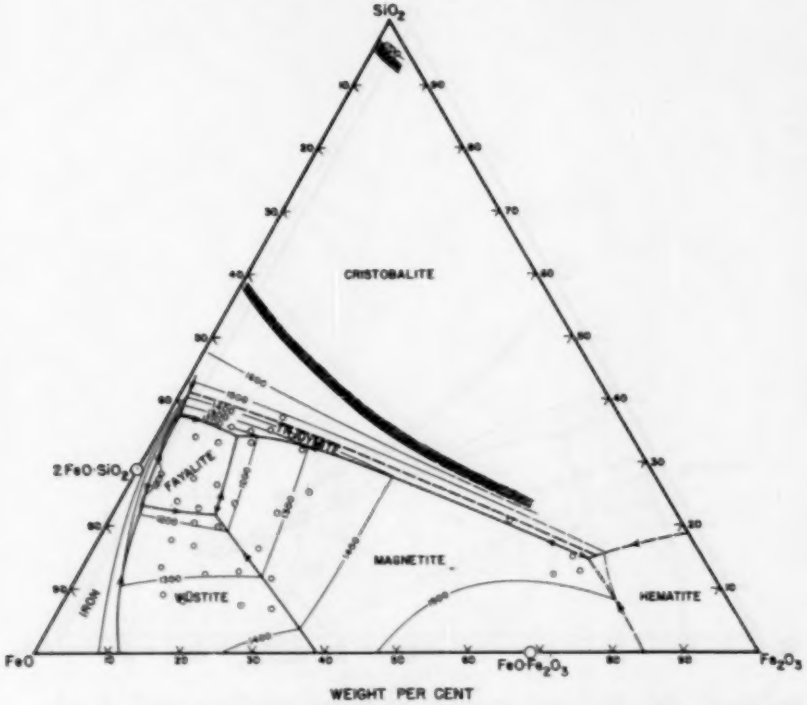

Fig. 5. Phase equilibrium diagram at liquidus temperatures for the system FeO—Fe_2O_3—SiO_2, after Muan (1955). Light lines are liquidus isotherms at 100°C intervals, and heavy lines are boundary curves, with arrows pointing in directions of falling temperatures. The tridymite-cristobalite boundary curve is dashed. Medium lines with stippling on one side indicate limit of two liquid region.

(O_2 isobars) of the gas phase in equilibrium with condensed phases along the liquidus surface. These lines are extensions into the triangle representing the FeO—Fe_2O_3—SiO_2 system of points of intersection between O_2 isobars and the liquidus curve in the Fe—O system (fig. 4). An example of such lines is illustrated in figure 6 (Muan, 1955). Similarly, one may draw lines representing equal p_{H_2O}/p_{H_2} (or p_{CO_2}/p_{CO}) ratios for points along the liquidus surface. Figure 7 gives an illustration of this for the system FeO—Fe_2O_3—SiO_2 (Muan, 1955).[10] It will be noticed that the lines of equal p_{CO_2}/p_{H_2} ratios are nearly parallel to the boundary curve between the fields of wüstite and metallic iron. This is in accordance with figure 3, where it was shown that this boundary curve is almost vertical (corresponding to constant p_{CO_2}/p_{CO} ratio)[10] over a large temperature interval.

[10] This diagram shows lines representing equal p_{CO_2}/p_{H_2} ratios rather than p_{CO_2}/p_{CO} ratios. However, the numerical values of these ratios are almost identical because the equilibrium constant for the "water gas reaction" $CO_2 + H_2 = CO + H_2O$ is not significantly different from 1 in the temperature interval considered.

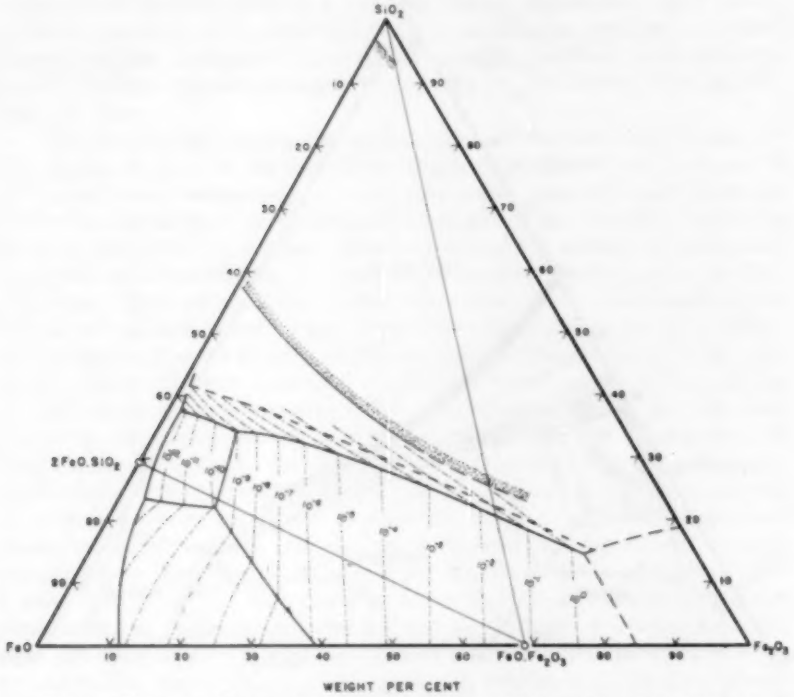

Fig. 6. Phase equilibrium diagram for the system FeO—Fe_2O_3—SiO_2. Heavy lines are boundary curves and dash-dot lines are lines of equal O_2 pressures for points on liquidus surface. Lines with stippling on one side indicate limit of two liquid region. (Diagram after Muan (1955)).

Liquidus temperatures were chosen for illustration in the present case. One may of course construct O_2 isobars or lines representing equal p_{H_2O}/p_{H_2} (or p_{CO_2}/p_{CO}) ratios at other temperatures as well, above or below liquidus temperatures.

In order to illustrate the relationships of compositions of crystalline phases in equilibrium with liquid and gas, the above diagrams are supplemented by the fractionation curves shown in figure 8. Fractionation curves are constructed from conjugation lines in such a way that the conjugation lines are tangent to the fractionation curves. (A conjugation line joins the composition of a liquid with the composition of the crystalline phase with which it is in equilibrium). The composition of a crystalline phase in equilibrium with a liquid, therefore, may be derived from the diagram of figure 8 as the intersection with the join FeO—Fe_2O_3 of the tangent to the fractionation curve at the point representing liquid composition.

In the case of a quaternary system the principles are the same, but it is much more difficult to illustrate the relationships geometrically. Take as an

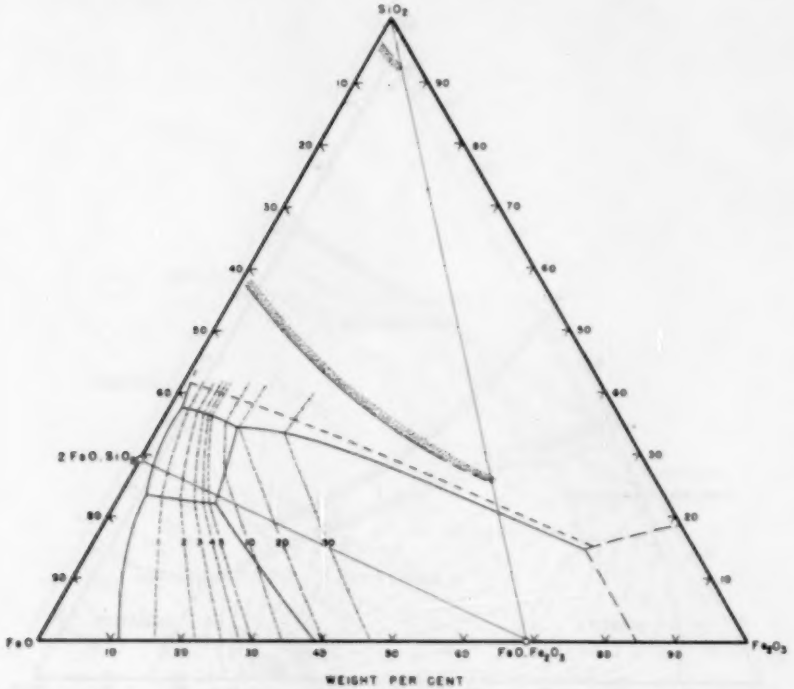

Fig. 7. Phase equilibrium diagram for the system FeO—Fe_2O_3—SiO_2. Heavy lines are boundary curves and dash-double dot lines are lines of equal p_{CO_2}/p_{H_2} ratios of the gas phase in equilibrium with liquids at liquidus temperatures. Lines with stippling on one side indicate limit of two liquid region. (Diagram after Muan (1955)).

example the quaternary[11] system MgO—FeO—Fe_2O_3—SiO_2 (Muan and Osborn, 1956). For our purpose it is most convenient to consider this system as formed from FeO—Fe_2O_3—SiO_2 by the addition of MgO. If, as before, we focus our attention on the liquidus temperature region, the O_2 isobars or the lines representing equal p_{CO_2}/p_{H_2} ratios along the liquidus surface in the ternary system FeO—Fe_2O_3—SiO_2 are starting lines for irregularly curved surfaces ("oxygen isobaric surfaces") extending through the tetrahedron representing the MgO—FeO—Fe_2O_3—SiO_2 system. These surfaces are difficult to illustrate in perspective drawings of the tetrahedron. An indication of their location is obtained in the following way: Phase equilibria at an O_2 pressure represented by such a surface are illustrated by projecting points in the surface into a chosen plane cutting through the tetrahedron, preferably a plane located close to the surface in question. The actual location of composition points of the mixtures at liquidus temperatures, and hence the location of the

[11] The system MgO—FeO—Fe_2O_3—SiO_2 is part of the quaternary system Mg—Fe—Si—O but is not in itself a completely quaternary system because metallic iron appears as a phase in certain composition-temperature ranges. For our purposes this may be disregarded, and the system will be considered quaternary.

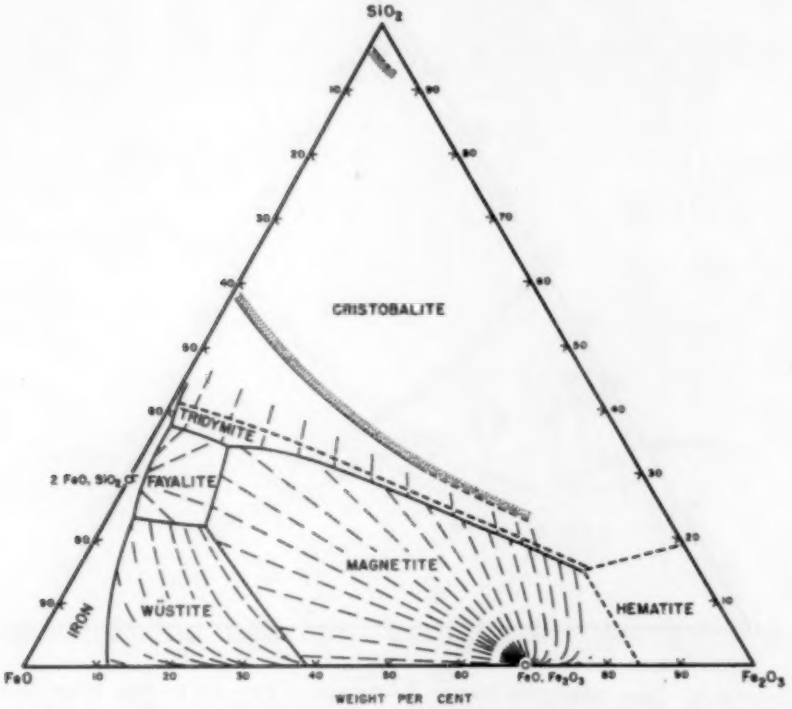

Fig. 8. Diagram of the system $FeO—Fe_2O_3—SiO_2$ presented in order to illustrate relationship of compositions of liquid and crystalline phases in equilibrium, after Muan (1955). Heavy lines are boundary curves and medium dash lines are fractionation curves. Lines with stippling on one side indicate limit of two liquid region.

isobaric surface at liquidus temperatures, is indicated by lines in the projected diagram representing equal Fe_2O_3/FeO ratios. An example of this is given by the phase diagram $MgO—FeO.Fe_2O_3—SiO_2$ (fig. 9) drawn to represent phase relationships in the system MgO—iron oxide—SiO_2 in air (Muan and Osborn, 1956). Points located exactly in the plane chosen for projection have Fe_2O_3/FeO ratios of 2.22 (on a weight % basis). Mixtures located on the Fe_2O_3 side of this plane have Fe_2O_3/FeO ratios larger than 2.22, and mixtures located on the FeO side of the plane have Fe_2O_3/FeO ratios below this value.

Similarly, approximate locations of fractionation curves may be indicated by projecting them into a chosen plane. An example of this is shown in figure 10, representing phase equilibria in the system $FeO—Fe_2O_3—Al_2O_3—SiO_2$ in air (Muan, 1957).

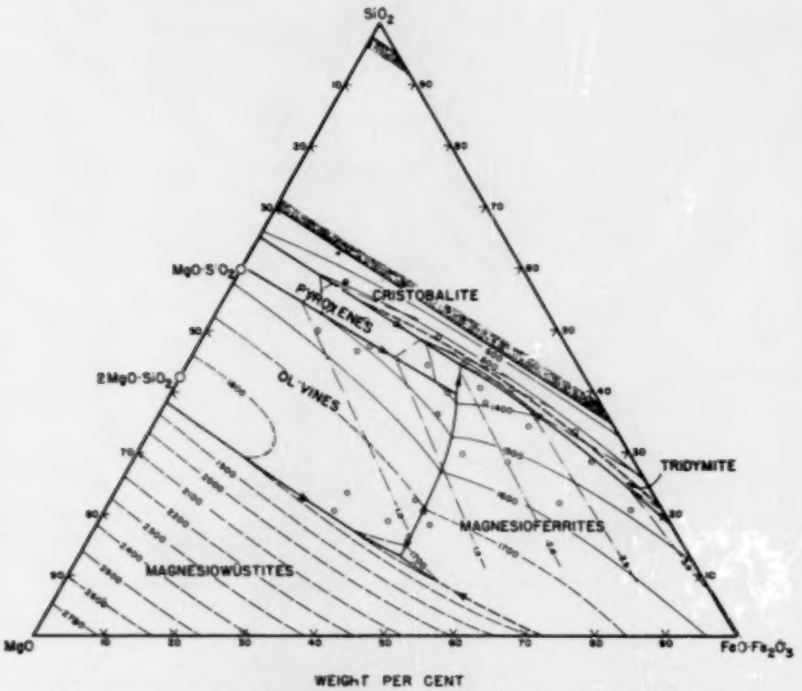

Fig. 9. Diagram to illustrate phase relationships in the system MgO—FeO—Fe_2O_3—SiO_2 in air. For the sake of simplicity the relationships are pictured as a ternary system with MgO, $FeO.Fe_2O_3$, and SiO_2 as components. Heavy lines are boundary curves (these curves are not boundary curves in the strict meaning of the term as applied to ternary systems but rather traces of the curved boundary surfaces between two adjacent primary-phase volumes in the "plane" which the diagram represents), with arrows pointing in the directions of falling temperatures, and light solid lines are liquidus isotherms at 100°C intervals. Boundary curves and isotherms are drawn as dashed lines in regions where quenching data were not obtained. Light dash-triple dot lines are curves approximately passing through points of equal Fe_2O_3/FeO ratios at liquidus temperatures. Medium lines with stippling on one side indicate limit of two liquid region.

PATHS OF EQUILIBRIUM CRYSTALLIZATION

Phase equilibrium relationships can best be described by derivation of paths of equilibrium crystallization. This term has been used primarily by petrologists concerned with the differentiation of a magma into various minerals and rocks, but because of its general usefulness in phase equilibrium considerations it deserves much wider attention. As originally defined the path of equilibrium crystallization means the course along which the liquid composition changes as heat is withdrawn from the system under equilibrium conditions. It also, however, implies the changes taking place in the composition of the gas and crystalline phases during crystallization. In a wider meaning, therefore, the path of equilibrium crystallization is a continuous description of the changes in phase assemblage taking place as the tempera-

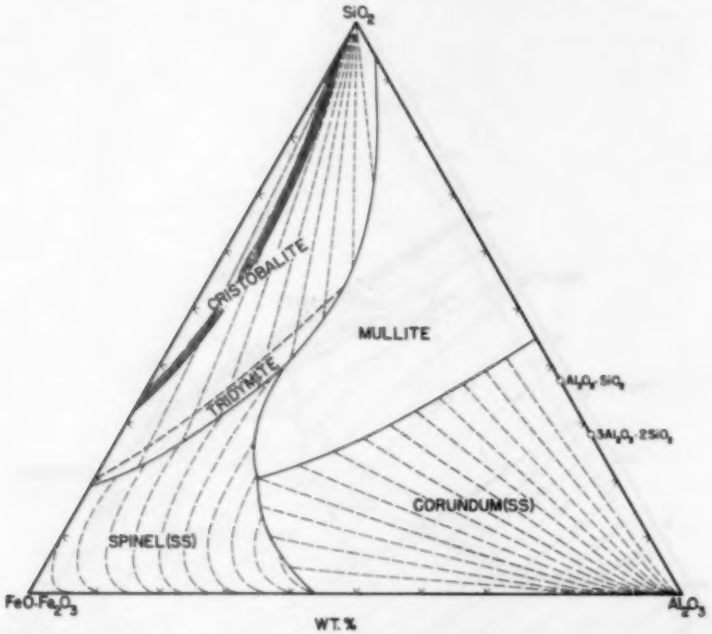

Fig. 10. Diagram of the system iron oxide Al_2O_3—SiO_2 in air presented in order to illustrate relationship of composition of liquid and crystalline phases in equilibrium. Heavy lines are boundary curves and medium dashed lines are fractionation curves. Lines with stippling on one side indicate limit of two liquid region. (Diagram after Muan (1957)).

ture is lowered from liquidus temperature, and equilibrium maintained among the phases. The same sequence of phase changes of course occurs upon heating under equilibrium conditions, only in the opposite direction, and one could equally well talk about a "path of melting". Thus a knowledge of the path of equilibrium crystallization in a system enables one to determine the composition of all phases present and their relative amounts at any temperature within the interval in which the system has been investigated.

In most dry oxide systems, where the gas phase can be neglected, the path of equilibrium crystallization can be derived on the assumption that the total composition of condensed phases remains constant. In systems where changes in oxidation states take place, this relationship usually does not hold. In reacting with the atmosphere, as temperature is changed, oxygen is added to or subtracted from the condensed phases concomitant to a proportional change in the MeO_x/MeO_y ratio. The total composition of the condensed phases thus changes continuously during crystallization of the liquid, but only with respect to the relative proportions of the two components MeO_x and MeO_y. This change can be described by straight lines passing through the O corner of the system in question. By combining these lines with liquidus isotherms, fractionation curves, O_2 isobars or lines of equal p_{CO_2}/p_{H_2} ratios,

one is able to derive paths of equilibrium crystallization for various idealized conditions, which conditions in practice approach more or less closely. In the following, methods for derivation of paths of equilibrium crystallization in binary, ternary and quaternary systems involving changes in oxidation states will be reviewed briefly, using the systems Fe—O, FeO—Fe_2O_3—SiO_2 and MgO—FeO—Fe_2O_3—SiO_2 as examples. Four different idealized conditions will be considered:

(1) Constant total composition of condensed phases
(2) Constant O_2 pressure
(3) Constant mixing ratio p_{CO_2}/p_{H_2} of the gas phase
(4) Crystallization in contact with metallic iron

The first of these conditions is closely approximated in a closed system when the volume of the gas phase is small. Conditions under (2) and (3) are easily realized experimentally and have been used extensively in recent phase equilibrium studies (Muan, 1955; Muan and Osborn, 1956; Muan and Gee, 1956; Muan, 1957a, b). Finally, the fourth condition obtains under the experimental conditions first used by Bowen and Schairer for studying iron silicate systems (Bowen and Schairer, 1932). Throughout the following discussion it is assumed that perfect equilibrium exists among the phases. Also, it is assumed that no reaction takes place between the sample and the material of the crucible in which the sample is contained, except where iron crucibles are used (case 4 above).

The System Fe—O.—In a binary system the situation is usually so simple that the term path of equilibrium crystallization is rarely used at all. However, for the sake of completeness and because the present system is more complicated than ordinary dry binary systems, the relationships will be discussed briefly. Under conditions of constant total composition of condensed phases (case 1) the path of equilibrium crystallization can be read from the diagram in figure 4 by following a vertical (constant composition) line from high to low temperatures. For instance, a mixture of composition 24 weight % oxygen will go through the following sequence of phase changes as heat is withdrawn from the closed system under equilibrium conditions. Above 1395°C the mixture is all liquid. At 1395°C the first traces of wüstite appear, and wüstite and liquid coexist in equilibrium over the temperature range 1395 to 1388°C. At the latter temperature the last trace of liquid disappears, and wüstite is the only condensed phase present in the interval 1388-740°C. Magnetite starts forming at 740°C, and this phase coexists in equilibrium with wüstite down to 560°C. At this temperature, corresponding to an invariant situation, the four phases wüstite, magnetite, metallic iron, gas are present together in equilibrium. Finally, below 560°C metallic iron and magnetite are the stable condensed phases. During the crystallization process the O_2 pressure changes continuously in a manner which may be read directly off the diagram in figure 4. The intersection of the vertical (constant composition) line and the O_2 isobar at any temperature gives the equilibrium O_2 pressure of the gas phase.

At constant O_2 pressure (case 2) the path of equilibrium crystallization

coincides with the O_2 isobar corresponding to the chosen O_2 pressure. As an example, consider crystallization at a constant O_2 pressure of 10^{-8} atm. Above 1626°C a metallic liquid is the only condensed phases present. At 1626° a metallic liquid and an oxide liquid coexist in equilibrium with the gas phase. Between 1626 and 1397°C liquid oxide is the only condensed phase existing under equilibrium conditions. At 1397°C liquid and crystals of wüstite and gas are present together in equilibrium. In the temperature interval 1397-1280°C wüstite is in equilibrium with the gas, and at 1280°C wüstite and magnetite coexist with the gas. From 1280 to 840° magnetite is the stable phase in an atmosphere of this O_2 pressure. At 840°C, magnetite and hematite coexist, and below 840°C hematite is in stable equilibrium with the gas. One important difference between this case and the case discussed under (1) should be emphasized: In the present case two condensed phases (such as for instance liquid and wüstite) can coexist in equilibrium only at one temperature. This is because we have "used up" one degree of freedom by choosing the O_2 pressure. Under the conditions stipulated under (1), however, no restrictions in the sense of the phase rule are imposed on the system, and two condensed phases can coexist over a temperature interval.

The third case, crystallization under conditions of constant p_{CO_2}/p_{H_2} ratios of the gas phase, is very similar to the case just discussed and needs no special description. Lines of equal p_{CO_2}/p_{H_2} ratios are paths of equilibrium crystallization under these conditions.

If the crystallization takes place in contact with metallic iron (case 4), the changes in phase assemblage can be read from the diagram (fig. 4) by following the boundary curve between metallic iron and the lowest stable oxide, from high to low temperatures. Between 1535 and 1524°C solid iron is in equilibrium with a metallic liquid and gas. At 1524°C solid iron, a metallic liquid and an oxidic liquid coexist in equilbrium with gas. Between 1524 and 1371°C liquid oxide is in equilibrium with iron and gas. In the temperature interval from 1371 to 560°C wüstite is the equilibrium condensed phase in contact with iron, and below 560°C magnetite coexists in equilibrium with iron. Again, the variation in O_2 pressure during crystallization is determined as the intersections between the O_2 isobars and the boundary curve along which iron is one of the equilibrium phases.

The System FeO—Fe_2O_3—SiO_2.—Paths of equilibrium crystallization under conditions of constant total composition of condensed phases (case 1) can be derived by methods analogous to those used for ordinary dry silicate systems. Such methods have been described in detail in many papers emanating from the Geophysical Laboratory of the Carnegie Institution of Washington.[12] The application of these principles to the system FeO—Fe_2O_3—SiO_2 has been described in detail elsewhere (Muan, 1955). Only one example will be given here for the purpose of illustrating the general relationships. The crystallization paths can be derived from diagrams showing liquidus isotherms (fig. 5), O_2 isobars along liquidus surface (fig. 6) and fractionation curves

[12] See for example Bowen's classic book (N. L. Bowen, Evolution of the igneous rocks, reprinted in 1956 by Dover Publications, Inc., New York, 332 p.)

(fig. 8) on the basis of the assumption that the total composition of condensed phases remains constant.

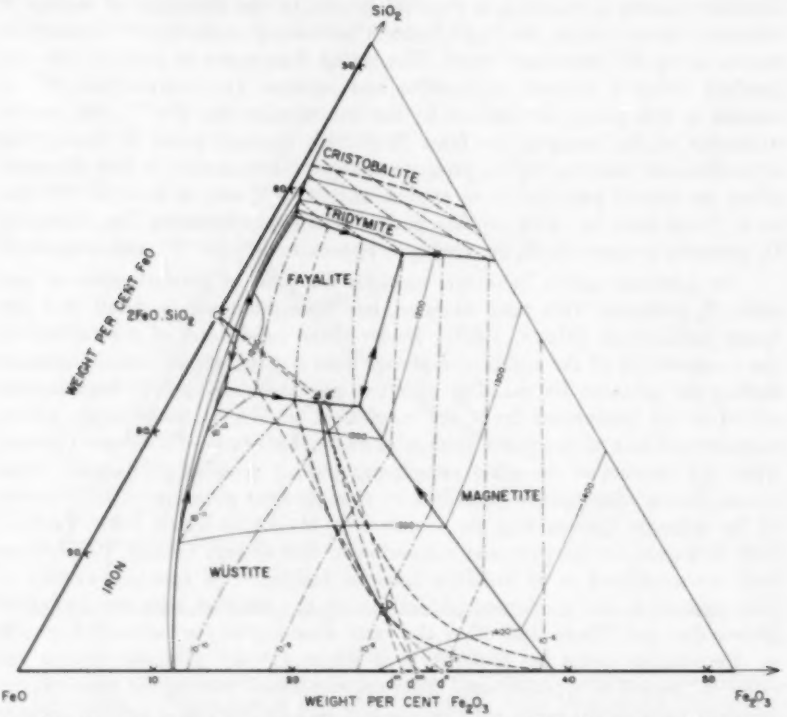

Fig. 11. Diagram of a part of the system$FeO—Fe_2O_3—SiO_2$ shown in order to illustrate paths of equilibrium crystallization under conditions of constant total composition of condensed phases. Heavy lines are boundary curves, medium solid line equilibrium crystallization curve and medium dash lines fractionation curves. Light solid lines are liquidus isotherms, light dash-dot lines O_2 isobars for points on liquidus surface, and light dash lines conjugation lines. (Diagram after Muan (1955)).

On the basis of these diagrams, paths of equilibrium crystallization for a part of the system $FeO—Fe_2O_3—SiO_2$ are shown in figure 11. Heavy lines are boundary curves. Medium dash lines are fractionation curves, medium solid lines are equilibrium crystallization curves and light dash lines are conjugation lines. Light solid lines are liquidus isotherms and light dash-dot lines are O_2 isobars.

Mixture *D* is chosen to illustrate paths of crystallization in the field of wüstite. At approximately 1370°C wüstite starts separating out and the liquid composition moves along the equilibrium crystallization curve *D-d* (mediun. solid line). The composition of the wüstite in equilibrium with liquid, determined by the tangent to the fractionation curve through the points represer'ing liquid composition, changes continuously from *d″* (31 weight % Fe_2O_3) to *d‴* (28 weight % Fe_2O_3). Fayalite starts separating out together with

wüstite from the liquid at point *d*, and the liquid composition moves along the boundary curve wüstite-fayalite towards *d'*. From the point *d* where the boundary curve is reached, a reversal occurs in the direction of change in composition of wüstite, the Fe_2O_3 content increasing as the liquid composition moves along the boundary curve. The liquid disappears at point *d'*, the end product being a mixture of fayalite and wüstite. The composition *d''''* of wüstite at this point, determined by the conjugation line *d'*-*d''''*, falls on the extension of the straight line from $2FeO.SiO_2$ through point *D*. During the crystallization process, the O_2 pressure changes continuously. It first decreases along the curved path *D*-*d* from approximately 10^{-8} atm. at *D* to $10^{-10.5}$ atm. at *d*. From here on, with fayalite and wüstite coprecipitating, the change in O_2 pressure reverses itself, increasing to approximately $10^{-10.4}$ atm. at point *d'*.

In contrast to this behavior, consider the path of crystallization at constant O_2 pressure. This case, likewise, has been discussed in detail in a previous publication (Muan, 1955). Under these conditions of crystallization, the composition of the condensed phases does not in general remain constant during the process. By reacting with the gas phase, oxygen is continuously added to or subtracted from the condensed phases as temperature varies, concomitant to a proportional change in Fe_2O_3/FeO ratio of condensed phases, while the amount of the other constituent (SiO_2) remains unchanged. These compositional changes are described by straight lines pointing to the O corner of the triangle representing the system Fe—Si—O, of which FeO—Fe_2O_3—SiO_2 is a part. In the previous discussion of this system (Muan, 1955) these lines were referred to as iso-silica lines to designate the constant amount of SiO_2 present in the condensed phases during the reaction between condensed phases and gas. These lines have the same meaning as the curves referred to as dissociation paths by Richards and White (1954). Beacuse oxygen can either be added to or subtracted from the condensed phases, the term oxygen reaction lines seems more appropriate and will be used as a general term to designate these lines in this and in future papers from this laboratory. An example of path of crystallization at constant O_2 pressure is illustrated in figure 12. Here the same line symbols have been used as before and in addition dash-cross lines are used to indicate changes in total composition of condensed phases.

In mixture *C* wüstite starts separating out at about 1350°C, and as heat is withdrawn, the liquid composition moves along the wüstite liquidus surface following the 10^{-8} atm. isobar. The wüstite composition changes continuously in a way which can be derived from the fractionation curves. These curves are not drawn in figure 12, in order to avoid the confusion caused by too many lines. When the liquid composition reaches point *c*, wüstite disappears and magnetite starts separating out with temperature remaining constant. When the last trace of wüstite disappears, the liquid composition starts moving along the magnetite liquidus surface following the 10^{-8} atm. isobar, with magnetite continuously separating out. When the boundary curve magnetite-tridymite is reached, at point *c'*, the liquid disappears, leaving as end product a mixture of magnetite and tridymite. The total composition during this

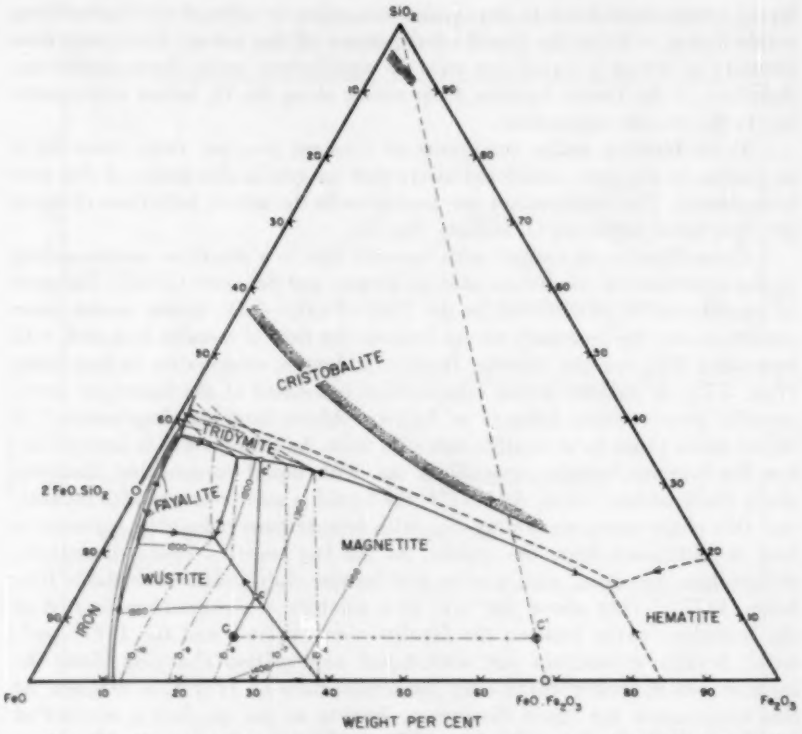

Fig. 12. Diagram of the system $FeO—Fe_2O_3—SiO_2$ shown in order to illustrate paths of equilibrium crystallization at constant O_2 pressure. In addition to the line symbols explained for fig. 11 light dash-cross lines are used to represent changes in total composition of condensed phases during crystallization, and lines with stippling on one side indicate limit of two liquid region. (Diagram after Muan (1955)).

process changes along the straight line from *C* to *C'*. The sudden discontinuous change in total composition of condensed phases as a boundary curve is reached (points *c* and *c'* in fig. 12) is analgous to the change along a horizontal line in a two phase (two *condensed* phases) region in the system Fe—O (fig. 4). This situation is caused by the requirement of disappearance of one phase before the temperature can change, due to the restrictions imposed on the system resulting from our choosing the O_2 pressure.

An O_2 isobaric section through the ternary system $FeO—Fe_2O_3—SiO_2$ is not a true binary system, because the compositions of all phases can not be represented in terms of two chosen components. However, aside from this limitation, the system can be treated like a binary system as far as the crystallization process is concerned. The liquid compositions will always be represented by points along the O_2 isobar in question, regardless of the nature of the crystalline phases separating out, whether they be pure phases or solid solution crystals. The O_2 of the atmosphere acts as a regulator to bring the

liquid composition back to its equilibrium value in spite of the crystallizing solids trying to bring the liquid compositions off the isobar. The lowest temperature at which a liquid can exist in equilibrium under these conditions, therefore, is the lowest liquidus temperature along the O_2 isobar corresponding to the chosen atmosphere.

Crystallization under conditions of constant p_{CO_2}/p_{H_2} ratio (case 3) is so similar to the case considered above that no special discussion of this case is necessary. The relationships are analogous to the above, with lines of equal p_{CO_2}/p_{H_2} ratios replacing O_2 isobars (fig. 7).

Crystallization in contact with metallic iron is a situation corresponding to the experimental conditions used by Bowen and Schairer (1932). The path of equilibrium crystallization in the $FeO—Fe_2O_3—SiO_2$ system under these conditions are the boundary curves between the field of metallic iron and, with increasing SiO_2 content, wüstite, fayalite, tridymite, cristobalite, in that order (figs. 5-7). A mixture whose composition is located at the boundary curve metallic iron—wüstite behaves as follows: Above liquidus temperatures[13] a liquid oxide phase is in equilibrium with iron. As temperature is lowered below the liquidus, wüstite crystallizes out, with liquid composition changing along the boundary curve. At 1177°C the liquid is also saturated with fayalite, and this phase starts separating out, with temperature remaining constant as heat is withdrawn from the system. As the last trace of liquid disappears, temperature decreases, with wüstite and fayalite coexisting with metallic iron below 1177°C (but above 560°C). In a mixture of composition located at the boundary curve between the fayalite composition[14] and the 1177° peritectic, fayalite crystallizes out, with liquid composition changing along the fayalite-iron boundary curve until the temperature of 1177°C is reached. At this temperature the liquid disappears, leaving as end product a mixture of fayalite and wüstite in equilibrium with metallic iron. A mixture with a composition corresponding to fayalite[14] is all liquid above 1205°C (Bowen and Schairer, 1932). At this temperature the mixture crystallizes completely to fayalite in equilibrium with metallic iron. Similarly, any mixture of composition on the SiO_2 side of the fayalite composition crystallizes to a mixture of fayalite and tridymite at the peritectic temperature of 1178°C. Fayalite is the primary crystalline phase in mixtures located between $2FeO.SiO_2$ and this peritectic, while tridymite or cristobalite is the primary phase in mixtures located between SiO_2 and the peritectic composition. The system iron oxide—SiO_2 in contact with metallic iron is not truly binary, because compositions of condensed phases can not be represented in terms of two chosen components. Aside from this limitation, however, the path of crystallization can be treated in a manner analogous to that for a binary system. The usual representation of the system in terms of a projection into the join $FeO—SiO_2$ as illustrated in figure 13, after Bowen and Schairer (1932), is therefore very instructive and quite sufficient for most purposes. It should be pointed out

[13] Liquidus temperature is used here to indicate highest temperature of stable existence of a crystalline *oxide* phase.

[14] The exact location of this composition is determined as the point of intersection between the boundary curve and the oxygen reaction line passing through the $2FeO.SiO_2$ composition point.

specifically, however, that the apparent eutectics in the join $FeO—SiO_2$ are in reality peritectics in the ternary system $FeO—Fe_2O_3—SiO_2$.

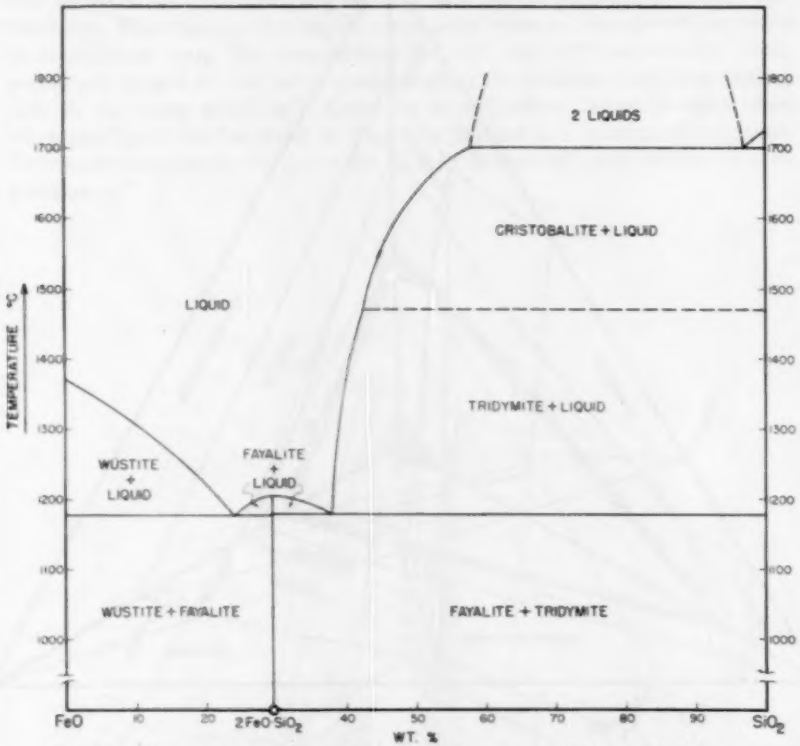

Fig. 13. Diagram illustrating phase equilibrium relationships at liquidus temperatures in the system iron oxide—SiO_2 in contact with metallic iron. The diagram has been plotted with the appearance of a binary system with FeO and SiO_2 as components. (After Bowen and Schairer (1932)).

The System MgO—FeO—Fe_2O_3—SiO_2.—Crystallization under conditions of constant total composition of condensed phases is analogous to the situation in ordinary dry oxide systems. Methods for describing path of crystallization in dry quaternary silicate systems have been discussed in the literature.[15] Applications of such methods to the system $MgO—FeO—Fe_2O_3—SiO_2$ were discussed in detail in a previous paper from this laboratory (Muan and Osborn, 1956). Suffice it here to summarize the relationships briefly: In figure 14 the system $MgO—FeO—Fe_2O_3—SiO_2$ is illustrated as a regular tetrahedron. Quaternary univariant lines along which three crystalline phases, one liquid and a gas phase coexist in equilibrium, extend through the tetrahedron from the left hand face to the right hand face. As an example of crystallization at constant total composition consider a mixture of composi-

[15] Compare footnote 12.

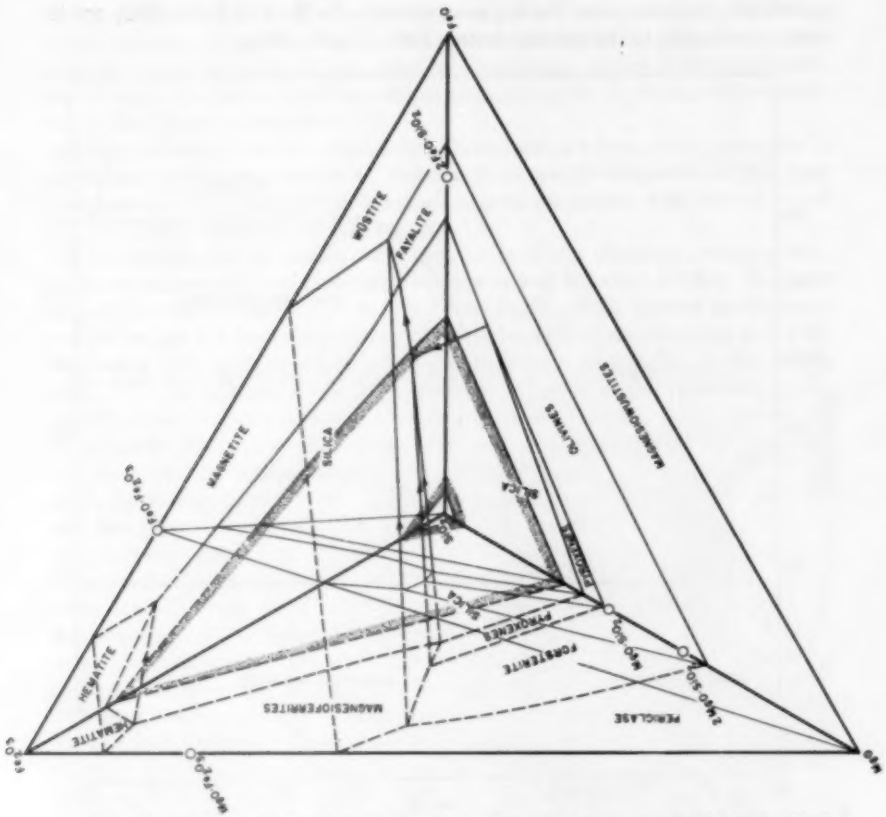

Fig. 14. Diagram illustrating phase relationships in the system MgO—FeO—Fe_2O_3—SiO_2, after Muan and Osborn (1956). The system is pictured as a regular tetrahedron with one component at each apex. Compounds, with compositions given in terms of the components, are plotted in weight per cent. The plane MgO—FeO—Fe_2O_3—SiO_2 is indicated with light solid lines. Boundary curves are drawn as medium solid lines in the base (the system MgO—FeO—SiO_2) and in the right-hand face (the system FeO—Fe_2O_3—SiO_2) and as light lines in the plane MgO—FeO.Fe_2O_3—SiO_2 (corresponding approximately to the system MgO—FeO—Fe_2O_3—SiO_2 in air). Quaternary univariant lines, extending into the tetrahedron from the bounding ternary systems, are also drawn as medium solid lines. Medium dashed lines represent inferred boundary curves in the bounding ternary systems MgO—Fe_2O_3—SiO_2 and MgO—FeO—Fe_2O_3. Medium lines with stippling on one side indicate limit of region of coexistence of two silicate liquids.

tion *c* as illustrated in figure 15. This point is located on the univariant line along which magnesioferrite, pyroxene, olivine, liquid and gas exist together in equilibrium. Immediately above liquidus temperature a liquid of composition *c* is in equilibrium with gas. At liquidus temperature, magnesioferrite (composition c′), pyroxene (composition c″) and olivine (composition c‴), start separating out, and as heat is continuously withdrawn from the system, the liquid composition changes to the right along the boundary curve from *c*

toward m. As crystallization proceeds, the three crystalline phases change compositions along the joins $MgO.Fe_2O_3$—$FeO.Fe_2O_3$, $MgO.SiO_2$—$FeO.SiO_2$, and $2MgO.SiO_2$—$2FeO.SiO_2$ respectively, and the O_2 pressure decreases continuously. When the liquid composition reaches point m, the crystalline phases in equilibrium have the compositions m', m'', and m''' respectively. These points are located so that point c, representing the constant total composition, falls in the plane m'-m''-m'''. Complete crystallization therefore takes place when the liquid reaches point m. The final product is a mixture of magnesioferrite of composition m', pyroxene of composition m'', and olivine of composition m'''.

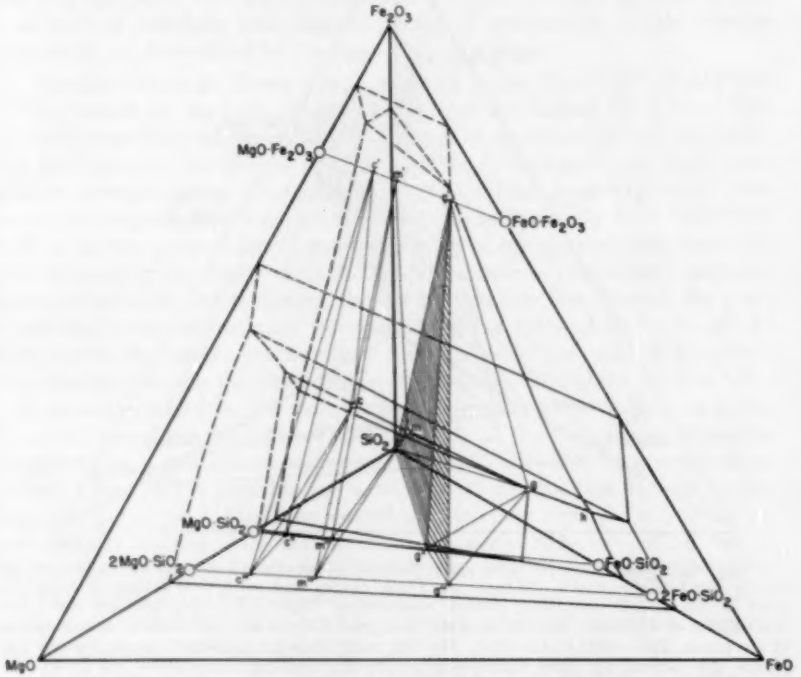

Fig. 15. Diagram to illustrate paths of equilibrium crystallization for mixtures in the system MgO—FeO—Fe_2O_3—SiO_2 under conditions of constant total composition of condensed phases. Open circles and solid dots represent compositions of liquid and crystalline phases, respectively, for mixtures whose paths of crystallization are discussed in the text. Light solid lines indicate the joins $MgO.Fe_2O_3$—$FeO.Fe_2O_3$, $MgO.SiO_2$—$FeO.SiO_2$, and $2MgO.SiO_2$—$2FeO.SiO_2$. The two shaded triangular planes are formed by lines connecting points representing compositions of crystalline phases in equilibrium with liquid at the quaternary univariant situation. (Diagram after Muan and Osborn (1956)).

A mixture located in the plane g'-g''-g''' will crystallize completely only after the liquid composition has reached point g. Here g', g'' and g''' represent compositions of magnesioferrite, pyroxene and olivine, respectively, that together with tridymite are in equilibrium with melt of composition g at the

quaternary liquidus invariant point. Thus, under conditions of constant total composition of condensed phases, the lowest temperature of liquid existence in a quaternary system is the temperature of a liquidus invariant point (eutectic or peritectic) or the temperature of that point on a quaternary univariant line representing composition of the liquid phase in equilibrium with crystalline phases whose composition points form a plane in which the composition of the original starting mixture is located.

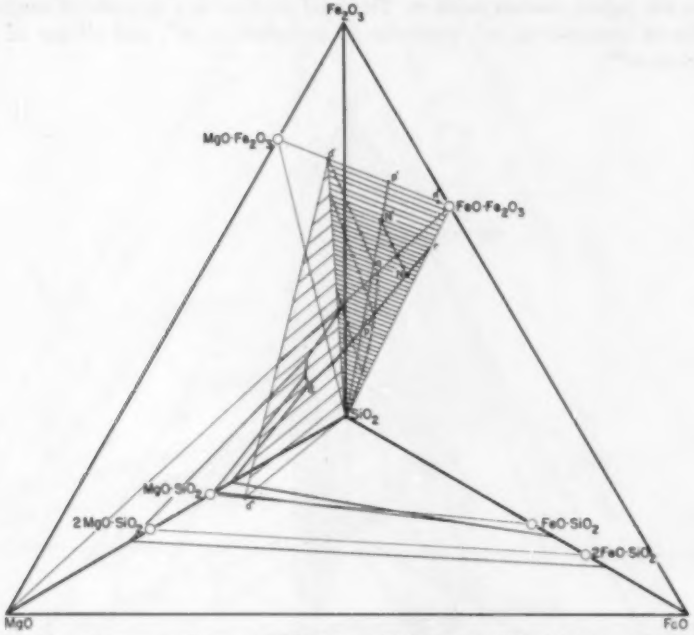

Fig. 16. Diagram to illustrate paths of equilibrium crystallization for mixtures in the system MgO—FeO—Fe_2O_3—SiO_2 in air. Open circles and solid dots represent compositions of liquid and crystalline phases, respectively. Light solid lines indicate the joins $MgO.Fe_2O_3$—$FeO.Fe_2O_3$, $MgO.SiO_2$—$FeO.SiO_2$, and $2MgO.SiO_2$—$2FeO.SiO_2$ and outlines of the plane MgO—$FeO.Fe_2O_3$—SiO_2. Medium solid lines are boundary curves. The shaded planes are formed by lines connecting points representing compositions of crystalline phases. (Diagram after Muan and Osborn (1956)).

In contrast to this behavior, consider crystallization at constant O_2 pressure, as demonstrated by a specific case illustrated in figure 16. Crystallization in air is chosen as an example, i.e. at a constant O_2 pressure of 0.21 atm. Compositions of mixtures at liquidus temperatures in air are located in an irregularly curved surface, the 0.21 atm. O_2 isobaric surface, which extends into the tetrahedron from the corresponding isobaric line in the system FeO—Fe_2O_3—SiO_2 (fig. 6). For the sake of simplicity this O_2 isobaric surface has been pictured as a plane MgO—$FeO.Fe_2O_3$—SiO_2 in figure 16. Consider a mixture of composition represented by point *N* on the boundary curve between tridymite and magnesioferrite in this plane. At the liquidus temperature for

this mixture, liquid of composition N is in equilibrium with infinitesimal amounts of tridymite (SiO_2) and magnesioferrite of composition n'. With magnesioferrite of changing composition and tridymite crystallizing out together, the liquid composition moves along the boundary curve in the surface $MgO—FeO.Fe_2O_3—SiO_2$. The total composition during this process changes along the oxygen reaction line[16] through the point of original composition from N in the direction toward N'. Complete crystallization takes place when the liquid composition reaches point p, at which point the magnesioferrite has a composition p'. This latter point is located so that a line from the silica corner to p' goes through N', the point of intersection of the oxygen reaction line with the plane $MgO.Fe_2O_3—FeO.Fe_2O_3—SiO_2$. The final product is thus a mixture of tridymite and magnesioferrite of composition p', the relative amounts being determined by the ratio $N'p'/SiO_2N'$.

Similarly it can be shown that all mixtures in the plane $MgO—FeO.Fe_2O_3—SiO_2$ located on the $SiO_2—FeO.Fe_2O_3$ side of the dashed curve from SiO_2 to q will crystallize completely to a mixture of magnesioferrite and tridymite. The significance of the dashed line SiO_2-q is the following: As the liquid composition changes along the tridymite-magnesioferrite boundary curve from r to d, the magnesioferrite composition changes continuously from $FeO.Fe_2O_3$ to d' (d' is the composition of magnesioferrite in equilibrium with liquid d). For mixtures in the $MgO—FeO.Fe_2O_3—SiO_2$ plane to crystallize completely to magnesioferrite and tridymite, the oxygen reaction line through the point of starting composition must intersect the plane $SiO_2—FeO.Fe_2O_3—d'$. In other words, the oxygen reaction lines through the SiO_2 d' edge of this plane, when cutting through the plane $MgO—FeO.Fe_2O_3—SiO_2$ along the line SiO_2-q, separate the mixtures into two groups with respect to crystallization paths. Mixtures located on the $SiO_2—FeO.Fe_2O_3$ side of the line SiO_2-q crystallize completely to a mixture of magnesioferrite and tridymite at a temperature corresponding to the liquidus for a mixture of composition located on the boundary curve $r—d$. Mixtures located on the other side of the line SiO_2-q have oxygen reaction lines that intersect the plane $SiO_2—d'—d''$, d'' being the composition of the pyroxene in equilibrium with liquid of composition d. The final product for these mixtures, therefore, is magnesioferrite, tridymite and pyroxene, and the last trace of liquid disappears at the liquidus temperature for a mixture of composition d.

Noteworthy among the relationships explained above is the fact that the liquid composition during crystallization remains in the 0.21 atm. O_2 surface (here pictured as the plane $MgO—FeO.Fe_2O_3—SiO_2$). The reason for this is the same as explained for $FeO—Fe_2O_3—SiO_2$. The O_2 of the atmosphere compensates for the tendency of the crystallizing solid phases to push the liquid composition out of the isobaric surface. Hence, at constant O_2 pressure, a liquid phase can never exist in equilibrium at a temperature lower than the lowest liquidus temperature in the O_2 isobaric surface corresponding to the chosen atmospheric conditions. This temperature is usually that correspond-

[16] The oxygen reaction lines have a direction pointing towards the O apex of the tetrahedron representing the system Mg—Fe—Si—O, and have the same significance as the corresponding lines for the system $FeO—Fe_2O_3—SiO_2$ (compare page 194).

ing to the intersection between the O_2 isobaric surface and a quaternary univariant line. Only on the O_2 isobaric surface which passes through the point representing composition of the liquid at a quaternary liquidus invariant situation will a liquid phase exist in equilibrium with four crystalline phases at the temperature of this situation. The isobaric surfaces are not true ternary systems, because the compositions of the phases can not be represented by three components. However, in spite of this limitation, in the derivation of paths of equilibrium crystallization at constant O_2 pressure, they can be treated like ternary systems.

The crystallization process at constant CO_2/H_2 ratios requires no detailed discussion. The relationships are analogous to above, with lines of equal CO_2/H_2 ratios replacing the O_2 isobars.

The paths of equilibrium crystallization of mixtures in the system MgO—FeO—Fe_2O_3—SiO_2 in contact with metallic iron can be derived by methods analogous to those described for the systems Fe—O and FeO—Fe_2O_3—SiO_2. The small primary field of metallic iron in the FeO—Fe_2O_3—SiO_2 system (figs. 5-7) extends as a thin phase volume into the tetrahedron MgO—FeO—Fe_2O_3—SiO_2, adjacent to the basal plane MgO—FeO—SiO_2. This phase volume was left out of figures 14-16 in order to simplify the drawings. A pure iron oxide liquid in contact with metallic iron contains approximately 10 weight % Fe_2O_3[17] at liquidus temperature. As SiO_2 is added, the Fe_2O_3/FeO ratio of the liquid in equilibrium with iron (see boundary curve between metallic iron and oxide phases in figs. 5-7) decreases. The decrease is caused by the increase in acidity[18] of the liquid as SiO_2 content increases. This effect more than balances the opposite effect on Fe_2O_3/FeO ratio of the decrease in liquidus temperatures caused by the first SiO_2 additions. As more SiO_2 is added, liquidus temperatures vary relatively little with SiO_2 content in the region where fayalite ($2FeO.SiO_2$) is the primary crystalline phase. When the liquid becomes saturated with SiO_2, liquidus temperatures rise sharply as SiO_2 content increases. This increase in liquidus temperatures magnifies the acidity effect of SiO_2 on Fe_2O_3/FeO ratios, and hence the boundary curve between metallic iron and cristobalite approaches the join FeO—SiO_2 as the temperature of melting of iron is reached. As MgO is added to silica-iron oxide mixtures, the basic character of MgO may be expected to increase the Fe_2O_3/FeO ratio of the liquid phase. However, the MgO addition at the same time raises liquidus temperatures very markedly. The Fe_2O_3 content of liquids in equilibrium with metallic iron is therefore very low for all compositions in the system MgO—iron oxide—SiO_2 except those close to the iron oxide apex of the tetrahedron representing the system. The relationships can be seen quantitatively from the analytical data of Bowen and Schairer (1935). The Fe_2O_3 content is less than 2 weight % for most compositions, and hence

[17] According to Darken and Gurry (1946) the Fe_2O_3 content is 8.22 weight %, while Bowen and Schairer (1932) give a value of 11.56 weight %.

[18] A quantitative acid-base scale is not available for melts like we have for aqueous solutions. The term acid is used here to describe the behavior of an ion of high field strength (Si^{4+}), in accordance with modern concepts of acid-base relationships in oxide systems (Weyl, 1956).

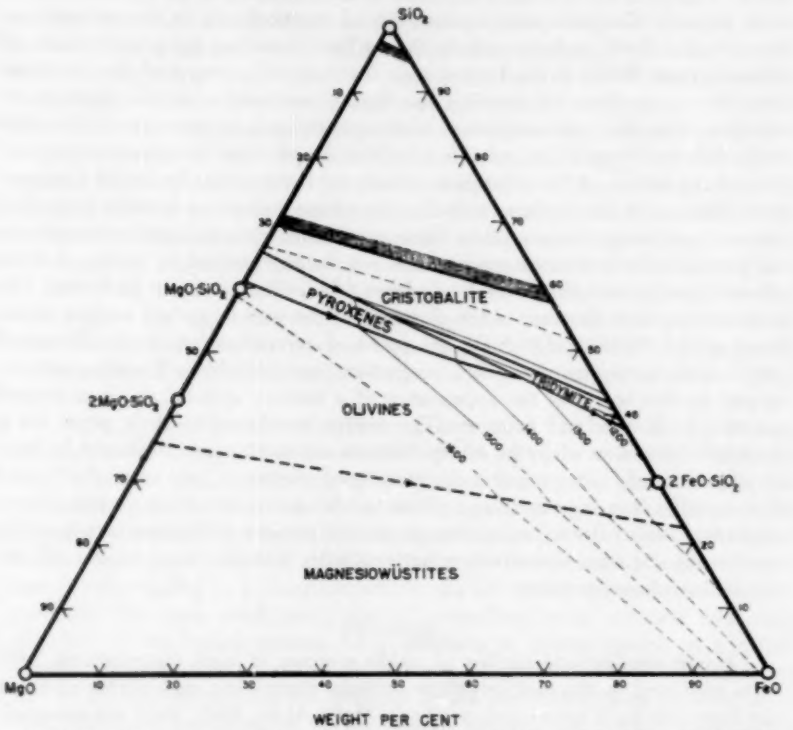

Fig. 17. Diagram illustrating phase relationships in the system MgO—FeO—SiO_2, after Bowen and Schairer (1935). Heavy lines are boundary curves with arrows pointing in the directions of falling temperatures. Light solid lines are liquidus isotherms at 100°C intervals. Boundary curves and liquidus isotherms are dashed in regions where liquidus data were not obtained. Medium lines with stippling on one side indicate limit of two-liquid region.

the iron phase volume extends only as a very thin slice into the tetrahedron of figures 14-16, adjacent to the basal plane.

It will be recalled that in the system FeO—Fe_2O_3—SiO_2 the path of crystallization for mixtures in contact with metallic iron was the boundary curve between metallic iron and the adjacent phase areas. In the present case, similarly, liquid compositions during crystallization must remain in the boundary surface between the primary phase volume of metallic iron and the adjacent phase volumes in the quaternary system, magnesio-wüstite, olivine, pyroxene, tridymite, cristobalite, depending on composition of the mixture. Projections of these phase volumes are indicated in figure 17, which is a reproduction of the system MgO—"FeO"—SiO_2 after Bowen and Schairer (1935). Their diagram is obtained by projecting actual compositions of mixtures located along the boundary surface limiting the iron phase volume, into the base (MgO—FeO—SiO_2) of the tetrahedron representing the MgO—

$FeO—Fe_2O_3—SiO_2$ system. Analogous to the situation in an O_2 isobaric section through the quaternary system, liquid compositions in the present case remain in a fixed surface, namely the surface bounding the phase volume of metallic iron. While in the former case reaction with oxygen of the gas phase was the mechanism for keeping the liquid composition in the appropriate surface, the same is accomplished in the present case by reaction of the oxide melt with the iron of the crucible in which the mixture is contained. Regardless of the nature of the crystalline phases separating out, the liquid composition remains in the surface bounding the phase volume of metallic iron. The system is not truly ternary under these conditions, because liquid compositions in the irregularly curved surface can not be represented in terms of three chosen components. However, aside from this limitation it can be treated like a ternary system. Because of the closeness of the iron boundary surface to the basal plane, $MgO—FeO—SiO_2$, the paths of crystallization can be discussed very satisfactorily in terms of a projection into this plane. The diagram obtained in this way has the appearance of a ternary system, and was treated as such by Bowen and Schairer. The reader is referred to their paper for a detailed discussion of paths of equilibrium crystallization. It should be kept clearly in mind, however, that the condensed phases contain some Fe^{3+}, and that metallic iron is present as a phase in addition to the oxide phases. Hence apparent ternary invariant situations in the projected diagram are actually quaternary liquidus invariant situations with metallic iron as one of the crystalline phases present.

SUMMARY

Phase equilibrium studies of oxide systems at high temperatures have been restricted in the past largely to systems containing only oxides of noble gas type ions such as for instance CaO, MgO, Al_2O_3, SiO_2. Data are essentially lacking on oxide systems involving elements where changes in oxidation states occur. The study of the latter systems is complicated because the composition of the gas phase must be controlled carefully and varied between wide limits. At reasonably high levels of O_2 pressures (1 atm.—10^{-3} atm.) such equilibria may be studied experimentally in O_2 atmospheres where the desired pressure is adjusted by vacuum techniques or by mixing O_2 with an inert gas. When the partial pressure of O_2 becomes low ($<10^{-3}$ atm.) the gas phase is so diluted in O_2 that a very substantial volume of gas would be necessary to change the composition of the condensed phases to the equilibrium value. With a moderate rate of flow of gas through the furnace in which the equilibrium study is made, it is therefore not possible to reach equilibrium within a reasonable period of time. In such cases indirect methods of obtaining the desired O_2 pressure must be used. The most convenient method is to use a mixed gas system containing an O_2 bearing species which upon heating dissociates under liberation of O_2. Convenient gases for this purpose are CO_2 or H_2O. The degree of dissociation and hence the O_2 pressure may be controlled by mixing CO or H_2 with the gas in controlled proportions.

Most of the few available phase diagrams for oxide systems involving changes in oxidation states are very incomplete. In addition to the usual

representation of composition of condensed phases such diagrams should contain information regarding the equilibrium composition of the gas phase as well. It is suggested that binary systems be represented in an usual composition-temperature diagram with O_2 isobars or lines of equal CO_2/H_2 equilibrium ratios superimposed to indicate gas composition. In ternary systems showing phase relationships at liquidus temperatures the ordinary projection of liquidus surface with liquidus isotherms should be supplemented by diagrams showing O_2 isobars (or lines of equal p_{CO_2}/p_{H_2} ratios) along the liquidus surface and fractionation curves. Quaternary systems are difficult to represent graphically. Phase relationships at liquidus temperatures are best illustrated by projecting compositions from their actual locations in irregularly curved O_2 isobaric surfaces into chosen planes. In the resulting diagrams, which have the *appearance* of ternary systems, the actual compositions of mixtures are indicated by lines of equal ratios (MeO_x/MeO_y) of the oxides of the element with changing oxidation state (such as for instance Fe_2O_3/FeO).

Path of equilibrium crystallization is a term used for the continuous description of changes in phase assemblage taking place as heat is withdrawn from a system and equilibrium is maintained among the phases during the process. Iron oxides and iron oxide containing silicates are chosen as examples of paths of equilibrium crystallization in systems where changes in oxidation states occur. Four idealized conditions of crystallization are considered, each one corresponding to a situation which can be closely approximated experimentally. The first condition is that of crystallization at constant total composition of condensed phases. This situation is approximated in a closed system when the volume of the gas phase is small. The path of crystallization can be derived by well known methods by the use of diagrams showing liquidus isotherms, fractionation curves and O_2 isobars. The second condition is crystallization at constant O_2 pressure. In this case the criteria used for derivation of crystallization path in ordinary dry silicate systems are not applicable, because total composition of condensed phases does not in general remain constant. By reaction with the gas phase oxygen is added to or subtracted from the condensed phases concomitant to a proportional change in the oxide ratio MeO_x/MeO_y. This composition change is described by oxygen reaction lines, which are straight lines pointing towards the O apex of the model representing the system in question. By choosing the O_2 pressure, we have "used up" one degree of freedom, and the system possesses one degree of freedom less than in the first case considered, for the same number of phases present. In a binary system, therefore, two condensed phases, such as for instance one crystalline and one liquid phase, can coexist only at one temperature at a chosen O_2 pressure. In a ternary system the O_2 isobars along the liquidus surface are the paths along which the liquid composition changes during crystallization. The lowest temperature of stable existence of a liquid phase is usually the intersection between a boundary curve and the O_2 isobar in question. In a quaternary system, similarly, the liquid composition remains in the particular O_2 isobaric liquidus surface corresponding to the chosen O_2 pressure. The lowest temperature of liquid formation under equilibrium con-

ditions is usually the intersection between a quaternary liquidus univariant line and the O_2 isobaric surface in question.

Crystallization under conditions of constant p_{CO_2}/p_{H_2} ratio is analogous to the case above, with p_{CO_2}/p_{H_2} ratios replacing the O_2 pressures in the discussion.

When crystallization takes place in contact with metallic iron, the liquid composition is forced to move along the boundary surface (or boundary curve) between the phase volume (area) of metallic iron and the adjacent oxide phase volumes (areas). In a binary system liquid oxide and a crystalline oxide phase can coexist in equilibrium with iron at one temperature only. In a ternary system the lowest temperature of stable existence of an oxide liquid is usually the temperature of a liquidus invariant situation where metallic iron is one of the phases present. In a quaternary system the lowest temperature of liquid formation, likewise, is usually the temperature of one of the quaternary liquidus invariant situations where metallic iron is one of the phases present.

ACKNOWLEDGMENTS

The ideas presented in this paper resulted mainly from studies of phase equilibria in oxide systems carried out in College of Mineral Industries, The Pennsylvania State University, as part of a research project sponsored by American Iron and Steel Institute. The author wishes to acknowledge the many stimulating discussions of the subject with E. F. Osborn.

REFERENCES

Bowen, N. L., and Schairer, J. F., 1932, The system FeO—SiO_2: Am. Jour. Sci., v. 24, p. 177-213.

———, 1935, The system MgO—FeO—SiO_2: Am. Jour. Sci., v. 29, p. 151-217.

Brewer, Leo, 1953, The thermodynamic properties of the oxides and their vaporization process: Chem. Reviews, v. 52, p. 1-75.

Chipman, John, and Marshall, Shadburn, 1940, The equilibrium $FeO + H_2 = Fe + H_2O$ at temperatures up to the melting point of iron: Am. Chem. Soc. Jour., v. 62, p. 299-305.

Coughlin, J. P., 1954, Contributions to the data on theoretical metallurgy. XII. Heats and free energies of formation of inorganic oxides: U. S. Bureau of Mines, Bull. 542.

Darken, L. S., and Gurry, R. W., 1945, The system iron-oxygen. I. The wüstite field and related equilibria: Am. Chem. Soc. Jour., v. 67, p. 1398-1412.

———, 1946, The system iron-oxygen. II. Equilibrium and thermodynamics of liquid oxide and other phases: Am. Chem. Soc. Jour., v. 68, p. 798-816.

Emmett, P. H., and Shultz, J. F., 1930, Equilibria in the Fe—H—O system. Indirect calculation of the water gas equilibrium constant: Am. Chem. Soc. Jour., v. 52, 4268-85.

Harker, R. I., and Tuttle, O. F., 1956, Experimental data on the P_{CO_2}-T curve for the reaction: Calcite + quartz = wollastonite + carbon dioxide: Am. Jour. Sci., v. 254, p. 239-256.

Harker, R. I., and Hutta, J. J., 1956, The stability of smithsonite: Econ. Geology, v. 51, p. 375-381.

Muan, Arnulf, 1955, Phase equilibria in the system FeO—Fe_2O_3—SiO_2: AIME Trans., v. 203, p. 965-967, Jour. Metals, Sept., 1955.

———, 1957a, Phase equilibria at liquidus temperatures in the system iron oxide—Al_2O_3—SiO_2 in air atmosphere: Am. Ceram. Soc. Jour., v. 40, p. 121-133.

———, 1957b, Phase equilibrium relationships at liquidus temperatures in the system FeO—Fe_2O_3—Al_2O_3—SiO_2: Am. Ceram. Soc. Jour., v. 40, p. 420-431.

Muan, Arnulf, and Gee, C. L., 1956, Phase equilibrium studies in the system iron oxide—Al_2O_3 in air and at 1 atm. O_2 pressure: Am. Ceram. Soc. Jour., v. 39, p. 207-214.

Muan, Arnulf, and Osborn, E. F., 1956, Phase equilibria at liquidus temperatures in the system MgO—FeO—Fe_2O_3—SiO_2: Am. Ceram. Soc. Jour., v. 39, p. 121-140.

Richards, R. G., and White, J., 1954, Phase relationships of iron-oxide containing spinels. Part I. Relationships in the system Fe—Al—O: Brit. Ceram. Soc. Trans., v. 53, p. 233-270.

Schuhmann, R., Jr., Powell, R. G., and Michal, E. J., 1953, Constitution of the FeO—Fe_2O_3—SiO_2 system at slag-making temperatures: AIME Trans., v. 197, p. 1097-1104; Jour. Metals, Sept., 1953.

Weyl, W. A., 1956, Acid-base relationship in glass systems. A new acid-base concept applicable to aqueous systems, fused salts, glasses, and solids: The Glass Industry, v. 37, p. 264-269, 286, 288, 325-331, 336, 344, 346, 350.

College of Mineral Industries
The Pennsylvania State University
University Park, Pennsylvania

[American Journal of Science, Vol. 256, March 1958, P. 208-218]

GROUP OPERATOR VARIANCE IN MORPHOMETRIC WORK WITH MAPS

RICHARD J. CHORLEY

ABSTRACT. Two groups of inexperienced operators delimited and measured certain linear, areal and slope aspects of the morphometry of seven drainage basins, exhibited on topographic maps on a scale of 1:25,000. A statistical comparison of the combined group results shows that there is no significant difference between the mean values of the lengths, areas and channel gradients of second and third order streams obtained by each group, nor between the mean drainage densities. The only important source of individual and group variation which appeared lay in the recognition of first order stream channels.

The application of statistical methods to the study of the geometry of landscape (Strahler, 1954) has made it necessary that relatively large samples of the values of particular morphometric units (e.g. stream lengths, basin areas, maximum valley-side slopes, etc.) be amssed before regions can be quantitatively described and before certain inter and intra-regional relationships can be established. The number of variates in each sample must often run into the hundreds, and this has created a purely mechanical sampling problem both for field workers and for those who carry out morphometric work with maps or aerial photographs. In the latter connection, it is interesting to determine the reliability of measurements made by operators with a minimum of experience and whether different operators obtain similar results in measuring identical landscape features. This paper concerns a comparison of the work of two groups of inexperienced operators, the members of which measured similar morphometric features from the same maps of identical drainage basins.

Fourteen students, including seniors and graduate students, were given class instruction in the delimitation and measurement of landscape features from topographic maps, together with less than one hour of training in the operation of the chartometer and compensating polar planimeter. They were then allowed to divide themselves into two groups of seven students each, meeting at different times, and each group was assigned the maps of seven different drainage basins with which to work. It was purely by chance that the two graduate students and, generally, a majority of the better students in geomorphology elected to attend at the same time, forming Group 2. Each operator within each group was therefore concerned with a different drainage basin, but the two groups were each working with the same seven basins. Each operator worked independently and, more important, the two groups were physically separated.

The drainage basins used were six fourth order and one third order, all located on the Dartmoor granite of Devon County, England, and depicted on Ordnance Survey 1:25,000 maps (Nos. 20/ 57, 58, 66, 67, 68, 76, 77 and 78).

Apart from a minimum of initial individual assistance in drawing drainage lines and watershed divides, each operator was left to delimit the morphometric features as he saw fit and to develop his own standards of accuracy of measurement. The principles of recognising first, second, third and fourth order stream segments and basin areas were based on those

modifications of Horton's method (1945, p. 281-283) established by Strahler (1952, p. 1120), as illustrated by Miller (1953, fig. 12). In this revised method, fingertip tributaries represent first order streams and a junction of two streams of the same order begins a stream segment of the next higher order. When the measurements were complete, the final results of each group were combined, and comparisons of the data collected by each group were made.

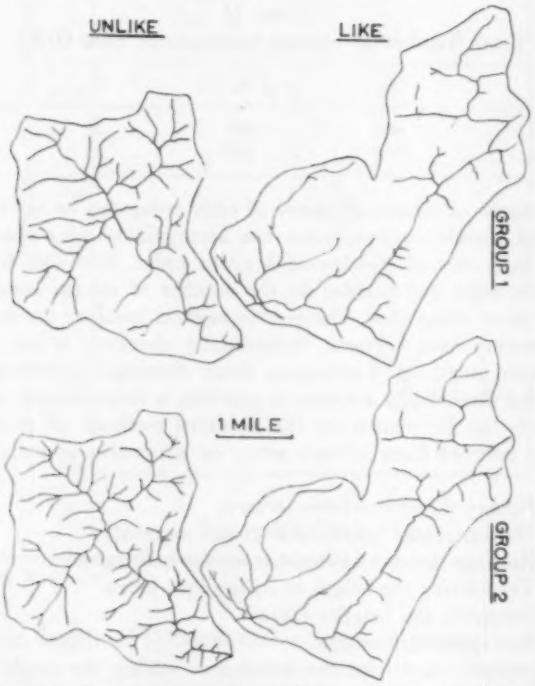

Fig. 1. The most unlike and like interpretations of stream channel networks by members of the two groups.

Table 1 shows the total number of stream segments of each order recognised by each group. The greatest discrepancy between the discrimination of the two groups is to be found in their recognition of finger-tip (first order) tributaries. The delimitation of first order streams involves a most subjective element of determining what constitutes a significant crenulation in a contour line, thereby determining the location and extent of a headwater gully. All operators continued their finger-tip tributaries headward to the highest contour which, in their individual estimation, contained a significant, aligned crenulation. Despite variation in the interpretation of first order stream segments, with Group 2 being apparently more assiduous in the search for headwater gullies (fig. 1), it is instructive to note that the total number of second order stream segments recognized by each group was identical, and that there

was only a difference of one in third orders. This similarity of results between the two groups can be tested statistically by applying an analysis of covariance (Walker and Lev, 1953) to determine whether the two sets of numbers of stream segments are best fitted by two separate regressions or by a single common line (fig. 2). In this instance the F ratio ($F = .37 < F_{.95} = 7.71$) indicates that the hypothesis of a common regression line, with a regression coefficient of – .633, should be accepted.

TABLE 1
Total Number of Stream Segments of each Order

	N_1	N_2	N_3	N_4
Group 1.	405	107	21	6
Group 2.	508	107	22	6

Mean lengths of stream segments of each order can be calculated in two different ways. Firstly, each operator can accumulate on the chartometer the total length in inches of streams of a given order, then this figure can be translated into miles and divided by the number of stream segments of that order which were recognised. The second method involves the more arduous task of measuring each segment, individually changing it into miles, summing the stream lengths and averaging them. Although the second method is to be preferred statistically because it provides a large sample of individual variates which can be treated by the standard methods of group statistics, there are six sources from whence error or subjective approximation may enter:

a. Setting the chartometer to zero.
b. Measuring the length of a stream segment.
c. Reading the measurement from the instrument.
d. Translating the length in inches into miles.
e. Summing the lengths.
f. Averaging the lengths.

In the first method; except for the initial zero setting, the single final instrument reading and the single calculation of total length inches into miles; sources a, c, d, and e are virtually eliminated, and for this reason it would seem that this method should produce the more accurate and consistent mean stream lengths.

Table 2 indicates the total stream lengths obtained by the first method, and these have been averaged to give the mean stream lengths which are listed in table 3.

TABLE 2
Total Length of Stream Segments of each Order, in Miles

	ΣL_1	ΣL_2	ΣL_3	ΣL_4
Group 1.	111.90	45.08	35.97	18.80
Group 2.	129.93	47.31	35.39	18.29

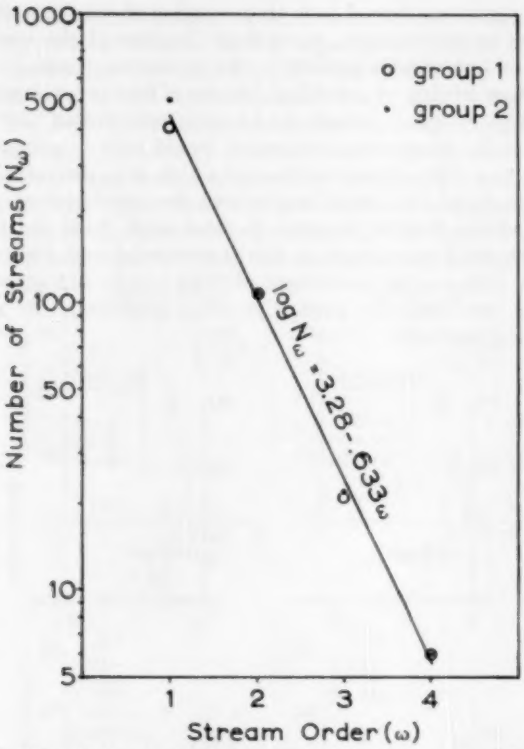

Fig. 2. Numbers of stream segments recognized by each group used to illustrate the Law of Stream Numbers.

TABLE 3

Mean Length of Different Order Stream Segments, in Miles

	First Method.		Second Method	
Order.	Group 1.	Group 2.	Group 1.	Group 2.
1	.276	.256	—	—
2	.421	.442	.400	.438
3	1.713	1.609	1.749	1.562
4	3.133	3.048	3.123	3.202

From the first, and in any case possibly the more accurate, method it is apparent that the mean length of first order stream segments shown on this scale of map of the Dartmoor region is about a quarter of a mile. The conventional chartometers which are economically available for class use have, as their finest graduation, divisions of one-half inch (representing, on this scale, approximately .200 miles); and are difficult to read with consistent ac-

curacy to within closer than .1 inch (representing about one sixth of the mean length of first order streams), particularly because of the small amount of 'play' which is unavoidably present in the measuring wheel. It seems, therefore, that the measuring of individual lengths of first order streams, the mean length of which is small enough to be only comparable with the smallest graduation on the measuring instrument, would introduce into the morphometric work just that subjective element which it is desirable to eliminate. The measurement of individual lengths and the calculation of means by the second method was limited therefore to the second, third and fourth orders, most of which are long enough so that instrumental and dial-reading errors could involve only a small percentage of their length, and which, in the first two instances, are numerous enough to admit confidently the application of group statistical methods.

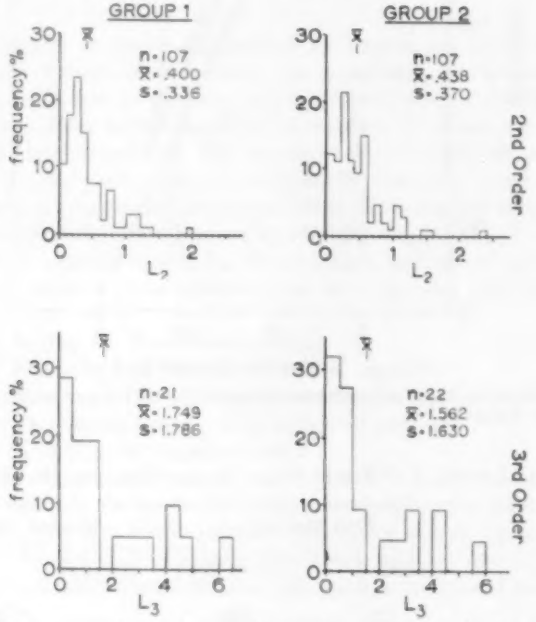

Fig. 3. Histograms of second and third order stream lengths for each group (in miles).

The results of these individual measurements by each group were combined (fig. 3) and strikingly exhibited the right skewness noted by Miller (1953) as characteristic of the frequency distributions of stream lengths and basin areas. As he suggested, this skewness was corrected by plotting the logarithms of stream lengths (fig. 4)—actually of one hundred times each individual length to avoid the use of negative logarithms. In order to test the normality of these logarithmic distributions, a chi-square test (Croxton and Cowden, 1939) was run on the distribution which seemed least obviously

normally distributed (the lengths of third order streams measured by Group 1), employing the conventional level of significance (P) of .05 (5%). This test resulted in a value of χ^2 of 2.19, indicating that, within the three degrees of freedom used, a normal curve is a good description of the frequency distribution ($.50<P<.70$). This precaution was necessary because, in order to employ simple tests of similarity between mean values, it must be shown that the samples are representative of normally distributed populations and that the variances—here represented by the standard deviations (S)—of the samples, the means of which are to be compared, are similar. The above chi-square test and visual inspection of the corresponding standard deviations of

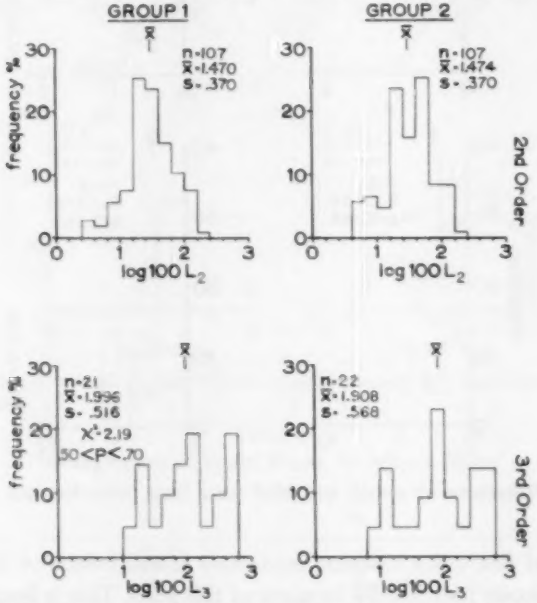

Fig. 4. Histograms of the logarithmic values of second and third order stream lengths for each group.

the two groups (fig. 4) indicate that both these conditions are satisfied and, again using a level of significance of .05, 't' tests were made comparing the means of the logarithmic values of second and third order stream lengths between Groups 1 and 2. The statistic 't', the calculation of which involves the arithmetic means, numbers of variates and a pooled standard deviation of two samples, enables one to determine the probability (P) that the observed difference between the two arithmetic means in question, either being the larger, with repeated sampling is due to chance sampling alone and does not represent a significant difference between the two populations from which the samples were drawn. Comparing, in this way, the means of the logarithmic values of second order ($P>.90$) and third order ($.50<P<.60$) stream lengths between the two groups, it was apparent—employing a critical level

of significance of .05—that there is no significant difference between the means of the logarithmic values of stream lengths of corresponding order between Groups 1 and 2 (fig. 4).

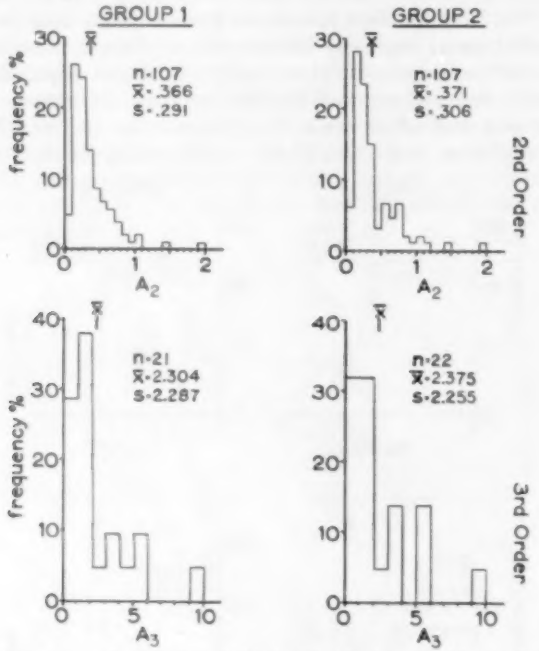

Fig. 5. Histograms of second and third order basin areas for each group (in sq. miles).

Areas of first order basins in landscapes of this texture of dissection are difficult to obtain individually on maps of this scale. This is because of their difficulty of delimitation on the map, either because they are so small or because the drawing of watershed lines on almost plane slopes becomes a highly subjective matter. Each group, however, delimited and measured individually the areas of second, third and fourth order basins; the composite mean values appearing in table 4 and frequency distributions for the second and third orders in figure 5. These distributions are strongly right-skewed and, as with the stream lengths, normal distribution were obtained by using the logarithms of the areas (fig. 6). A chi-square test on the logarithms of third order areas obtained by Group 2 showed them to be normally distributed ($.20<P<.30$). 't' tests revealed no significant difference between the means of the logarithmic distributions obtained by each group for either the second order basins ($P>.90$) or those of third order ($P>.90$).

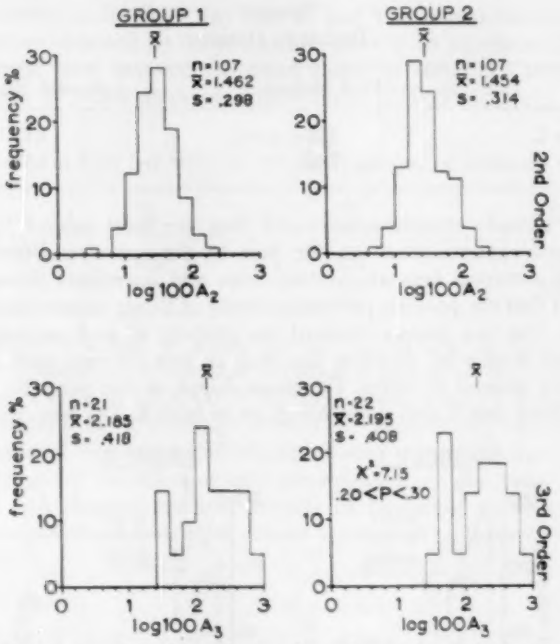

Fig. 6. Histograms of the logarithmic values of second and third order basin areas for each group.

TABLE 4

Mean Values of Basin Areas, in Square Miles

	$\overline{A_1}$	$\overline{A_2}$	$\overline{A_4}$
Group 1.	.366	2.304	9.623
Group 2.	.371	2.375	9.645

The most important morphometric measure involving both linear and areal aspects is the drainage density. For the region under investigation this was calculated in two ways (table 5). The first method was to take the mean of the seven calculated drainage densities for each group of seven individual drainage basins; the second, to divide the total measured length of channels in all seven basins by the sum of the seven basin areas, for each group. Naturally, whichever method was employed, the greater number of first order streams recognised by Group 2 resulted in a larger drainage density calculated by that group. A 't' test involving small samples (Croxton and Cowden, 1939, p. 329), however, showed no significant difference ($.30<P<.40$) between the means of the drainage densities calculated by the first method.

Slope aspects of topography are generally the most difficult and refined of morphometric measures to obtain from maps, involving as they do both

TABLE 5
Drainage Density

	First Method.	Second Method.
Group 1.	3.24	3.17
Group 2.	3.52	3.45

linear and altitude considerations; and they are most subject to error, inaccuracy and approximation on the part of the operator. Often one must estimate an elevation between contour lines and sometimes linear distances are so short that the possible percentage error of linear measurement becomes quite large. The two groups obtained the gradient of each second, third and fourth order stream by dividing the drop in feet between each end by the length of the channel in miles. The mean slopes, in feet per mile, of streams of second, third and fourth order are given in table 6. The frequency distribu-

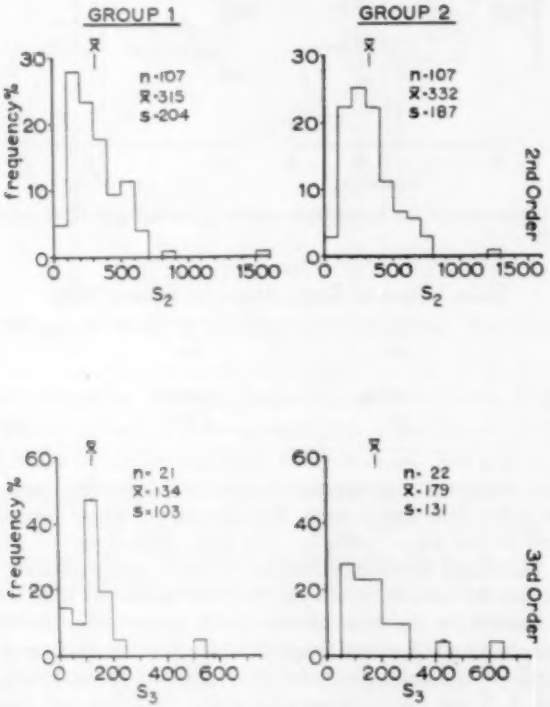

Fig. 7. Histograms of second and third order channel mean slopes for each group (in feet per mile).

tions of these slopes (fig. 7) show a pronounced right-skewness, which contrasts with the normal distribution of valley-side slopes (Strahler, 1950).

This was corrected in the usual way (fig. 8) and 't' tests between the logarithmic distributions obtained by the two groups showed no significant difference at the 5 percent level between the mean slopes of either the second order stream channels ($P>.90$) or those of third order ($.20<P<.30$).

TABLE 6

Mean Slopes, in Feet per Mile, of Stream Segments of Different Order

	$\overline{S_2}$	$\overline{S_3}$	$\overline{S_4}$
Group 1.	315	134	124
Group 2.	332	179	126

The conclusion which one would seem to be able to draw from the above preliminary investigation of operator variance in morphometric work is that, using maps on a scale of 1:25,000 of drainage basins having a texture of dissection represented by a drainage density of about 3.50, two groups of relatively unskilled operators collectively showed no significant difference between their group delimitation and measurement of the mean values of linear, areal and channel gradient aspects of landscape geometry—except where the recognition of first order stream segments was concerned.

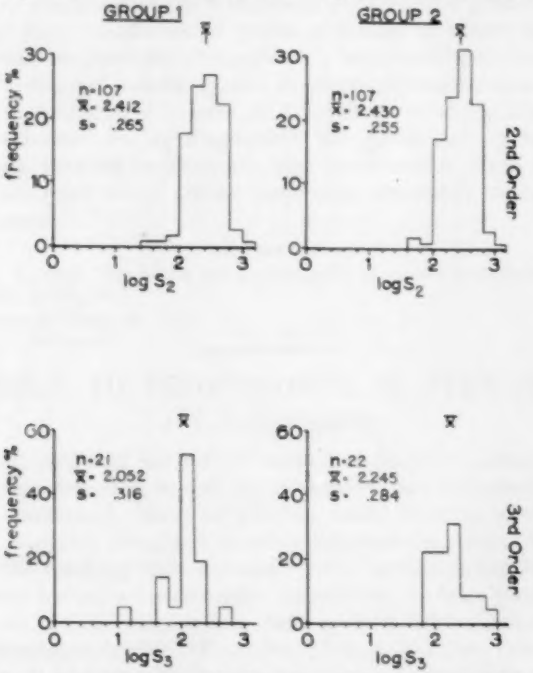

Fig. 8. Histograms of the logarithmic values of second and third order channel mean slopes for each group.

References

Croxton, F. E., and Cowden, D. J., 1939, Applied general statistics: New York, Prentice-Hall, Inc., 944 p.

Horton, R. E., 1945, Erosional development of streams and their drainage basins; hydrophysical approach to quantitative morphology: Geol. Soc. America Bull., v. 56, p. 275-370.

Miller, V. C., 1953, A quantitative study of drainage basin characteristics in the Clinch Mountain area, Virginia and Tennessee: Dept. of Geology, Columbia Univ., New York, Technical Rept., No. 3, Office of Naval Research, Contract N60NR 271-30.

Strahler, A. N., 1950, Equilibrium theory of erosional slopes approached by frequency distribution analysis: Am. Jour. Sci., v. 248, p. 673-698 and 800-814.

————, 1952, Hypsometric (area-altitude) analysis of erosional topography: Geol. Soc. America Bull., v. 63, p. 1117-1142.

————, 1954, Statistical analysis in geomorphic research: Jour. Geol., v. 62, p. 1-25.

Walker, H. M., and Lev, J., 1953, Statistical inference: New York, Henry Holt, 501 p.

Geology Department
Brown University
Providence, Rhode Island

DISCUSSION

THE NOMENCLATURE OF EVAPORITE TEXTURES

F. H. STEWART

In a recent paper, Dr. J. T. Greensmith (1957) has suggested a number of new names for evaporite grains and textures, for which I feel that there is no real justification.

The border between diagenesis and metamorphism is a diffuse one and is especially so in salts which are highly susceptible to only moderate changes in temperature and pressure. I have not found, however, that this raises any real practical difficulties in nomenclature. I do not see any objection to using some metamorphic textural terms in the description of evaporites (whether stratified or unstratified is immaterial) which have suffered widespread recrystallisation or mineralogical reconstitution in response to increased temperature or pressure due to load. Evaporites commonly show excellent examples of changes controlled by rise of temperature on burial, classed under the well-established heading of "Geothermal Metamorphism". The fact that such deposits may lie between relatively unaltered beds of limestone is irrelevant to their metamorphic status.

I do not see any need for the special terms 'evapocrysts' and 'neocrysts' to describe individual primary or secondary evaporite grains; surely *primary* and *secondary* grains would do. A statement as to whether *primary* or *secondary linear* or *platy parallelism* of grains is present or absent is better than using the terms 'evapocrystic', 'evapolensic', 'neocrystic' and 'neolensic'. The word 'porphyroblastic' can be applied to metamorphosed evaporites. Would it really cause confusion if it were used for those in which large secondary crystals have formed during diagenesis? We should not try to establish a sharp division between sedimentary and metamorphic rocks where none exists, and we must avoid adding more than absolutely necessary to our geological jargon.

REFERENCE

Greensmith, J. T., 1957, The Status and nomenclature of stratified evaporites: AM. JOUR. SCI., v. 255, p. 593-595.

GRANT INSTITUTE OF GEOLOGY
EDINBURGH 9, SCOTLAND

REPLY TO PROFESSOR F. H. STEWART

J. T. GREENSMITH

It is gratifying that the current method of describing evaporites should be so vigorously defended, as only by these means can the complexities of the subject be illuminated. Most petrologists would heartily agree about the necessity of avoiding new, and possibly cumbersome, terms. On the other hand, from the teaching (and students') point of view it can be rather confusing if terms having a metamorphic connotation, such as 'porphyroblastic', and others an igneous connotation, such as 'poikilitic' (Dunham, 1948, p. 220) and 'pseudoporphyritic' (Pettijohn, 1949, p. 355), are used to describe similar rocks. It is partly this inconstancy in usage which first suggested the need for a rationalisation in terminology.

Likewise, there is no doubt that metamorphic textural terms are often genetically appropriate, but there must be occasions when that particular origin is doubtful. Anhydrite beds at depth sometimes grade into secondary gypsum beds at outcrop presumably, but not always certainly, as a result of weathering (Pettijohn, 1949, p. 359). Surely, unless one can be reasonably certain that no genetic implication is involved, it is unwise to use a metamorphic-type description for those secondary gypsum beds. It is precisely to avoid problems of this type that the proposed system may be most useful and can be positively justified.

References

Dunham, K. C., 1948, A Contribution to the Petrology of the Permian Evaporite Deposits of North-eastern England: Yorks. Geol. Soc. Proc., v. 27, p. 217-227.

Pettijohn, F. J., 1949, Sedimentary Rocks: New York, Harper, 526 p.

Queen Mary College
London, England

REVIEWS

Handbuch der Physik. vol. 47, *Geophysics I: The Earth's Body*; I. S. Flugge, editor. P. 659. Berlin, 1956 (J. Bartels, Group Ed. Springer Verlag, DM. 118).—Geophysics I is the first of two volumes dealing with geophysics in the new edition of the *Encyclopedia of Physics*. The volume consists of 16 chapters: one each on rotation of the earth, radioactivity, telluric currents, interior of the earth, and forces in the crust; two on magnetism; two on gravity and figure of the earth; and seven on related topics of seismology, structure of the crust, and elastic properties. The book serves as an excellent summary of the fields of geophysics concerned with the solid earth.

The volume opens with a clear and concise treatment of the rotation of the earth and the derivation of a constant time unit by Sir H. Spencer-Jones. Irregular variations in the rate of rotation are explained by Munk and Revelle's theory of thermal convection in the core and electromagnetic coupling of the core with the mantle.

The second chapter, the first of several on seismology, is by J. Coulomb (in French) and treats the theory and mechanical principles of seismographs. In the next chapter K. E. Bullen develops the basic equations of seismic wave transmission, discusses the cause and energy content of earthquakes and interprets the physical properties of materials in the deep interior of the earth. Next follows an outstanding chapter on surface waves by M. Ewing and F. Press. This chapter summarizes much new material that has never before been brought together. Geologists will be interested to note that Lg waves are interpreted as channel waves in a low-velocity channel the top of which is the surface of the earth, instead of requiring a rather special low-velocity channel inside the crust. The chapter also provides necessary background for a chapter on structure of the earth's crust by the same two authors. In the latter chapter seismic refraction studies and gravity measurements are also brought to bear on the problems of crustal structure in the continents and oceans. The continental crust is about 35 km. thick and the oceanic crust only 5 km. The favored theory on oceanic trenches associated with island arcs is depression of

the crust without thickening or development of a "tectogene." Other chapters on seismology and related subjects are one by J. Coulomb on microseisms (in French), a very short chapter on seismic prospecting by Ewing and Press, and a chapter on measurement of elastic constants of rock. The latter, by H. Baule, Bochum, and E. Müller (in German) reviews static, dynamic and seismic methods of measurement.

In a chapter on gravity and isostasy, G. D. Garland describes absolute and relative measurements, their reduction, and their mathematical interpretation. An especially interesting section on the meaning of anomalies includes a description of the Bouguer anomaly on the Canadian shield, where the anomalies (with a relief of 90 milligals) follow structural trends and seem to indicate major lateral changes within the crust rather than simply variations in thickness of the crust. Correlation of negative anomalies with glaciated regions is also challenged. The subject of gravity and geodesy is completed in a chapter by K. Jung on the figure of the earth (in German). This topic covers nearby a hundred pages and includes a thorough, lucidly illustrated discussion of the geoid, the figures of reference and movements of the earth's axis of rotation.

The difficult and elusive subject of forces in the earth's crust is developed by A. E. Scheidegger, avoiding "obviously fantastic postulates." Some readers may take exception to basic premises in this paper, for example the premise that mountain building occurred in only about ten diastrophisms "separated by long periods of acquiescence," or the assumption of a two-layer crust following Jeffries' 1939 model, or especially, the claim that gravity data eliminate the possibility of normal faults along the African Rift Valleys. The latter premise is widely recognized as probably in error (see for instance, Vening Meinesz, F. A., 1950, Les "graben" Africains, résultat de compression ou de tension dans la croûte terrestre?: Institut Royal Colonial Belge, Bulletin des Séances, v. 21, p. 539-552). A comparatively long article on radioactivity and age of minerals by J. T. Wilson, R. D. Russell and R. M. Farquhar covers the subject historically as well as analytically. A chapter on the earth's interior by J. A. Jacobs is concerned with seismic data, mass and moment of inertia, thermal and electrical effects, and the geomagnetic field as explained by the dynamo theory. Electrical currents in the earth are treated in an article by L. Cagniard (in French). The chapter includes general theory, electrical prospecting and relations between magnetic and electrical variations.

Magnetism is treated in two chapters, both by S. K. Runcorn. The first is a concise summary of rock magnetism: mineralogy, physical theory, measurement, and variations from the Precambrian to the present. The other chapter summarizes the magnetism of the whole earth and theories of the earth's magnetism.

A useful German-English and English-German index completes the book.

The volume is attractive, except for its high price, to specialists in geophysics and to everyone interested in geophysical problems.

GEORGE A. THOMPSON

Elasticity, Fracture and Flow, with engineering and geologic applications; by J. C. JAEGER. P. viii, 152. London, 1956 (Methuen & Co., Ltd., $2.50).—

This splendid little book by the author of "An Introduction to Applied Mathematics" and co-author of "Conduction of Heat in Solids" is a concise mathematical treatment of the behavior of stressed solids. Professor Jaeger, in his own words, has "attempted to set out in as elementary form as possible the basic mathematics of elasticity, plasticity, viscosity and rheology, together with a discussion of the properties of the materials involved and the way in which they are idealized to form the basis for the mathematical theory".

The book treats three topics in approximately equal length: stress and strain, behavior of actual materials, and equations of motion and equilibrium. Stress and infinitesimal strain are presented first for two and then for three dimensions. Invariants, quadrics, Mohr's representation of stress and strain then follow, with a careful elementary treatment of finite homogeneous strain. This section is extremely good although the notation is not best suited for extension to tensor analysis.

The behavior of actual materials is described in an extraordinarily compact fashion which nevertheless achieves the stated purpose of the book. The equations of isotropic elasticity are followed by review of crystal elasticity, as an example of anisotropic elastic behavior. Treatment of finite strain under hydrostatic pressure next suggests to the reader what can be done with finite elasticity. Fracture of solids is treated according to Coulomb-Navier theory, with Anderson's extension to faulting. The Mohr, Griffith and Becker theories of failure are summarized, although unfortunately the reader is not given references to the original work. The yielding of perfectly plastic solids according to the Tresca and Huber-Mises theories conclude this section, with a brief summary of rheological models which combine elastic, plastic and viscous behavior; 19 references are provided.

The final third of the book develops the equations of motion and equilibrium of isotropic bodies, and uses the stress function to analyze a few problems of plain stress and strain. Wave propagation, a few elementary relationships in seismic prospecting, the equations of motion of a viscous fluid, and the slip line theory of two-dimensional plastic flow of ideal materials conclude the book.

Geologic applications briefly mentioned are Anderson's theory of faulting, Becker's finite strain theory, elastic properties of rocks, stresses at depth due to gravity, seismic prospecting and creep of rocks. Engineering applications include, in addition, the tensile test, plastic torsion of cylinders, and the Rankine theory of earth pressures.

This book should be useful to geologists who want a rather complete elementary survey of those mathematical tools presently available for analysis of rock deformation, or who want to review the assumptions one must make about rocks in order to treat them mathematically. For mathematical preparation the reader should have facility with calculus through partial differentiation and vector calculus, and some acquaintance with three-dimensional analytical geometry and the complex variable. The book is nicely subdivided for classroom use; an elementary course in structural geology could use sec-

tions 1, 2, 3, 6, 7, 10, 21 and 22, which treat two-dimensional stress and strain, Mohr circle and strength theory, and general properties of materials. Remaining sections might be used in an advanced course in mechanics of rock deformation or crystal plasticity or as an introduction to seismology. Compactness of the book and the need for supplementary reading and problems mean that this book will find its greatest application in the hands of a teacher.

Probably the greatest weakness of Professor Jaeger's book is that it is in places forced to touch on the physics of deformation, but for lack of space cannot really survey this field. For example, the most recent work reported on rock or mineral deformation is from 1939, the rich field of crystal plasticity is totally unrepresented, and thermodynamic variables are not considered. Furthermore it is implied that with present knowledge we can idealize the flow of rock by a simple rheological model (p. 105). In this respect the title is somewhat misleading for there is regretably little in geology that can now be treated by the methods of this book without further experimental guidance. However, the book succeeds admirably in its expressed intent, and as a well-written synthesis of material now scattered through six or seven books on plasticity, elasticity, metallurgy and beam theory, it is highly recommended.

W. F. BRACE

Principles of Stratigraphy; by CARL O. DUNBAR and JOHN RODGERS. P. 356; 123 figs., 21 tbls. New York, 1957 (John Wiley & Sons, Inc., $10.00).—The present status of stratigraphic principles is ably and clearly described by Dunbar and Rodgers in *Principles of Stratigraphy*, a readable, scholarly survey well-suited for use as a college textbook and equally valuable to the professional geologist as a reference work. It is comprehensive, up-to-date, and attractively presented, the outstanding book in the field.

Eighteen chapters are divided into four sections as follows: *Environments of deposition* (sedimentary processes, non-marine environments, marine environments, mixed environments), *basic stratigraphic relations*, (stratification, breaks in the record, facies and facies change), *interpretation of lithotopes* (sedimentary rock nomenclature, rudites, terrigenous arenites, lutites, redbeds, carbonate rocks, siliceous non-fragmental rocks), *synthesis* (the local section, correlation, the stratigraphic system, broad patterns in the distribution of sedimentary rocks). A combination of bibliography and author's index, listing 685 titles, and a subject index are included.

The method chosen by the authors for dealing with inconsistent and multiple use of terms is logical. It should go far to resolve semantic conflicts that abound in stratigraphy. They believe that "what can be dangerous to scientific understanding and progress is not so much that a term is being used in two senses, annoying as that may be, as that the men so using it are unaware of their difference." They recognize that uniform usage, although desirable, cannot be forced. So, they describe differences and inconsistencies that exist and make their own recommendations.

A few minor points invite comment. Microcrystalline texture in carbonate rocks is, in some cases, clearly related to fine dimensions of the original grains. However, there are well-authenticated cases (*e.g.*, in the Guadalupe

Mountains area, Texas) of development of secondary microcrystalline texture in carbonate rocks by recrystallization of coarse clastic sediment. The clastic texture and fabric of the original rock are progressively obliterated by recrystallization.

The authors devote much space to recent studies on turbidity flows, but they do not make a clear distinction between them and submarine slides (termed submarine "landslides"). The slides may cause turbidity flows, as has been postulated for certain Permian rocks in the Delaware Basin, but the deposits of the two processes are very different. Turbidity current deposits are characterized by graded bedding and, according to Kuenen, the coarsest fragments do not exceed 10 cm in diameter. It is doubtful, and certainly not demonstrated, that turbidity currents "are capable of transporting very large blocks."

The authors use the term *biotope* for the environment in which a community of organisms lives or lived in the past. They do not distinguish, however, between organic environments (habitats) and depositional environments. It seems to me that these are usually different and should not be confused. In ecological usage, the biotope is a map unit. It is synonymous and coextensive with niche or habitat. But many habitats are not closely related to conditions of sedimentation. By simple analogy one would suppose that a lithotope would be the depositional (and diagenetic) conditions under which a rock was formed, and it is so used by some writers. However, Dunbar and Rodgers define this term as the local rock record of the biotope.

Biocoenosis, another ecological term, is used by the authors in the conventional sense for a local community or assemblage of living organisms. If this definition is to be maintained, however, it cannot very well be applied to fossil assemblages which bear little resemblance to living communities. Very few species of the living community, perhaps rarely more than a few percent, are capable of leaving a fossil record. Fossil assemblages are records by which biocoenoses may be inferred.

A few points on coral reefs raised by the authors are debatable. They subscribe to a currently popular view that the broad sea-level flat, so characteristic of Pacific coral reefs, is cut mainly by solution. There is, however, an opposed view supported by much evidence that the reef flat is of complex origin in which sea-water solution is subordinate. According to this thesis planation near the inner margin of the reef is by organic erosion, aided by wave attack at the intertidal nip. Elsewhere, over most of the area of the reef, the intertidal platform is built upward to sea level by organisms. The surface represents the ceiling of organic accretion. This, essentially, was the conclusion of Darwin and Dana and is the view shared by a number of modern students.

The Marquesas Islands near Key West cited by the authors as an atoll are not of coral reef origin. They form a pseudoatoll.

These are relatively unimportant details chosen at random. They do not detract significantly from the general effect of objectivity and comprehensive treatment of *Principles of Stratigraphy*. The authors and publisher are to be congratulated for the outstanding and timely result. NORMAN D. NEWELL

VOL. 256 No. 3, 1958

American Journal of Science

MARCH 1958

CONTENTS

Structural Petrology of Cambro-Ordovician Limestones of the North-West Highlands of Scotland ..... *C. B. Crampton* 145

Dynamic Interpretation of the Fabric of a Dolomite from the Moine Thrust-Zone in North-West Scotland ..... *John M. Christie* 159

Phase Equilibria at High Temperatures in Oxide Systems Involving Changes in Oxidation States ..... *Arnulf Muan* 171

Group Operator Variance in Morphometric Work with Maps *Richard J. Chorley* 208

DISCUSSION

The Nomenclature of Evaporite Textures ..... *F. H. Stewart* 219

Reply ..... *J. T. Greensmith* 219

REVIEWS

Handbuch der Physik, vol. 47; I. S. Flugge, editor ..... *George A. Thompson* 220

Elasticity, Fracture and Flow; by J. C. Jaeger ..... *W. F. Brace* 222

Principles of Stratigraphy; by Carl O. Dunbar and John Rodgers *Norman D. Newell* 223